



# **UNIVERSIDAD DE INVESTIGACIÓN DE TECNOLOGÍA EXPERIMENTAL YACHAY**

**Escuela de Ciencias Físicas y Nanotecnología**

**TÍTULO: Designing a Passive Cooling Material Based on Wood**

Trabajo de integración curricular presentado como requisito para la  
obtención del título de Ingeniera en Nanotecnología

**Autor:**

Bermeo Alvaro Domenica Romina

**Tutor:**

Ph.D.- Medina Dagger Ernesto

**Cotutor:**

Ph.D. - Chacón Julio

Urcuquí, Imbabura, Ecuador, June 8, 2021



Urcuquí, 3 de junio de 2021

**SECRETARÍA GENERAL**  
**(Vicerrectorado Académico/Cancillería)**  
**ESCUELA DE CIENCIAS FÍSICAS Y NANOTECNOLOGÍA**  
**CARRERA DE NANOTECNOLOGÍA**  
**ACTA DE DEFENSA No. UITEY-PHY-2021-00009-AD**

A los 3 días del mes de junio de 2021, a las 15:30 horas, de manera virtual mediante videoconferencia, y ante el Tribunal Calificador, integrado por los docentes:

<b>Presidente Tribunal de Defensa</b>	Dr. BRAMER ESCAMILLA , WERNER , Ph.D.
<b>Miembro No Tutor</b>	Dra. BRICEÑO ARAUJO, SARAH ELISA , Ph.D.
<b>Tutor</b>	Dr. MEDINA DAGGER, ERNESTO ANTONIO , Ph.D.

El(la) señor(ita) estudiante **BERMEO ALVARO, DOMENICA ROMINA**, con cédula de identidad No. **0105515118**, de la **ESCUELA DE CIENCIAS FÍSICAS Y NANOTECNOLOGÍA**, de la Carrera de **NANOTECNOLOGÍA**, aprobada por el Consejo de Educación Superior (CES), mediante Resolución **RPC-SO-13-No.156-2015**, realiza a través de videoconferencia, la sustentación de su trabajo de titulación denominado: **Designing a Passive Cooling Material Based on Wood**, previa a la obtención del título de **INGENIERO/A EN NANOTECNOLOGÍA**.

El citado trabajo de titulación, fue debidamente aprobado por el(los) docente(s):

<b>Tutor</b>	Dr. MEDINA DAGGER, ERNESTO ANTONIO , Ph.D.
<b>Co - Tutor</b>	Dr. CHACON TORRES, JULIO CESAR , Ph.D.

Y recibió las observaciones de los otros miembros del Tribunal Calificador, las mismas que han sido incorporadas por el(la) estudiante.

Previamente cumplidos los requisitos legales y reglamentarios, el trabajo de titulación fue sustentado por el(la) estudiante y examinado por los miembros del Tribunal Calificador. Escuchada la sustentación del trabajo de titulación a través de videoconferencia, que integró la exposición de el(la) estudiante sobre el contenido de la misma y las preguntas formuladas por los miembros del Tribunal, se califica la sustentación del trabajo de titulación con las siguientes calificaciones:

Tipo	Docente	Calificación
Presidente Tribunal De Defensa	Dr. BRAMER ESCAMILLA , WERNER , Ph.D.	10,0
Tutor	Dr. MEDINA DAGGER, ERNESTO ANTONIO , Ph.D.	10,0
Miembro Tribunal De Defensa	Dra. BRICEÑO ARAUJO, SARAH ELISA , Ph.D.	9,5

Lo que da un promedio de: **9.8 (Nueve punto Ocho)**, sobre 10 (diez), equivalente a: **APROBADO**

Para constancia de lo actuado, firman los miembros del Tribunal Calificador, el/la estudiante y el/la secretario ad-hoc.

Certifico que *en cumplimiento del Decreto Ejecutivo 1017 de 16 de marzo de 2020, la defensa de trabajo de titulación (o examen de grado modalidad teórico práctica) se realizó vía virtual, por lo que las firmas de los miembros del Tribunal de Defensa de Grado, constan en forma digital.*

**BERMEO ALVARO, DOMENICA ROMINA**  
**Estudiante**

**Dr. BRAMER ESCAMILLA , WERNER , Ph.D.**  
**Presidente Tribunal de Defensa**

WERNER  
BRAMER  
ESCAMILLA  
Digitally signed by  
WERNER BRAMER  
ESCAMILLA  
Date: 2021.06.03  
16:58:14 -05'00'



Dr. MEDINA DAGGER, ERNESTO ANTONIO , Ph.D.  
**Tutor**

ERNESTO  
ANTONIO  
MEDINA DAGGER

Digitally signed by  
ERNESTO ANTONIO  
MEDINA DAGGER  
Date: 2021.06.03  
16:54:02 -05'00'

Dra. BRICEÑO ARAUJO, SARAH ELISA , Ph.D.  
**Miembro No Tutor**



Firmado electrónicamente por:

**SARAH ELISA  
BRICENO  
ARAUJO**

CIFUENTES TAFUR, EVELYN CAROLINA  
**Secretario Ad-hoc**

EVELYN  
CAROLINA  
CIFUENTES TAFUR

Digitally signed by EVELYN  
CAROLINA CIFUENTES  
TAFUR  
Date: 2021.06.03 16:52:21  
-05'00'

## **AUTORÍA**

Yo, **DOMENICA ROMINA BERMEO ALVARO**, con cédula de identidad 0105515118, declaro que las ideas, juicios, valoraciones, interpretaciones, consultas bibliográficas, definiciones y conceptualizaciones expuestas en el presente trabajo; así cómo, los procedimientos y herramientas utilizadas en la investigación, son de absoluta responsabilidad de el/la autora (a) del trabajo de integración curricular. Así mismo, me acojo a los reglamentos internos de la Universidad de Investigación de Tecnología Experimental Yachay.  
Urcuquí, Abril 2021



Doménica Romina Bermeo Alvaro

CI: 0105515118



## **AUTORIZACIÓN DE PUBLICACIÓN**

Yo, **DOMENICA ROMINA BERMEO ALVARO**, con cédula de identidad 0105515118, cedo a la Universidad de Investigación de Tecnología Experimental Yachay, los derechos de publicación de la presente obra, sin que deba haber un reconocimiento económico por este concepto. Declaro además que el texto del presente trabajo de titulación no podrá ser cedido a ninguna empresa editorial para su publicación u otros fines, sin contar previamente con la autorización escrita de la Universidad.

Asimismo, autorizo a la Universidad que realice la digitalización y publicación de este trabajo de integración curricular en el repositorio virtual, de conformidad a lo dispuesto en el Art. 144 de la Ley Orgánica de Educación Superior

Urcuquí, Abril 2021.



Doménica Romina Bermeo Alvaro

CI: 0105515118

## **Dedication**

A mis hermanos: Diana, Meche, Hernan, Ferdi y Milo.

A mis padres: Henry y Paola.

A mi compañero de vida: Leandro

A mis angelitos: Daniel, Mamaluca, Hernan, Sparky y Muñeca.

Domenica Romina Bermeo Alvaro

## **Acknowledgements**

I would like to thank my supervisor Ernesto Medina, my co-advisor Julio Chacón, as well as Werner Bramer and Floralba with out them the realisation of this thesis project would not be possible. At the same time I would like to thank my teachers who guided me along my career as a professional and as a person. Also Evelyn Cifuentes who always was there for the students.

I also would thank my family of Cuenca and Ibarra. I always keep one of them in my heart. I also would like to thank my friends Dale, Gaby, Emi, Will, Anthony, Pablito, Mau, Mati, Brandon who made Yachay my second home. Thank to my friends of the career who made this adventure more special: Cris, Carito, Pato, Majito, Nico. Finally, to my new family Leandro.

Domenica Romina Bermeo Alvaro

## Resumen

Hoy en día, utilizamos sistemas de refrigeración como un refrigerador, aire acondicionado, e incluso ventiladores eléctricos, pero no somos conscientes del consumo de energía de estos dispositivos y la entrada de energía que se necesita para enfriar un cuerpo. Como parte del proceso de reducción del cambio climático, es necesario reducir nuestro consumo de energía. Por lo tanto, se propone un proceso de refrigeración radiativa pasiva como alternativa a los aires acondicionados y dispositivos de refrigeración<sup>1</sup>. Este proceso puede enfriar una superficie por debajo de la temperatura ambiente, sin entrada de energía, emitiendo radiación a través de ventanas atmosféricas naturales (principal de 8-13  $\mu\text{m}$ ) al espacio (temperatura alrededor de 2,8 K). Este proceso es aún más eficaz por la noche, y los estudios de su funcionamiento durante el día están apareciendo actualmente<sup>1</sup>. Por lo tanto, en este proyecto, nuestro objetivo es estudiar el proceso de enfriamiento pasivo radiativo de las maderas seleccionadas presentes en Ecuador (*Eucalyptus globulus* (Eucalipto), *Guarea kunthiana* (Manzano Colorado/Colorado), y *Dacryodes peruviana* (Copal)) delignificándolas (por medio de blanquear la madera) para tener un material que emita en la ventana atmosférica (8-13  $\mu\text{m}$ ) y refleje la radiación solar. En el proyecto, se obtuvieron maderas blanqueadas con poder de enfriamiento por la noche y menor poder de enfriamiento durante el día. El material más eficiente para el enfriamiento pasivo es cooling wood Colorado, la diferencia de temperatura con respecto a la temperatura ambiente se encontró que es por la noche  $2,7 \pm 0,2$  ° C y en el día  $0,6 \pm 0,2$  ° C con un poder de enfriamiento sobre área de  $80 \pm 20$   $\text{Wm}^{-2}$  y  $60 \pm 20$   $\text{Wm}^{-2}$  respectivamente.

**Palabras clave:** Poder de enfriamiento, celulosa, XPS, FTIR, emisividad.

## Abstract

Nowadays, we use cooling systems like a refrigerator, air conditioner, and even electric fans, but we are not aware of the energy consumption of these devices and the power input that is needed to cool a body. As part of the process of reducing climate change, it is necessary to reduce our energy consumption. Thus, a passive radiative cooling process is proposed as an alternative to air conditioners and cooling devices<sup>1</sup>. This process can cool a surface below ambient temperature, without power input, by emitting radiation through naturally occurring atmospheric windows to space (temperature around 2.8 K). This process is even more effective at night, and studies of its operation at daytime are currently appearing<sup>1</sup>. Thus, in this project, we aim to study the passive radiative cooling process of selected woods present in Ecuador (*Eucalyptus globulus* (Eucalipto), *Guarea kunthiana* (Manzano Colorado/Colorado), and *Dacryodes peruviana* (Copal)) by delignifying them (by means bleach the wood) to have a material that emits in the atmospheric window (8-13  $\mu\text{m}$ ) and reflects solar radiation. In the project, bleached woods were obtained with cooling power at night and lower cooling power at day. The most efficient material for passive cooling is Colorado cooling wood, the difference in temperature with respect to ambient temperature was found to be at night  $2,7 \pm 0.2$  °C and at day  $0,6 \pm 0.2$ °C with a cooling power over an area of  $80 \pm 20$   $\text{Wm}^{-2}$  and  $60 \pm 20$   $\text{Wm}^{-2}$  respectively.

**Keywords:** Cooling power, cellulose, XPS, FTIR, emissivity.

# Contents

<b>List of Figures</b>	<b>xvii</b>
<b>List of Tables</b>	<b>xxii</b>
<b>1 Introduction</b>	<b>1</b>
1.1 Problem Statement . . . . .	4
1.2 General and Specific Objectives . . . . .	5
1.2.1 General Objectives . . . . .	5
1.2.2 Specific Objectives . . . . .	5
<b>2 Theoretical Framework</b>	<b>7</b>
2.1 Thermal radiation . . . . .	7
2.2 Atmospheric window . . . . .	10
2.3 Passive Cooling Phenomenon . . . . .	10
2.3.1 Radiative cooling power of the system $P_{rad}$ . . . . .	12
2.3.2 Environmental thermal absorption $P_{atm}$ . . . . .	13
2.3.3 Solar Absorption $P_{solar}$ . . . . .	14
2.3.4 Non radiative heat loss $P_{norad}$ . . . . .	14
2.3.5 Effect of tilt angle . . . . .	15
2.4 Materials . . . . .	15

2.4.1	Photonic Materials . . . . .	16
2.4.2	Metamaterials . . . . .	18
2.4.3	Coatings . . . . .	18
2.4.4	Natural Materials . . . . .	20
2.5	Nanowood . . . . .	22
2.5.1	Improvements Nanowood material . . . . .	24
2.6	Ecuadorian Woods . . . . .	25
2.6.1	<i>Guarea kunthiana</i> (Manzano Colorado) . . . . .	25
2.6.2	<i>Eucalyptus globulus</i> (Eucalipto) . . . . .	26
2.6.3	<i>Dacryodes peruviana</i> (Copal) . . . . .	27
2.7	Characterization of Materials . . . . .	27
2.7.1	Fourier transform infrared spectroscopy (FTIR) . . . . .	27
2.7.2	X-ray photoelectron spectroscopy (XPS) . . . . .	30
<b>3</b>	<b>Methodology</b>	<b>33</b>
3.1	Delignification Process . . . . .	33
3.1.1	Delignification by NaOH and Na <sub>2</sub> SO <sub>3</sub> . . . . .	34
3.1.2	Delignification by NaClO . . . . .	36
3.1.3	Delignification by NaClO <sub>2</sub> . . . . .	37
3.2	Characterization using FTIR . . . . .	39
3.3	Characterization using XPS . . . . .	39
3.4	Cooling performance . . . . .	40
<b>4</b>	<b>Results &amp; Discussion</b>	<b>45</b>
4.1	Materials obtained . . . . .	45
4.2	FTIR . . . . .	45
4.2.1	Colorado . . . . .	47

4.2.2	Eucalipto . . . . .	52
4.2.3	Copal . . . . .	54
4.3	XPS . . . . .	58
4.3.1	Colorado . . . . .	59
4.3.2	Eucalipto . . . . .	62
4.3.3	Copal . . . . .	69
4.4	Cooling Performance . . . . .	78
4.4.1	Colorado . . . . .	81
4.4.2	Eucalipto . . . . .	84
4.4.3	Copal . . . . .	86
<b>5</b>	<b>Summary and Conclusions</b>	<b>91</b>
5.1	Summary . . . . .	91
5.2	Conclusion . . . . .	92
5.3	Outlook . . . . .	94
<b>A</b>	<b>Cooling performance closed box</b>	<b>95</b>
<b>B</b>	<b>XPS data of fitting</b>	<b>99</b>
<b>C</b>	<b>Arduino</b>	<b>103</b>
	<b>Bibliography</b>	<b>109</b>



# List of Figures

2.1	Here we depict the infrared spectrum of the atmospheric transmission above Mauna Kea, with air mass 1.5 and water column 1 mm. This represents an overview of the wavelength of 8-14 $\mu\text{m}$ which is the main atmospheric transparency window. The figure can be obtained from the data generated by ATRAN <sup>2</sup> , thanks to the Gemini Observatory. It is important to notice that transmission is dimensionless <sup>3</sup> . . . . .	11
2.2	Here we depict the scheme for a passive radiative material and the factors that affect the net cooling power: the radiative cooling power $P_{rad}$ , environmental thermal absorption $P_{rad}$ , solar absorption $P_{solar}$ , heat transferred as conduction or convection (nonradiative) $P_{norad}$ and an extra term, the thermal leakage $P_{leak}$ , when we are working with a thermally isolated measurement box. . . . .	11
2.3	Scheme of different photonic materials for passive radiative cooling. a) metal-dielectric photonic structure <sup>4</sup> and b) photonic solar reflector and thermal emitter <sup>5</sup> . These figures are based on bibliography . . . . .	17
2.4	Scheme of the different metamaterials for passive radiative cooling. a) A symmetrically shaped conical metamaterial (CMM) pillars of Germanium (red) and Aluminium (gray) <sup>6</sup> . b) Resonant polar dielectric microspheres of $SiO_2$ randomly oriented in a polymeric matrix <sup>7</sup> . These figures are inspired from bibliography . . . . .	19

2.5	Scheme of the (P(VdF-HFP)HP) coating that created a network of air voids in polymer. This figure is inspired from paper Hierarchically porous polymer coatings for highly efficient passive daytime radiative cooling <sup>8</sup> . . . . .	20
2.6	Monomer of cellulose structure, here one observes the three reactive hydroxyl groups in the carbon C6, C2 and C3. . . . .	21
2.7	Graphical illustration of hierarchical alignment of nanowood structure at the top panel, at bottom panel, one can observe its cellulose chain, aligned to form fibril aggregate. Based on bibliography <sup>9</sup> . . . . .	23
3.1	Graphical illustration of experimental scheme of chemical treatment with NaOH (2.5 M)/Na <sub>2</sub> SO <sub>3</sub> (0.4M) and H <sub>2</sub> O <sub>2</sub> (2.5 M, 50 % solution) . . . . .	35
3.2	Possible mechanism of delignification using firstly A) NaOH, Na <sub>2</sub> SO <sub>3</sub> and B) H <sub>2</sub> O <sub>2</sub> . . . .	36
3.3	Possible mechanism of delignification using NaClO . . . . .	37
3.4	Possible mechanisms of delignification using NaClO <sub>2</sub> adapted from <sup>10</sup> . . . . .	38
3.5	Equipment for the measurement of temperature differences and cooling power. . . . .	40
3.6	Graphical illustration of experimental setup for the measurement of temperatures and cooling power. . . . .	41
3.7	Graphical illustration of experimental setup for the measure of temperatures and cooling power. . . . .	41
4.1	In this figure one observes the materials obtained from Colorado, Copal an Eucalipto woods, after chemical treatment with NaOH/Na <sub>2</sub> SO <sub>3</sub> and H <sub>2</sub> O <sub>2</sub> (cooling wood), NaClO and NaClO <sub>2</sub> . . . . .	46
4.2	Wood structure is present here where cellulose, lignin and hemicellulose are observed. The main structure of wood is cellulose. The hemicellulose shown is for hardwood. In lignin Me means a methyl group (CH <sub>3</sub> ) <sup>11</sup> . . . . .	47
4.3	FTIR spectra of Colorado wood before the delignification, during the delignification and after of the delignification treatment to obtain Colorado cooling wood material. . . . .	48

4.4	FTIR spectra of Eucalipto wood before the delignification, during the delignification and after of the delignification treatment to obtain Eucalipto cooling wood material . . . . .	53
4.5	FTIR spectra Copal wood before the delignification, during the delignification and after of the delignification treatment to obtain Copal cooling wood material . . . . .	55
4.6	SEM XPS . . . . .	58
4.7	C1s and O1s XPS spectra of Colorado for non-treated wood (NTW), treated wood (TW) and cooling wood (CW). . . . .	63
4.8	N1s and Si2p XPS spectra of Colorado for non-treated wood (NTW), treated wood (TW) and cooling wood (CW). . . . .	64
4.9	C1s and O1d XPS spectra of Eucalipto for non-treated wood (NTW), treated wood (TW) and cooling wood (CW). . . . .	70
4.10	N1s and Si2p XPS spectra of Eucalipto for non-treated wood (NTW), treated wood (TW) and cooling wood (CW). . . . .	71
4.11	C1s and O1s XPS spectra of Copal for non-treated wood (NTW), treated wood (TW) and cooling wood (CW). . . . .	75
4.12	N1s and Si2p XPS spectra of Copal for non-treated wood (NTW), treated wood (TW) and cooling wood (CW). . . . .	76
4.13	Emissivity of cooling woods: Colorado (blue), Copal (purple) and Eucalipto (pink) with respect to the atmospheric transmission where the atmospheric window is observed. Transmission and emissivity is dimensionless <sup>3</sup> . . . . .	78
4.14	Manzano Colorado cooling wood temperature during the day (a), and during the night (b), where (green) is the temperature of Colorado cooling wood, (purple) ambient temperature, and (pink) untreated Colorado wood over time in an open box. . . . .	83
4.15	Colorado net cooling power with respect to time expected during the day. . . . .	84
4.16	Eucalipto cooling wood temperature during the day (a) and during the night (b), where (green) is the temperature of Eucalipto cooling wood, (purple) ambient temperature, and (pink) untreated Eucalipto wood over time in an open box. . . . .	85

4.17	Eucalipto net cooling power expected over time . . . . .	86
4.18	Copal cooling wood temperature during the day (a) and during the night (b), where (green) is the temperature of Copal cooling wood, (purple) ambient temperature, and (pink) untreated Copal wood over time in an open box. . . . .	87
4.19	Copal net cooling power expected. . . . .	88
A.1	Manzano Colorado registered temperature differences closed. . . . .	96
A.2	Eucalipto registered temperature differences closed. . . . .	97
A.3	Copal registered temperature differences closed box. . . . .	98
C.1	Arduino code part 1 (page 1 and 2) . . . . .	104
C.2	Arduino code part 2 (page 3 and 4) . . . . .	105
C.3	Arduino code part 3 (page 5 and 6) . . . . .	106
C.4	Arduino code part 4 (page 7) . . . . .	107
C.5	Arduino code part 5 (page 8 and 9) . . . . .	108

# List of Tables

2.1	FTIR peaks for wood and its main components: cellulose, hemicellulose and lignin, the * refers to the peaks in the atmospheric window, the peaks intensity are denoted by (s) strong, (m) medium and (w) weak. . . . .	29
4.1	Ratio of intensities $I(1421/898)$ measured for the spectra in order to identify the increase of crystallinity. . . . .	56
4.2	FTIR peaks of wood and its main components: cellulose, hemicellulose and lignin measured in the samples, * refers to the peaks in the atmospheric window regions of 8 to 13 $\mu m$ , the peaks intensity are denoted by (s) strong, (m) medium and (w) weak. . . . .	57
4.3	Peaks assignments for XPS spectra C1s, O1s, N1s and Si2p for Colorado for non-treated wood (NTW), treated wood (TW) and cooling wood (CW). . . . .	65
4.4	Peaks assignments for XPS spectra C1s, O1s, N1s and Si2p for Eucalipto for non-treated wood (NTW), treated wood (TW) and cooling wood (CW). . . . .	72
4.5	Peaks assignments for XPS spectra C1s, O1s, N1s and Si2p for Copal for non-treated wood (NTW), treated wood (TW) and cooling wood (CW). . . . .	77
4.6	Emissivity in the range of the atmospheric window (8 to 13 micrometers). It is important to notice that emissivity is dimensionless. <sup>3</sup> . . . . .	80
4.7	Cooling performance results for Colorado, Eucalipto and Copal cooling wood (CW). . . .	88

B.1	Area and FWHM (full width in a half maximum) of peaks present in XPS spectra C1s, O1s, N1s and Si2p for Colorado (COL) non-treated wood (NTW), treated wood (TW) and cooling wood (CW) . . . . .	100
B.2	Area and FWHM (full width in a half maximum) of peaks present in XPS spectra C1s, O1s, N1s and Si2p for Eucalipto (EUC) non-treated wood (NTW), treated wood (TW) and cooling wood (CW) . . . . .	101
B.3	Area and FWHM (full width in a half maximum) of peaks present in XPS spectra C1s, O1s, N1s and Si2p for Copal (COP) non-treated wood (NTW), treated wood (TW) and cooling wood (CW) . . . . .	102

# Chapter 1

## Introduction

Today, we use cooling systems like refrigerators or air conditioners in many spheres of our lives. But we are rarely aware of the energy consumption of these devices and the power input needed to comfortably cool a room. From a climate perspective, Ecuador is usually subdivided into four regions: "Sierra," "Costa," Amazon, and Galapagos; however, 54% of all national electric consumption comes from the Costa region according to ARCONEL ("Agencia de regulación y control de electricidad")<sup>12</sup>. This is obviously because this region is warmer than the rest by a considerable margin, making it necessary for its inhabitants to spend more electricity on cooling devices, such as air conditioners, during long parts of the day<sup>13</sup>. Not only that, but the Costa region also contains the largest Fishing industries in the country. This sector also requires a vast input of electrical energy into the refrigeration of their products<sup>13</sup>. This is not an isolated issue in Ecuador. Nowadays, a considerable segment of the global electrical production goes to cooling, from food preservation, air conditioning to even large-scale computation. Currently, compression-based cooling systems are commonly used for cooling. However, they consume large amounts of electricity and generate a large quantities of CO<sub>2</sub><sup>14</sup>. Also, that cooling strategy only moves heat from one location to another on the earth's surface, together with converting work to heat. Thus, the net effect is heating instead of cooling, leading to various issues such as the urban heat island (UHI) effect and thermal pollution. Under global warming, these issues are getting worse which requires more energy for cooling. Hence, inexpensive and

eco-friendly approaches with net cooling capability are desirable for reducing energy costs and associated adverse effects above<sup>14</sup>.

Passive radiative cooling during the day is a new, eco-friendlier alternative that has recently been in the scientific spotlight as a possible alternative to traditional cooling methods<sup>1</sup>. Radiative cooling is then a natural method for cooling since heat is dissipated to space via thermal radiation. But the technique is not as easy as it sounds. It is more affordable at night. During the daytime, cooling is difficult to achieve because of solar radiation, and some cooling power is lost due to the wind or by conduction or convection. In that way, it is essential to study the cooling system<sup>15</sup>. For a material to have passive radiative cooling at night should have high emissivity in the atmospheric transparency window close to that of a perfect *Blackbody*. But for a material to have passive radiative cooling during the day, it should have high emissivity in the infrared window and simultaneously reflect or scatter visible sunlight efficiently. This means ideally that it has an emissivity of almost 0 in the whole spectrum (except at the atmospheric window).

The atmosphere has its own mechanism to cool itself due to the existence of dust and various greenhouse gases, including water vapor<sup>16</sup>. The atmospheric window is known as a part of the atmospheric electromagnetic spectrum in which the atmosphere is particularly transmissive<sup>17</sup>. There are mainly three major atmospheric transmission windows: one in the near-infrared (NIR) 0.7–2.5  $\mu\text{m}$ , the other in the mid-infrared (MIR) 3–5  $\mu\text{m}$ , and the most important in far-infrared (FIR), 8–14  $\mu\text{m}$  (can be observed in figure 2.1 ). At the same time, in the atmospheric window, energy absorption by water vapor and carbon dioxide is weak, so then photons escape more easily to space<sup>18</sup>. So, some infrared radiation originates near the earth's surface, leaving the atmosphere through this window unimpeded.

Studies of passive cooling operation in the daytime are currently appearing in the literature<sup>1</sup>. Different materials such as photonic structures<sup>4</sup>, metamaterials<sup>6</sup>, and coatings<sup>8</sup> have been probed for their applicability as passive cooling radiators by day. Similarly, a composite from wood can have a desirable behavior for passive radiative cooling<sup>9</sup>. We will study some materials derived from different woods existing in Ecuador, like *Eucalyptus globulus* (Eucalipto), *Guarea kunthiana* (Manzano Colorado), and *Dacryodes peruviana* (Copal).

Wood is mainly composed of amorphous lignin and hemicellulose, which are intertwined between the



cellulose nanofibril<sup>9</sup>. The cell wall consists mainly of cellulose fibrils of 3-5 nm in diameter, lignin, and pectin. One of the most important features of wood is its anisotropic structure since wood has aligned vertical channels. As is observable when you take a piece of wood, inside it there exist aligned vertical channels. These are used to pump ions, water, and other nutrients needed for photosynthesis from the roots to the leaves<sup>19</sup>. Inside the wood, cellulose and hemicellulose are linked by hydrogen bonds and between lignin and hemicellulose by covalent linkage<sup>20</sup>. Cellulose and hemicellulose are colorless, and the lignin complex structure has a dark color. Mesoporous wood structure leads to large light scattering in the visible range making wood ready for this propose<sup>19</sup>.

Natural lignin is a 2D amorphous polymer with a dark color comprising three types of lignin units: syringyl units (S), guaiacyl units (G), and p-gydoxylphenil units (H). Some studies have proposed a wood composite obtained from different chemical treatments<sup>9,19</sup>. The idea of this experimental procedure is to delignify (remove the lignin) and remove the hemicellulose from the wood by bleaching it<sup>9,20</sup>. After the chemical treatment, the cellulose aggregates in the cell wall layer. The resulting material consists of cellulose nanofibrils in the form of fibril aggregates. Each cellulose nanofibril, that constitutes the cell walls, is packed and aligned parallel to each other and leads to a hierarchical alignment of nanowood. Also, the removal of lignin and hemicellulose increases the wood's porosity and eliminates any traces of other colors from the material<sup>21</sup>, therefore creating a better nanofibril alignment of cellulose as well as a whiter and more diffusely reflective material surface.

Finally, each fibril aggregate is composed of aligned crystalline cellulose packed with several tens of glucan chains in a crystalline order, held together by intermolecular hydrogen bonds and van der Waals forces. The material shows a lower density, high mechanical strength, and low emissivity in visible range, yielding a high efficient block to thermal radiation from the sun. Among the benefits of the new material is its anisotropic thermal conductivity. That property allows heat to spread along the nanofibril direction, reducing the heat flow in a transverse direction<sup>9</sup>. Then this composite is ideal for the study of passive radiative cooling<sup>9</sup>. This material can be used for high-scale production since its procedure is easy and environmentally friendly.

In this thesis project, we study the theory behind passive radiative cooling. We design passive cooling

materials and design how to measure their cooling power. In Chapter 2, we study the parameters involved in a material in order to have passive cooling behavior. We present some materials recently reviewed with this performance. An explanation of the structure of wood is given to understand the material designed in this thesis. In Chapter 3 we explain the methodology used to obtain the passive cooling material based on wood, how FTIR and XPS did the characterization of the materials, and how we will study the cooling power of the materials. Finally, in Chapter 5 is discussed the results of the materials obtained, their characterization, and their cooling performance.

## 1.1 Problem Statement

Passive radiative cooling at night has been studied since the 70s<sup>1</sup>. However, its use during the day as an alternative to air conditioners and cooling systems has recently gained huge relevance<sup>1,5,22</sup>. The problem with obtaining passive cooling during the day is solar radiation in the visible range. Therefore, to achieve passive cooling during the day it is essential to have a material that reflects almost all solar radiation in the visible range and, at the same time, is highly emissive in the atmospheric window<sup>23</sup>. Some materials that have been studied for passive cooling in daylight have complex structures, metamaterials<sup>6</sup>, photonic materials<sup>5</sup>, and to obtain them a complex chemical and physical processes are needed. On the other hand, we have wood that emits efficiently in the atmospheric window between 8 to 13 micrometers thanks to cellulose<sup>24</sup>. Therefore in this thesis project, we will perform different chemical treatments to delignify three different kinds of wood (*Eucalyptus globulus* (Eucalipto), *Guarea kunthiana* (Manzano Colorado), and *Dacryodes peruviana* (Copal)) and consequently bleached them in order for them to reflect sunlight in the visible range and concomitantly be emissive at the atmospheric infra-red window.

## 1.2 General and Specific Objectives

### 1.2.1 General Objectives

Design a passive cooling material based on wood present in Ecuador (*Eucalyptus globulus* (Eucalipto), *Guarea kunthiana* (Manzano Colorado), and *Dacryodes peruviana* (Copal)) and measure its passive cooling performance.

### 1.2.2 Specific Objectives

- To understand passive radiative cooling process by studying its physical meaning.
- To create the cooling material based on wood by removing Lignin.
- To develop data collecting equipment containing two insulated boxes and electronics to measure temperatures and net cooling power.
- To identify the best wood with possible cooling performance from the three measured.
- To understand, FTIR and XPS, the chemical changes done by the chemical treatment that lead us to the final material.
- To compare cooling power measured by the equipment with the expected model for the passive radiative cooling based on the emissivity of the samples and temperature measurements.



## Chapter 2

# Theoretical Framework

### 2.1 Thermal radiation

Electromagnetic radiation commonly present in our surroundings comprises, among many others, gamma rays, x rays, ultraviolet/visible/infrared radiation, and radio waves in order of their wavelengths. Matter in general by molecular and atomic agitation can emit electromagnetic radiation in various frequencies. Thermal radiation, commonly in the infrared range and visible light, is emitted by the agitation of matter according to their temperature<sup>25</sup>. Most of solar radiation that reaches our earth's surface is in the thermal radiation range. Electromagnetic radiation is classified by frequency and wavenumber. Then frequency  $\nu$  is defined as

$$\nu = \frac{c_o}{\lambda_{vac}} = \frac{c}{\lambda_{med}}, \quad (2.1)$$

where  $c_o$  is the speed of propagation in vacuum,  $c$  is the speed of light in the medium and  $\lambda$  is the wavelength. In vacuum,  $c_o$  is  $2.998 * 10^8 m/s$ , then the speed of the medium  $c$  is given by its index of refraction  $n$ :  $n = c_o/c$ .

Thermal radiation is in the wavelength range from  $0.2-1001 \mu m$ , while the visible spectrum comprises from  $0.39-0.77 \mu m$ , ultraviolet  $0.001-0.4 \mu m$ , infrared (ir): near ir  $0.77-25 \mu m$  and far ir  $25-1000 \mu m$ <sup>25</sup>. For passive radiative cooling applications, it is essential to understand the solar radiation arriving on the

Earth's surface. The concept of *Irradiance* indicates the rate of solar energy arriving at a surface per unit time per unit area. It refers to the rate of incident energy, and its units are  $\text{W m}^{-2}$ . *Irradiation* refers to the radiation arriving at the surface whether or not the origin of the radiation is the sun and its units are  $\text{kJ m}^{-2}$ . Solar energy is obviously the major contributor to most radiative heat transfer applications<sup>26</sup> when we don't have radiation sources based on the Earth, such as heat vents or, for example, volcanoes. In the following, we will survey a set of critical concepts to understand the passive cooling phenomenon.

### Blackbody model

A black body is considered an ideal surface that serves as a reference when the behavior of real surfaces is analyzed. A perfect Blackbody, at a given temperature absorbs radiation perfectly at all wavelengths and emits at all wavelengths in all directions<sup>25</sup>. If  $P_i(\mathbf{k}, \alpha)$  is the power incident on the blackbody in the  $\mathbf{k}$  direction and with polarization  $\alpha$  and  $P_e(-\mathbf{k}, \alpha)$  is the power emitted in the opposite direction by the Blackbody, then

$$P_e(-\mathbf{k}, \alpha) = a(\mathbf{k}, \alpha)P_i(\mathbf{k}, \alpha), \quad (2.2)$$

where  $a(\mathbf{k}, \alpha)$  is the fraction of power absorbed at  $(\mathbf{k}, \alpha)$ . For the ideal Blackbody  $a(\mathbf{k}, \alpha) = 1$ . In other words A Blackbody is an ideal material that absorbs and emits all frequencies<sup>27</sup> and it reflects no radiation at all.

### Planck's Law

The spectral distribution of the power emission for a Blackbody is described by<sup>28</sup>

$$I_{BB}(T, \lambda) = \frac{2h\nu^3}{nc^2} \frac{1}{\exp(h\nu/(k_B T)) - 1}, \quad (2.3)$$

also known as the spectral radiance emitted from a small hole in a 'box' in one unit of solid angle<sup>29</sup>. Here,  $\nu$  is the frequency,  $c$  the vacuum velocity for light,  $h$ , Planck's constant,  $k_B$  the Boltzmann constant,  $T$  the absolute temperature and  $n$  the refractive index of the medium (generally  $n=1$ ). The SI-dimension

of spectral radiance is  $W/m^2$ . Then the expression as a function of wavelength is obtained by replacing  $\lambda = c/\nu$ <sup>29</sup> and then:

$$I_{BB}(T, \lambda) = \frac{2hc^2}{n^2\lambda^5} \frac{1}{\exp(hc/(\lambda k_B T)) - 1}, \quad (2.4)$$

with dimension of  $W/m^3$ .

### Kirchoffs radiation law

All matter radiates when heated; then, the resulting spectral intensity depends on absorption coefficient, refractive index, and the superficial characteristics like geometry and surface roughness. For limiting conditions, relations of emissivity, apparent reflectivity, and apparent transmissivity can be expressed as<sup>30</sup>.

$$J(\lambda, T) = J_b(\lambda, T) * \frac{[1 - \mathcal{R}(\lambda, T)][1 - \mathcal{T}(\lambda, T)]}{1 - \mathcal{R}(\lambda, T)\mathcal{T}(\lambda, T)}, \quad (2.5)$$

where  $J(\lambda, T)$  is the emissivity power of the body at temperature  $T$  and wavelength  $\lambda$ ,  $J_b$  is the spectral emissivity power of an ideal Blackbody,  $\mathcal{R}$  is the reflectivity and  $\mathcal{T}$  the transmissivity of the body.

The emissivity, by definition, is the ratio of the actual emitted energy to that of a Blackbody  $J/J_b$ :

$$\varepsilon(\lambda, T) = \frac{J(\lambda, T)}{J_b(\lambda, T)}. \quad (2.6)$$

Therefore

$$\varepsilon(\lambda, T) = \frac{[1 - \mathcal{R}(\lambda, T)][1 - \mathcal{T}(\lambda, T)]}{1 - \mathcal{R}(\lambda, T)\mathcal{T}(\lambda, T)}. \quad (2.7)$$

Kirchoff's law outlines the equivalence between emission and absorption of a opaque body in thermal equilibrium. In the case of opaque bodies  $\mathcal{T} = 0$ <sup>31</sup>. Then

$$\varepsilon(\lambda, T) = 1 - \mathcal{R}(\lambda, T). \quad (2.8)$$

On the other hand for non reflective glasses or for luminous gas bodies with  $\mathcal{R} = 0$ <sup>31</sup>. As in our case where

we consider our reflectivity equal to zero<sup>22</sup>, the emissivity is

$$\varepsilon(\lambda, T) = 1 - \mathcal{T}(\lambda, T). \quad (2.9)$$

## 2.2 Atmospheric window

The atmosphere has its own mechanisms to cool itself when heated by dust and various greenhouse gases, including water vapor, CO<sub>2</sub>, and CH<sub>4</sub><sup>16</sup>. The atmospheric window is known as a part of the atmosphere electromagnetic spectrum in which the atmosphere is particularly transmissive<sup>17</sup> and thus, any emission from the surface in that frequency range leaves uncontested to outer space. This is a very efficient cooling mechanism for the Earth in the midst of global warming, regulating the Earth's temperature.

There are mainly three major atmospheric transmission windows: one in the near-infrared (NIR) 0.7–2.5  $\mu\text{m}$ , the other in the mid-infrared (MIR) 3–5  $\mu\text{m}$ , and the most important in far-infrared (FIR), 8–14  $\mu\text{m}$  (that can be observed in Fig. 2.1 ). At the same time, in the atmospheric window, energy absorption by water vapor and carbon dioxide is weak, so then photons scape more easily to space<sup>18</sup>. So some of the infrared radiation originating near the Earth's surface leaves the atmosphere through this window unimpeded. Finally, the emission to space can occur from the tops of clouds at different atmospheric levels and also by gases present in the atmosphere that absorb and emit infrared radiation. The majority of the atmosphere consists of nitrogen and oxygen, transparent to infrared radiation. On the other hand, water vapor, CO<sub>2</sub>, and some other minor gases present in the atmosphere, in much smaller quantities, can absorb some of the thermal radiation leaving the surface and reemit it from much higher and colder levels out to space<sup>32</sup>.

## 2.3 Passive Cooling Phenomenon

The earth has its main atmospheric transparency window between 8 and 13  $\mu\text{m}$  through which the earth can emit radiation to outer space, and that contributes to radiative cooling. But this mechanism is not



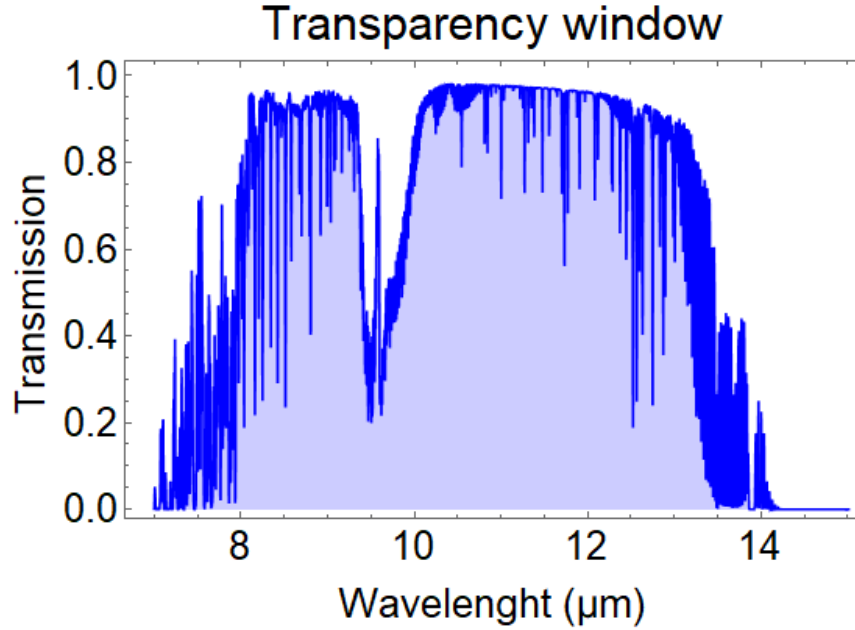


Figure 2.1: Here we depict the infrared spectrum of the atmospheric transmission above Mauna Kea, with air mass 1.5 and water column 1 mm. This represents an overview of the wavelength of 8-14  $\mu\text{m}$  which is the main atmospheric transparency window. The figure can be obtained from the data generated by ATRAN<sup>2</sup>, thanks to the Gemini Observatory. It is important to notice that transmission is dimensionless<sup>3</sup>

easy to take advantage of. It is more effective at night since, at day time, net cooling is difficult to achieve because of solar radiation absorption. At the same time, some lost cooling power is due to the wind by conduction and convection. Thus, it is essential to study all the physical factors that hinder the proposed cooling mechanism<sup>15</sup>.

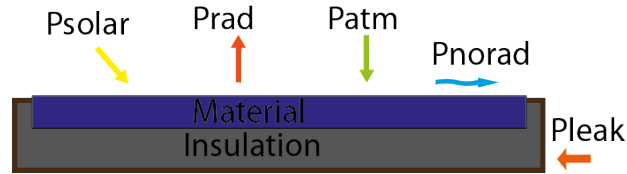


Figure 2.2: Here we depict the scheme for a passive radiative material and the factors that affect the net cooling power: the radiative cooling power  $P_{rad}$ , environmental thermal absorption  $P_{rad}$ , solar absorption  $P_{solar}$ , heat transferred as conduction or convection (nonradiative)  $P_{norad}$  and an extra term, the thermal leakage  $P_{leak}$ , when we are working with a thermally isolated measurement box.

We introduce the system to be studied in figure 2.2, where we illustrate the terms that are involved in the net radiative cooling power  $P_{rad}$ . When our material is facing a clear sky, we need to consider the radiative cooling power of the system  $P_{rad}$ , the environmental thermal absorption  $P_{atm}$ , the solar absorption  $P_{solar}$ , and the heat that is transferred from the ambient to the material either by conduction or convection (non-radiative heat loss)  $P_{norad}$ <sup>15,22,23</sup>. Also, an additional term needs to be considered when we are working in a thermally isolated measurement box, the thermal leakage  $P_{leak}$ . The  $P_{rad}$  is the outgoing heat flux that allows cooling. The remaining terms,  $P_{atm}, P_{solar}, P_{norad}, P_{leak}$ , work against the cooling<sup>23</sup>. Then the net cooling power  $P_{net}$  is

$$P_{net} = P_{rad} - P_{atm} - P_{solar} - P_{norad} - P_{leak}. \quad (2.10)$$

In order to understand how these terms are involved in the cooling performance of the system, we will review the meaning of each of the terms in the above relation.

### 2.3.1 Radiative cooling power of the system $P_{rad}$

The radiative cooling power is defined as the power of the material to emit thermal radiation to the sky in the transparency window (8-13  $\mu$  m). Thus the material losses heat and can be cooled. The equation expressing the cooling power is<sup>23</sup>:

$$P_{rad}(T) = \int d\Omega \cos(\theta) \int_0^\infty I_{BB}(T, \lambda) \xi_{film}(\lambda, \theta) d\lambda, \quad (2.11)$$

or doing the integration in the azimuthal angle

$$P_{rad}(T) = 2\pi \int_0^{\pi/2} \int_0^\infty I_{BB}(T, \lambda) \xi_{film}(\lambda, \theta) \sin(\theta) \cos(\theta) d\lambda d\theta \quad (2.12)$$

Where  $T$  is the surface temperature of the material,  $\lambda$  the wavelength and  $\theta$  the angle of incidence. As seen in the formula, it depends on the hemispherical spectral emissivity of the material at the average temperature  $T$ <sup>22,23</sup>. Here  $\xi_{film}(\lambda, \theta)$ , the spectral emissivity of the film<sup>22</sup>. It is the value defined in terms

of the absorptivity and is obtained from the Kirchoff's radiation law<sup>4</sup>. The factor  $I_{BB}(T, \lambda)$  is the spectral irradiance of the Blackbody at the surface defined by Planck's law, at temperature  $T$  (in this case, the surface temperature of the material) and a radiation wavelength  $\lambda$ <sup>22</sup> is defined as:

$$I_{BB}(T, \lambda) = \frac{2hc^2}{\lambda^5} \frac{1}{\exp(hc/(\lambda k_B T)) - 1}, \quad (2.13)$$

where  $h$  is the Planck's constant,  $k$  the Boltzmann constant and  $c$  the speed of light in vacuum<sup>15</sup>.

### 2.3.2 Environmental thermal absorption $P_{atm}$

$P_{atm}$  is the power absorb by the material from atmospheric irradiance at a temperature  $T_{amb}$ <sup>15</sup>, i.e. the power radiated downward from the atmosphere<sup>23</sup>. This term opposes the cooling the system and subtracts from the cooling power. It is defined then as

$$P_{atm}(T_{amb}) = \int d\Omega \cos(\theta) \int_0^\infty I_{BB}(T_{amb}, \lambda) \xi_{film}(\lambda, \theta) \xi_{atm}(\lambda, \theta, pw) d\lambda, \quad (2.14)$$

or

$$P_{atm}(T_{amb}) = 2\pi \int_0^{\pi/2} \int_0^\infty I_{BB}(T_{amb}, \lambda) \xi_{film}(\lambda, \theta) \xi_{atm}(\lambda, \theta, pw) \sin(\theta) \cos(\theta) d\lambda d\theta, \quad (2.15)$$

where  $\xi_{atm}(\lambda, \theta, pw)$  is the spectral dependent atmospheric emissivity. This factor should be calculated from the precipitable water (PW) content. The precipitable water represents the relative humidity (RH) and is the depth of water in a column if all the water vapor present in the atmosphere is precipitated as rain. The precipitable water is measured in millimeters. The emissivity of the atmospheric window is low but if PW is high, the emissivity increases hindering cooling<sup>22</sup>. The optical depth is the measure of how far light travel through a partially transparent medium before the light is scattered or absorbed<sup>33</sup>. If is assumed that the optical depth increases with the zenith angle  $\theta$  at a rate  $1/\cos(\theta)$ , then the spectral emissivity for any  $\theta$  is

$$\xi_{atm}(\theta, \lambda) = 1 - [1 - \xi_{atm}(0, \lambda)]^{1/\cos(\theta)}, \quad (2.16)$$

then  $\xi_{atm}(0, \lambda)$  is the spectral emissivity when  $\theta = 0$  (with the vertical direction)<sup>22</sup>.

### 2.3.3 Solar Absorption $P_{solar}$

Solar absorption is the result of the heating power due to the absorption of solar irradiance<sup>23</sup>. It reduces the cooling power depending on how much incident solar power is absorbed by the surface<sup>22</sup>. The formula that defines it is

$$P_{solar} = \cos\varphi \int_0^\infty \xi_{film}(\lambda, \varphi) I_{solar}(\lambda) d\lambda. \quad (2.17)$$

Here,  $I_{solar}(\lambda)$  is the solar spectral irradiance and  $\varphi$  is the angle between the normal to the module and solar irradiance. Here  $\xi_{film}(\lambda, \theta)$ , the spectral emissivity of the film<sup>22,23</sup>

### 2.3.4 Non radiative heat loss $P_{norad}$

At the same time, as the material starts to cool, heat can be transferred from the ambient surroundings to the material either by convection or conduction. This is the non-radiative heat loss convection heat flux ( $P_{conv}$ )<sup>23</sup> or conductive power ( $P_{cond}$ ) from the top of the surface of the material<sup>22</sup>. It can be computed following

$$P_{norad} = P_{conv} + P_{cond} = h_c(T_{amb} - T), \quad (2.18)$$

where  $h_c$  is the heat transfer coefficient<sup>15</sup>. If we consider convection and conduction we have  $h_c = h_{cond} + h_{conv}$ <sup>4</sup>. When we consider a steady-state flow over a flat surface with uniform surface heat flux, we can evaluate the convective heat transfer coefficient with a theoretical method or experimental methods.

$$P_{conv} = h_{air}(T_{amb} - T). \quad (2.19)$$

The theoretical method is based on dimensionless parameters and wind tunnel measurements. If we are outdoors, we notice that the wind direction speed changes constantly in time. Then in different studies<sup>34–36</sup>, it was suggested that the wind speed affects the heat transfer coefficient of the ambient air  $h_{air}$  over a flat

surface as<sup>22</sup>:

$$h_{air} = a + bV_{wind}. \quad (2.20)$$

Where a and b coefficients are obtained from the correlation of experimental data of heat transfer coefficient with the wind velocity. Thus, it is well-documented<sup>22,35,36</sup> that when we have a rectangular surface without a windshield, the heat transfer coefficient can be expressed approximately with the equation from bibliography :

$$h_{air} = 8.6(\pm 0.9) + 2.6(\pm 0.3)V_{wind} \quad (2.21)$$

With these phenomenological relations, we can determine the non-radiative heat loss contribution.

In general, to measure the cooling power, there is an additional term that should be taken in the count when we have a measurement box; it is the thermal leakage  $P_{leak}$  from the thermally insulated measurement box<sup>22,23</sup>.

### 2.3.5 Effect of tilt angle

If it is necessary to use a surface panel for the passive radiative cooling experiment, it is important to consider the tilt angle of the sample. The solar incidence on the panel surface is proportional to  $\cos(\theta_{solar} + \theta_{tilt})$  where  $\theta_{solar} + \theta_{tilt}$  is  $\varphi$ ,  $\theta_{solar}$  is the zenith angle and  $\theta_{tilt}$  tilt angle. Then, the tilt angle causes a reduction in the solar irradiance. The overestimation in cooling power due to the tilt angle needs to be added as an error of uncertainty. According a study of Aili *et al.*, the impact of  $\theta_{tilt} = 15^\circ$  on radiative cooling performance is almost negligible<sup>22</sup>.

## 2.4 Materials

With the passive radiative cooling method, one can exploit the transparency window and cool a body. This mechanism is broadly studied at night time. Nonetheless, it is more necessary in the daytime for useful applications. To obtain daytime cooling, the material needs not only to emit strongly in the atmospheric

transparency window. It also needs to be a broadband mirror for solar light. This is the opposite concept to a Blackbody in the optical range. The ideal radiative cooler should have a 0% solar absorption<sup>4</sup>. Some materials have been used to achieve these two main characteristics. In the next section, we will analyze some of them.

### 2.4.1 Photonic Materials

#### Ultrabroadband Photonic Structures To Achieve High-Performance Daytime Radiative Cooling

In this case Rephaeli *et al.* developed a metal-dielectric photonic structure with a net cooling power of  $100\text{W}/\text{m}^2$  at ambient temperature. They present a compact planar device that achieves radiative cooling in the daytime. The material consists of 2 thermally emitting photonic crystal layers comprised of *SiC* and quartz. They used those two materials with phononpolariton resonances in the  $8 - 13\ \mu\text{m}$  range, and quartz has a sharp resonance at  $9.3\ \mu\text{m}$  and *SiC* at  $12.5\ \mu\text{m}$ . So they complement the resonances and maximize the emission selectively in the atmospheric window at the same time that they minimize the absorption of visible light, making it so that the whole structure has a minimal amount of solar power absorption<sup>4</sup>. Reduction of the absorbed solar radiation was achieved by introducing a broadband solar reflector made of chirped 1D photonic crystals below the two layers photonic crystal of *SiC* and quartz. Then, the 1D photonic crystal consists of 3 sets of 5 bilayers of  $\text{TiO}_2$  and  $\text{MgF}_2$  with different thicknesses (to have three overlapping photonic bandgaps). The thickness of the first set of five bilayers is 25 nm of  $\text{TiO}_2$  and 35 nm of  $\text{MgF}_2$ , the second set 50 nm of  $\text{TiO}_2$  and 70 nm  $\text{MgF}_2$ , and the third set 75 nm of  $\text{TiO}_2$  and 105 nm of  $\text{MgF}_2$ . Then the 1D photonic crystal lay over a silver substrate<sup>4</sup>.

Then by coupling between material layers, they can control the emission, absorption, and reflection. By nanophotonic concepts, they can suppress solar absorption simultaneously as they enhance thermal emission in the atmospheric transparency window: an ultra-broadband performance<sup>4</sup>.

### Passive radiative cooling below ambient air temperature under direct sunlight

Other photonic materials can be fabricated. In a research performed by Raman *et al.*, they study the use of a photonic solar reflector and a thermal emitter that reflects 97 % of incident sunlight while emitting selectively in the atmospheric transparency window. When the material is exposed to direct sunlight exceeding  $850 \text{ W/m}^2$  on a rooftop, the photonic radiative cooler cools to  $4.9^\circ \text{C}$  below ambient air temperature and has a cooling power of  $40.1 \text{ W/m}^2$ <sup>5</sup>.

The photonic material they present consists first 200 nm silicon wafer over which a 200 nm silver is deposited. Above this base, the photonic radiative cooling has seven alternating layers of hafnium dioxide ( $\text{HfO}_2$ ) and silicon dioxide ( $\text{SiO}_2$ ) of varying thicknesses. The bottom four layers of  $\text{HfO}_2$  and  $\text{SiO}_2$  have thicknesses less than 100 nm and assist in optimizing solar reflection using periodic one-dimensional photonic crystals<sup>5</sup>.

$\text{HfO}_2$  serves as a high-index material that also presents low ultraviolet absorption, a useful feature when optimizing for solar reflectance, while  $\text{SiO}_2$  is optically transparent and is the low-index layer. They make an observation that the use of  $\text{HfO}_2$  is not essential, and can be replaced with titanium dioxide ( $\text{TiO}_2$ ), which is less expensive<sup>5</sup>.

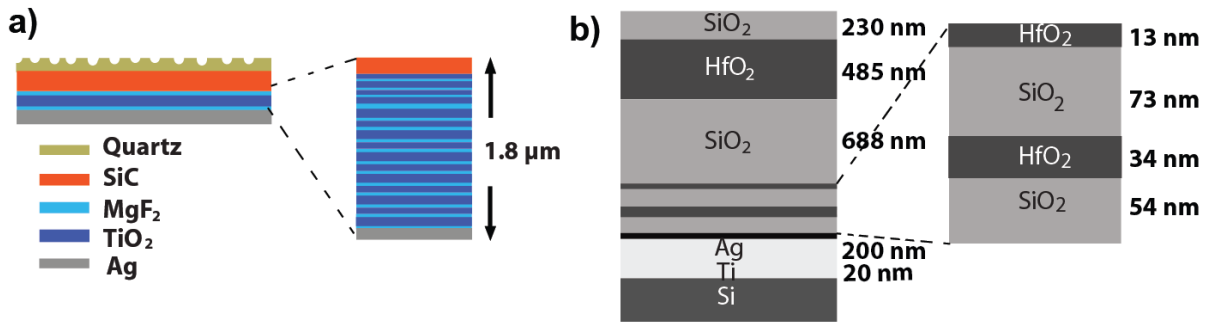


Figure 2.3: Scheme of different photonic materials for passive radiative cooling. a) metal-dielectric photonic structure<sup>4</sup> and b) photonic solar reflector and thermal emitter<sup>5</sup>. These figures are based on bibliography

### 2.4.2 Metamaterials

#### A metamaterial emitter for highly efficient radiative cooling

In the research from Hossain *et al.*, they propose an anisotropic material with an array of symmetrically shaped conical metamaterial (CMM) pillars. They obtained a near-unity absorption of unpolarized light. The CMM structure that they obtain has a radiative cooling power of  $116.6 \text{ W/m}^2$ <sup>6</sup>. They designed a meta dielectric conical metamaterial (CMM). First, a 5 nm thick chromium layer followed by a 150 nm thick aluminum layer was deposited on a bare silicon substrate. Over this, a  $3 \mu\text{m}$  thick PMMA polymer film was spin-coated. The general meta dielectric conical metamaterial (CMM) consists of 14 alternating layers of aluminum and germanium; between each, a 2 nm thick chromium layer is deposited as an adhesive layer. All of those layers are deposited on PMMA film. The thickness of the aluminum layer is 30 nm and of germanium 110 nm. The layers are circular and are symmetric along the vertical axis. The diameters of the layers increase from top to bottom, giving a structure with a conical shape<sup>6</sup>.

#### Scalable-manufactured randomized glass-polymer hybrid metamaterial for daytime radiative cooling

In a 2017 published study by Zhai *et al.*, they present resonant polar dielectric microspheres randomly distributed in a polymeric matrix, which results in a fully transparent metamaterial. They obtained an infrared emissivity greater than 0.93 across the atmospheric window when the material is backed with silver coating, and a noontime radiative cooling power of  $93 \text{ W/m}^2$  was achieved. Also, the material with  $50 \mu\text{m}$  thick reflects 96% of solar irradiance and has a  $110 \text{ W/m}^2$  cooling power at night<sup>7</sup>. The material consist in a polymer matrix of polymethylpentene (TPX) that encapsulates randomly silicon dioxide  $\text{SiO}_2$  microspheres. TPX has an excellent solar transmittance and along with the microspheres both are lossless in the solar spectrum direct solar irradiance, then the solar irradiance do not heat the metamaterial<sup>7</sup>.

### 2.4.3 Coatings

Another way to achieve passive radiative cooling is by coating existing materials.



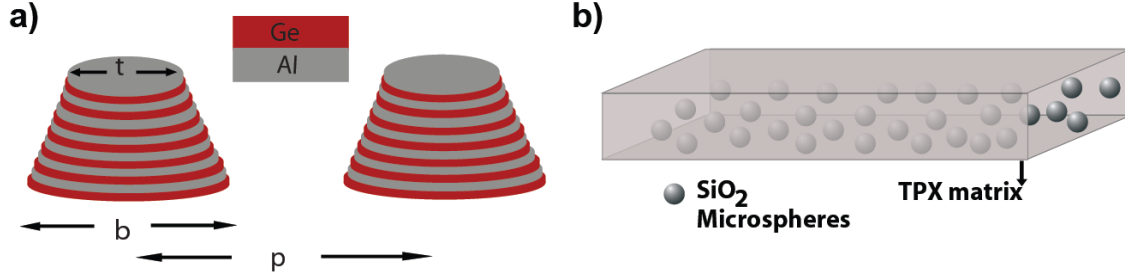


Figure 2.4: Scheme of the different metamaterials for passive radiative cooling. a) A symmetrically shaped conical metamaterial (CMM) pillars of Germanium (red) and Aluminium (gray)<sup>6</sup>. b) Resonant polar dielectric microspheres of  $SiO_2$  randomly oriented in a polymeric matrix<sup>7</sup>. These figures are inspired from bibliography

### Hierarchically porous polymer coatings for highly efficient passive daytime radiative cooling

In 2018, the research performed by Mandal *et al.* proposed a radiative cooling capable coating. They proposed a hierarchically porous poly(vinylidene fluoride-co-hexafluoropropene) (P(VdF-HFP)HP) coating. With this methodology, they obtained a high substrate-independent hemispherical solar reflectance of  $0.96 \pm 0.03$ , long-wave infrared emittances of  $0.97 \pm 0.02$ , which makes it ideal for a passive day radiative cooling. Finally, they achieved sub-ambient temperature drops of  $6^\circ\text{C}$  and cooling powers of  $96\text{ W/m}^2$  under solar intensities of 890 and  $750\text{ W/m}^2$  respectively<sup>8</sup>.

For the production of the material, they use a precursor solution of P(VdF-HFP) (polymer) and water (non-solvent) in acetone (solvent), and they apply the film onto a substrate and let it dry. As the acetone is very volatile, it rapidly evaporates, which causes the P(VdF-HFP) to phase-separate from the water, forming micro and nanodroplets. The P(VdF-HFP)HP coating is formed after the water evaporates. The material ideally has a coating of  $300\text{ }\mu\text{m}$ , and an approximant of 50% of porosity<sup>8</sup>.

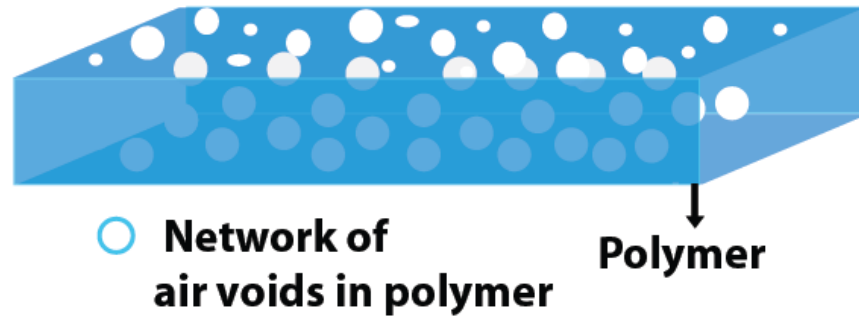


Figure 2.5: Scheme of the (P(VdF-HFP)HP) coating that created a network of air voids in polymer. This figure is inspired from paper Hierarchically porous polymer coatings for highly efficient passive daytime radiative cooling<sup>8</sup>

#### 2.4.4 Natural Materials

##### Wood

Similar to the previous materials, a composite from wood can have desirable behaviors for passive radiative cooling. As this project aims to study this material, we will be focused mostly on this application. Wood is mainly composed of amorphous lignin and hemicellulose, which are intertwined between the cellulose nanofibril<sup>9</sup>. The cell wall mainly consists of cellulose fibrils of 3-5 nm in diameter, lignin, pectin. One of the most important features of wood is its anisotropic structure since wood has aligned vertical channels. As is observable when you take a piece of wood, inside the wood, there exist aligned vertical channels. These are used to pump ions, water, and other nutrients needed for photosynthesis from the roots to the leaves.<sup>19</sup>. Inside the wood, cellulose and hemicellulose are linked by hydrogen bonds, and lignin and hemicellulose are joined by covalent linkage<sup>20</sup>. The structural components of cellulose is a linear homopolymer made up of D-anhydroglucose structural units linked by  $\beta$ -1,4 glycosidic bonds; hemicellulose is a heteropolysaccharides; finally, natural lignin is a tridimensional complex, amorphous polymer biologically synthesized mainly from phenolic structural units (p-hydroxyphenyl unit (H); guaiacyl

unit (G); and syringyl unit (S), respectively)<sup>37</sup>. Cellulose and hemicellulose are colorless, and the lignin complex structure has a dark color. Mesoporous structure in wood leads to large light scattering in the visible range making wood ideal for our purposes<sup>19</sup>.

Some studies have proposed a wood composite obtained from different chemical treatments<sup>9,19</sup>, the idea of this experimental procedure is to delignify the wood(remove the lignin). Some processes involve bleaching of wood<sup>9,20</sup>. Since natural wood is mostly uniform, bleaching wood can be highly effective<sup>20</sup>. The wood composite that we will study is sometimes named nanowood. The material obtained from the removal of hemicellulose and lignin leaves the cellulose nanofibril as the main backbone of the remaining structure. As cellulose will be the main component, we will briefly describe it<sup>9,20</sup>.

Cellulose consists of D-glucopyranose ring units in C1 chair configuration, the one that exhibits the lowest energy. Those units mentioned are linked then by  $\beta$ -1, 4-glycosidic bands, which results in an alternate turning of the cellulose chain axis by a  $180^\circ$ <sup>38</sup>. Then the repeating unit of cellulose is cellobiose with an approximated size of 1.3 nm it is observed in figure 2.6. Cellulose is formed by the repetition of cellobiose (n times). It has three reactive hydroxyl groups OH in each anhydroglucose unit (AGU) within the cellulose chain, primary at C6, secondary C2, and C3, which are in the plane of the ring. The next figure is a scheme of the cellulose structure<sup>38</sup>.

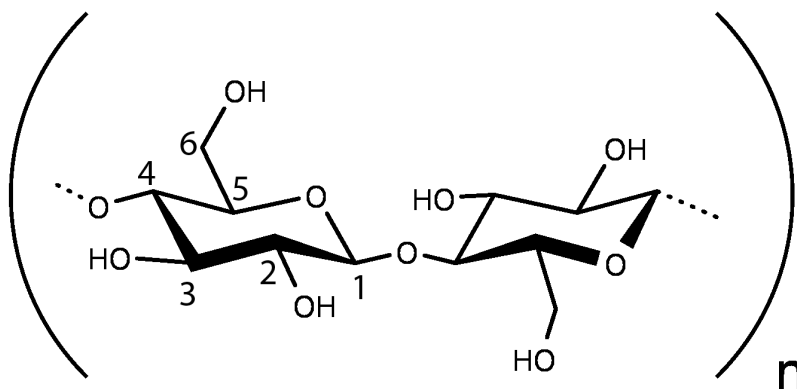


Figure 2.6: Monomer of cellulose structure, here one observes the three reactive hydroxil groups in the carbon C6, C2 and C3.

## 2.5 Nanowood

By removing lignin and hemicellulose we can increase the porosity of the wood<sup>21</sup>, resulting in a better nanofibril alignment of cellulose. After the chemical treatment, the cellulose aggregates in the cell wall layer. The resulting material is cellulose nanofibrils in the form of fibril aggregates named nanowood. Each cellulose nanofibril that constitutes the cell walls is packed and aligned parallel to each other and leads to a hierarchical alignment of nanowood<sup>9</sup>. Figure 2.6 shows the structure of nanowood. Finally, each fibril aggregate is composed of aligned crystalline cellulose packed with several tens of glucan chains in a crystalline order, held together by intermolecular hydrogen bonds and van der Waals forces. The material shows a lower density, high mechanical strength, and low emissivity, yielding a high efficiency in blocking thermal radiation from the sun. Among the benefits of the new material is its anisotropic thermal conductivity. That property allows heat to spread along the nanofibril direction, reducing the heat flow in a transverse direction<sup>9</sup>.

### Thermal properties

Natural wood is commonly used as a thermally insulating material. Nanowood preserves such superior insulating properties. Thermal conductivity of natural wood perpendicular and parallel to cellulose nanofiber alignment direction is 0.1 and 0.15 W/m·K, and the values for nanowood are 0.028 and 0.12 W/m·K. At the same time, when an incident laser heats the surface of wood or nanowood, heat is accumulated around the hot spot due to insufficient heat dissipation<sup>21</sup>. The temperature gradient is an elliptical shape around the heating spot due to anisotropy of the thermal conductivity in the transverse and axial direction<sup>9</sup>. Then, the maximum temperature achieved by nanowood is higher than that of the natural wood (approximately 3 °C), which suggests a better insulation property<sup>21</sup>.

The attained low thermal conductivity, especially along the radial direction, is due to the high porosity of nanowood. This is also enhanced by the nanowood having a lower density than natural wood. Nanowood exhibits anisotropic thermal conductivity with an anisotropy factor of 4.3. This anisotropy in thermal conductivity is mainly due to the anisotropic structure of the nanowood<sup>9</sup>. Under compression pressure,

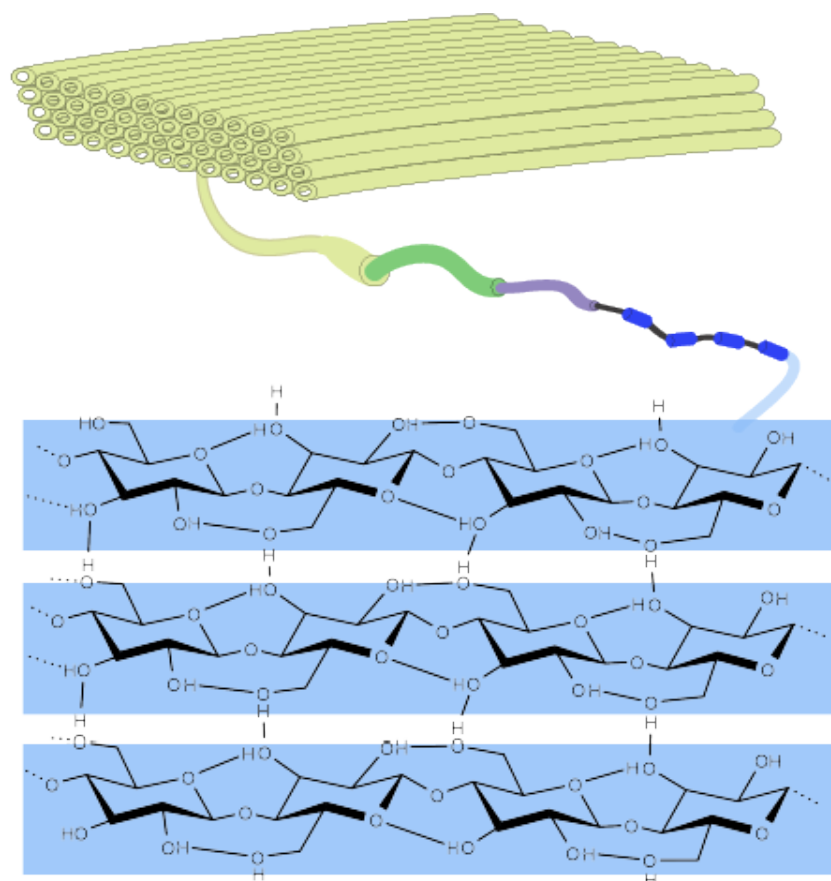


Figure 2.7: Graphical illustration of hierarchical alignment of nanowood structure at the top panel, at bottom panel, one can observe its cellulose chain, aligned to form fibril aggregate. Based on bibliography<sup>9</sup>

a slightly lower thermal conductivity is observed. Under compression, the air gaps between layers are minimized, then the contact between layers increases, leading to an overall reduction in thermal resistance<sup>21</sup>. The size of the porosity influences thermal conductivity. The larger the porosity, the smaller the thermal conductivity. Finally, most of the void channels in the nanowood are between 10-100  $\mu\text{m}$  in diameter, although the individual cellulose fibrils in the cell wall fibril aggregates exhibit an interfibril aggregate spacing in the nanometer range. Then, when the interspacing is smaller than the mean free path of air, thermal conduction through the air will be impeded. Nanosized pores can reduce the thermal

conductivity in axial and transverse direction<sup>9</sup>.

### 2.5.1 Improvements Nanowood material

After lignin removal and having obtained the nanowood structures, some changes can be made to the structure to improve performance. Here we discuss some of them.

#### Transparent wood

Another material studied is transparent wood. It has outstanding properties as optical transmittance and haze, strong durability, strong mechanical properties, and low thermal conductivity<sup>20</sup>. In general, transparent wood is obtained by performing two processes: 1) The delignification process or bleaching treatment, and 2) polymer infiltration along the lumina<sup>19</sup>. We can say that after obtaining the nanowood, they infiltrate its structure with a polymer. For the second process, epoxy resin can be used in a composition of 300 resin, and 21 non blushing cycloaliphatic hardener<sup>19</sup>, MMA impregnation and polymerization<sup>20</sup> among others.

In the transparent wood, polymers cross-link with the cellulose backbone after the removal of lignin, and it forms a 3D network, which leads to a higher mechanical strength compared to natural wood. The polymer fills the porous structure and leads to a high transmittance up to 44 %<sup>20</sup> or 90 %<sup>19</sup>. The results can vary due to the different cuts of the wood: cut along the growth direction and transverse to it. Transparent wood has anisotropic optical properties and mechanical properties. It also has higher strength and ductility (when it is cut along growth directions)<sup>9</sup>.

#### Hydrophobic structure

After the lignin removal, one can make a hydrophobic treatment to improve further its thermal characteristics. The process present by Hou *et al.* consists in creating a mixture of 95 weight % (wt%) ethanol, 2 wt% FAS ( perfluorodecyltrethoxysilane  $C_{16}H_{19}F_{17}O_3Si$ ) and 3 wt % Milli-Q water (pH adjusted at 5 with acetic acid). It will be used as a silane solution. The mixture is magnetically stirred for 24 hours for

silane hydrolysis. This material can be used as a membrane distillation since its high thermal conductivity along the fiber enables thermal dissipation along the axial direction and has an excellent intrinsic vapor permeability<sup>39</sup>.

### Wood carbon sponge

Another material of interest is known as wood carbon sponge (WCS) and can be obtained by the following procedure: After delignification, the material is stabilized in the air at 260°C for 6 h and then carbonized in Ar at 1000 °C for another 6 h. The lamella structure of nanowood does not change by carbonization step<sup>40</sup>. Then the WCS material has excellent mechanical compressibility. Also, it has a sensitive electrical conductivity change upon compression. These properties make this material ideal for highly sensitive strain sensors<sup>40</sup> apart to their thermal properties.

As observed in this section, some additions to the nanowood structure can be made to get materials for different applications. Since our primary goal is to achieve a passive radiative cooling material, functional day and night, we should get a material that reflects almost all solar visible light and has high emissivity in the atmospheric window<sup>1</sup>. For that, we aim to reduce some functional groups of lignin structure.

## 2.6 Ecuadorian Woods

Ecuador has one of the greatest diversity floristics worldwide. The flora is cataloged in 18,198 plant species. From those 4500 (25%) are endemic species<sup>41</sup>. Thus we will analyze three main kinds of wood found in Ecuador: *Guarea kunthiana* (Manzano Colorado), *Eucalyptus globulus* (Eucalipto), and *Dacryodes peruviana* (Copal).

### 2.6.1 *Guarea kunthiana* (Manzano Colorado)

*Guarea kunthiana* are species of the genus *Guarea* and family *Meliaceae*. It is native to the tropical rainforest of Ecuador and is known for its importance in the industry of construction<sup>42</sup>. In Ecuador it is a Native tree

of the Coast and Amazon and is present in the provinces from: Azuay, Bolívar, Carchi, Los Ríos, Napo, Pastaza, Morona Santiago, Zamora Chinchipe, Santo Domingo de los Tsachilas, Sucumbios. It is found between 0-1000 masl (meters above sea level)<sup>43,44</sup>.

The color of Manzano Colorado is wood pink (7.5YR 8/3) to very pale brown (10YR 8/3). This has no transition between sapwood and heartwood, non-smell neither taste. Colorado has undefined growth rings and diffuse porosity; its pores have not a defined pattern of arrangement, they can be: solitary, multiple 2-3 (-4-7) radials, and some clustered. *Guarea kunthiana* has 6 to 10 pores per mm<sup>2</sup>, and it has separate fibers. Its texture is medium, which means it is moderately hard and heavy, to hard and heavy, and it is medium luster. To work with wood is important to know the grain direction. Colorado is straight to crisscross grain. Straight means the grain runs parallel to the longitudinal axis of wood. Woods with straight grains are the easiest to work. On the other hand, cross-grain means that the grain deviates from the longitudinal axis<sup>45</sup>.

### 2.6.2 *Eucalyptus globulus* (Eucalipto)

The most frequently cultivated eucalyptus species is the *Eucalyptus globulus*. In Ecuador, *Eucalyptus globulus* is very important; however, it is an introduced species from Australia. The tree was introduced and cultivated from the Coast and Andes and is distributed from 0 to 4000 masl in the provinces of Chimborazo, Cotopaxi, Guayas, Imbabura, and Pichincha<sup>43,44</sup>. Eucalipto is a type of hardwood and is the most widely planted type of them. Eucalipto represents an important biomass source for the production of fuels, chemicals, and materials<sup>46</sup>. In general, Eucalipto has relatively high density, favorable chemical characteristics, low moisture content, and easy harvest. It has the ability to grow in localities where there are marked water shortages during substantial parts of the year<sup>37</sup>. Therefore, Eucalipto wood is used for construction like posts, piers, deck support, roofs, and struts; and even the branches are used as fuel. The flowers are melliferous, and the leaves are used medicinally to cure various conditions<sup>44</sup>. Its wood has a high value; it serves as a source of wood and paper and, for the manufacture of furniture for veneer boards<sup>47</sup>. The main components of Eucalipto wood are cellulose, hemicellulose, lignin, and some extractives. The



cellulose content of Eucalipto wood is comparatively high, making the pulp and paper industry one of its conventional users. From the pulp produced worldwide, about 50% comes from hardwoods, and half of this amount is made from Eucalipto. In the case of Eucalipto wood Hemicelluloses, heteropolysaccharides are largely dominated by acetylated glucuronoxylan<sup>37</sup>.

### 2.6.3 *Dacryodes peruviana* (Copal)

*Dacryodes peruviana* is a tree of the burseráceas family known as Copal. It grows in the humid forests of Colombia, Peru, and Ecuador<sup>43</sup>. In Ecuador, it is an Andean and Amazon native tree; it exists in the provinces: Morona, Napo, Pastaza, Zamora Chinchipe and can be found between 0-1500 masl<sup>43</sup>. Its trees are up to 20 m. It is straight and has a cylindrical shaft. Its color is Pale brown 2.5Y 8/4. Generally, this wood is used for the manufacture of furniture and in civil construction as formwork. Wood density is 0.61 gr/cm<sup>3</sup><sup>41</sup> The wood is used for the construction of houses of the local populations and also commercialized; the color of the sapwood is greyish white, and the heartwood is creamy white or pinkish white. The resin is used as a glue, aromatic, and fuel to light bonfires.<sup>48</sup> In the External bark is identified light brown lenticels, circular lenticels, about 3-5 mm in diameter, regularly distributed and little protruding. The internal bark of the tree is homogeneous, with whitish-pink color and a strong and resinous smell, similar to that of incense or turpentine. After the cut of Eucalipto, it exudes a translucent, oily resin with the strong odor described<sup>49</sup>.

## 2.7 Characterization of Materials

### 2.7.1 Fourier transform infrared spectroscopy (FTIR)

Fourier transform infrared spectroscopy is used to obtain an infrared spectrum of absorption or emission of a solid, liquid, and gas<sup>50</sup>. Commonly, FTIR spectrometer is composed of a source, sample cell, detector, amplifier, A/D converter, and a computer. In summary, radiation from the source reaches the sample, then its emission passes through the interferometer and finally reaches the detector. Then, the signal obtained

is amplified and converted to a digital signal by the A/D converter and amplifier. Finally, the signal is transferred to the computer where FTIR gets the actual spectrum by translating the raw data (interferogram) using the Fourier transform<sup>51,52</sup>. The infrared radiation of about 10,000–100  $\text{cm}^{-1}$  is sent through the sample where part of the radiation is absorbed and some passes through. The radiation absorbed is converted to vibrational or rotational energy by the sample. The resultant signal that we can commonly obtain at the detector is a spectrum generally from 4000 to 400  $\text{cm}^{-1}$ , which represents the samples' molecular fingerprint<sup>51</sup>. Typical FTIR resolution is 4  $\text{cm}^{-1}$ .<sup>50</sup> FTIR analysis is commonly used to identify organic, inorganic, and polymeric materials by using infrared light for scanning the samples. If some alterations in the characteristic pattern of absorption bands are observed, it indicates a change in the material composition. Therefore, FTIR is a useful technique for identifying and characterizing unknown materials, detecting contaminants, finding additives, and identifying decomposition and oxidation. Thanks to every molecule have a unique fingerprint, which makes FTIR an invaluable tool for chemical identification<sup>51</sup>.

As mentioned before Wood cell wall is mainly composed by cellulose, hemicellulose, and lignin. Then in an FTIR spectrum of wood, there are contributions from these components: mainly O-H stretching and C-H absorption bands. Then it follows that the fingerprint region is from 2000-600  $\text{cm}^{-1}$  where functional groups, in this part, are used to distinguish differences<sup>53</sup> from one wood to another, and in our case can serve to identify differences from non-treated wood to treated wood. In Table 2.1, we report a recompilation of the main peaks of the FTIR spectrum from wood for lignin, hemicellulose, and cellulose itself. It is important to understand the contributions of different functional groups in order to define which peaks we want to remove and which ones we want to enhance for having a passive radiative cooling performance.

FTIR performed on the nanowood, shows that peak in 1730  $\text{cm}^{-1}$  attributed to acetyl groups in hemicellulose weakened or disappeared<sup>20,21</sup>, in the 1593 and 1505  $\text{cm}^{-1}$  (indicative of aromatic skeleton) peaks disappear, indicating removal of lignin<sup>21</sup>, at 1370  $\text{cm}^{-1}$  the peak becomes smaller<sup>20</sup>, and 1235  $\text{cm}^{-1}$  (C-O stretching) the peak is reduced due to hemicellulose removal<sup>20,21</sup>. The peak at nearly 1000<sup>23</sup> is

Wavenumber ( $\text{cm}^{-1}$ )	Functional Groups	Compounds	R
*3000-3600 (s)	O-H stretching	Acid, methanol	20,53,54
*2860-2970 (m)	C-H stretch	Alkyl, aliphatic and aromatic	20 53 54
1700-1736 (m)	C=O stretch hemicellulose	Ketone and carbonyl	20,21,54
1590-1593 (m)	C=C stretching vibration	Lignin	20,21
1500-1505 (m)	C=C stretching vibration	Lignin	20,21
1370 (w)	C-H deformation vibration	Cellulose and hemicellulose	20
*1235-1240 (s)	C-O stretching	Lignin and hemicellulose	20,21
*1170,1082 (s)	C-O-C stretching vibration	Pyranose ring skeletal	54
* 1108 (m)	O-H association	C-OH	54
*1060 (w)	C-O stretching and C-O deformation	Ethanol C-OH	54
*700-900 (m)	C-H	Aromatic hydrogen	54
*700-400 (w)	C-C stretching		54

Table 2.1: FTIR peaks for wood and its main components: cellulose, hemicellulose and lignin, the \* refers to the peaks in the atmospheric window, the peaks intensity are denoted by (s) strong, (m) medium and (w) weak.

the highest peak in the FTIR absorbance spectrum of nanowood or cellulose, which is in the range in the atmospheric window. Then this composite is ideal for the implementation of passive radiative cooling<sup>9</sup>. This material can be used for high-scale production since the processing procedure is simple, low cost, and more environmentally friendly. It was confirmed by Li *et al.*<sup>23</sup>. In their project, they obtained nanowood material from basswood and studied its passive radiative cooling. During the night, they obtained an average cooling power of  $101 \text{ Wm}^{-2}$  and during the day of  $37 \text{ Wm}^{-2}$ .

### 2.7.2 X-ray photoelectron spectroscopy (XPS)

X-ray photoelectron spectroscopy (XPS) is by far the most commonly used technique in areas of materials science, chemistry, and chemical engineering to assess surface chemistry, bonding structure, and composition of surfaces and interfaces. XPS is nowadays a well-established characterization technique based on the photoelectric effect evidenced by Hertz in 1887<sup>55</sup>. The XPS technique indirectly calculates the binding energy (BE) of photoelectrons via the measurement of their kinetic energy (KE) using an electrostatic analyzer. The strength of the XPS technique relies on that an atom's chemical environment has a pronounced effect on the assessed binding energies (BEs) of core-level electrons, the effect commonly referred to as the chemical shift. First, XPS allows the assessment of the chemical composition of the sample. All chemical elements except hydrogen and helium can be probed. The atomic concentration for each element is calculated using the corresponding photoelectric cross-section which depends on the original electronic state of the photoelectron and the incident photon energy<sup>55</sup>. For an element, the BE of a given electronic state will also vary from this element's binding state. The measurement of these chemical shifts is immensely helpful to identify the binding states of elements. The information about existing bonds is typically extracted by comparing measured BE values to literature databases<sup>55-57</sup>.

When XPS is performed in wood samples, the most predominant peaks identified are C-C/C-H (C1), C-O (C2), C=O/C-O-C (C3), and O-C=O (C4). C-C comes mainly from aliphatic and aromatic carbons of lignin and extractives, and C-H mainly from cellulose. The peak of C-O carbon bonded to oxygen comes from carbohydrates and lignin constituents, but mainly from cellulose and hemicelluloses<sup>58</sup>. In cellulose structure, this is the most abundant bond. The peak related to C=O carbon bonded to carbonyl or C-O-C, two noncarbonyl oxygen atoms also come mainly from cellulose and hemicellulose. In the same way, O-C=O carbon bonded to carbonyl and non-carbonyl oxygen atom is related to hemicellulose and extracts<sup>59</sup>. It is important to highlight that cellulose can have contamination in the oxygen region due to adsorption of water since cellulose is hydrophilic<sup>58,59</sup>.

In a study of the delignification of poplar wood with lactic acid-based deep eutectic solvents<sup>24</sup>, they measure a XPS before and after the delignification process. They obtained that lignin has more

C1 contribution than cellulose and hemicellulose. Therefore an decrease of the relative peak area was observed after the delignification process. Also in that research C2 and C3 peaks have more contribution from polysaccharose. Then after the delignification an increase of C3 was observed but for C2 and C4, the changes were not significant<sup>24</sup>.



## Chapter 3

# Methodology

This chapter presents the methodology to design the cooling materials, characterize them and measure their cooling performance. In order to concoct our passive cooling material from wood, we will first delignify the wood by chemical treatment as thoroughly as possible. Then the materials will be characterized by FTIR and XPS. In order to test the performance of the materials, we built an insulating box and a controlling device to measure the box temperatures at different points, the ambient temperature, and the cooling power of the cooling wood. Finally, the cooling performance expected will be calculated based on the emissivity and the temperatures obtained.

The woods used for this thesis were obtained locally at Ibarra and Urcuquí. The chemical treatment was done in the laboratory of the School of Physical Sciences and Nanotechnology of the Yachay Tech University. The characterization of the materials was done in the laboratory facilities of Yachay Tech University.

### 3.1 Delignification Process

For the delignification process, we tested three different treatments: with sodium hydroxide (NaOH)/sodium sulfite ( $\text{Na}_2\text{SO}_3$ ) and hydrogen peroxide ( $\text{H}_2\text{O}_2$ ), with sodium hypochlorite NaClO with acetic acid

and with sodium chlorite ( $\text{NaClO}_2$ ). For the three procedures, the samples were cut in the wood growth direction, obtaining samples of  $2\text{ cm} \times 2\text{ cm} \times 0.5\text{ cm}$ . The selected wood species were *Eucalyptus globulus* (Eucalipto), *Guarea kunthiana* (Manzano Colorado/Colorado), and *Dacryodes peruviana* (Copal).

### 3.1.1 Delignification by $\text{NaOH}$ and $\text{Na}_2\text{SO}_3$

In the figure 3.1 is shown the samples before the delignification process and after it. The samples were treated first with sodium hydroxide  $\text{NaOH}$  (2.5 M) and sodium sulfite  $\text{Na}_2\text{SO}_3$  (0.4 M) dissolved in distilled water and kept boiling for approximately 12 hours. After this process, the samples were rinsed in hot distilled water three times. The samples from the first part were then treated with hydrogen peroxide  $\text{H}_2\text{O}_2$  (2.5 M, 50 % solution) to remove the lignin and most of the hemicellulose. We kept boiling without stirring until the sample's yellow color disappeared (10 h approximately). Then the samples were removed from the solution for rinsed with cold water. The samples were preserved in ethanol until some were dried in a small vacuum and others in a freeze drier to preserve the nanoporous structure. The experiment procedure is an adaptation of previous bibliography<sup>9,19</sup>. The samples taken in this section were measured by FTIR and XPS.

The chemical process involved in the chemical treatment with sodium hydroxide with sodium sulfite followed by the treatment with hydrogen peroxide is proposed in the figure 3.2. There is observed the G unit of lignin to visualize the chemical process. In the first part of the treatment figure 3.2 A with  $\text{NaOH}$  and  $\text{Na}_2\text{SO}_3$  of the wood, lignin suffers from sulfonation. This sulfonation was done by substituting the sulfonate group with aliphatic hydroxy groups of lignin. This leaves the lignin negatively charged<sup>60</sup>. Similarly, methyl groups could be removed (demethylation). The  $\text{CH}_3$  groups will be removed by a nucleophilic substitution reaction, then it leads to lower methyl groups and then a higher content of phenolic groups<sup>61</sup>. Both processes could happen, and then after this chemical treatment, the solution where the wood samples were embedded ended with a purple-brown color. After this part, lignin will be more soluble and will be diluted. Then with the washes we will lost the part of lignin that suffered sulfonation. Then the remaining for the next part of the delignification is the lignin part that was just demethylated. In the figure 3.2 B



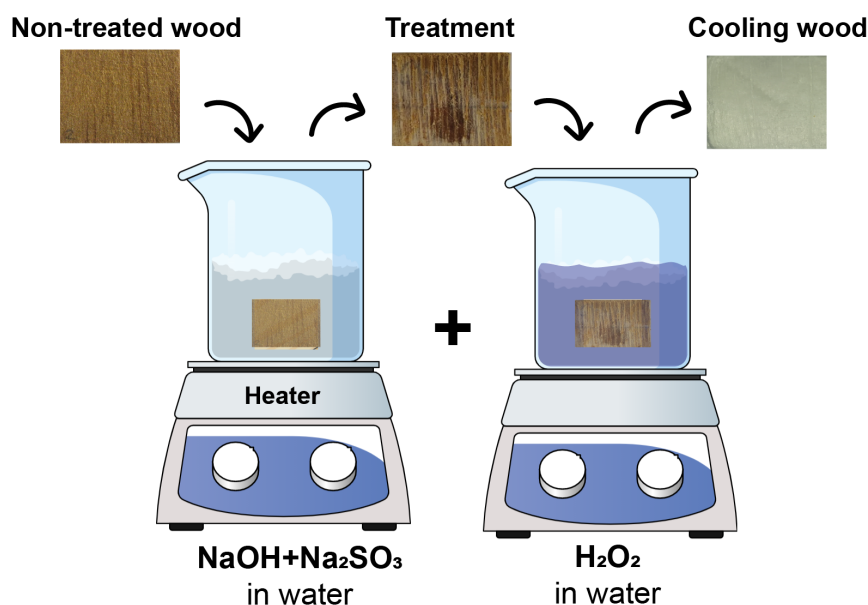


Figure 3.1: Graphical illustration of experimental scheme of chemical treatment with NaOH (2.5 M)/Na<sub>2</sub>SO<sub>3</sub> (0.4M) and H<sub>2</sub>O<sub>2</sub> (2.5 M, 50 % solution) .

is observed the chemical process after the hydrogen peroxide treatment. Hydrogen peroxide can help to oxidize the lignin by introducing carboxylate groups. In some bibliography<sup>60,62</sup>, it was stated that hydrogen peroxide acts on lignin by decomposing phenolate groups while creating carboxylate groups into lignin. Most of the hydrogen peroxide decomposes the lignin structure by cleavage the lignin ether bonds. Then, two reactions can occur for lignin oxidation. First, There is a nucleophilic attack to the hydroxyl anions that removes lignin chromophores. At the same time, the remaining radical species by the decomposition of hydrogen peroxide produces the oxidative degradation of the phenolic structures of lignin. Those can be converted to carboxylic acid groups. Second, perhydroxyl anion attacks the side chains of lignin that allow the opening of the benzene ring and the production of new compounds with carboxylate or chromophore groups. Using severe conditions, there would be further degradation of the ring by cleavage, giving us compounds with low molecular weight like oxalic acid, malonic acid, and formic acid. This oxidation promotes the solubility of lignin thanks to the increased carboxylate groups making it easy to remove most of the lignin from the wood samples<sup>60,62</sup>.

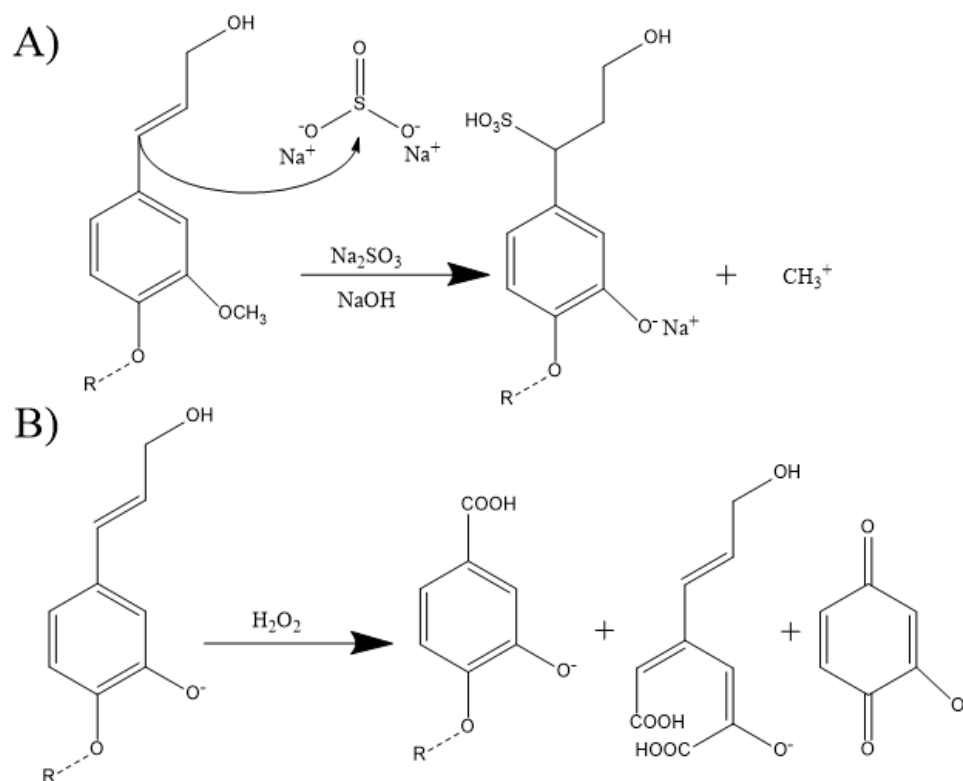


Figure 3.2: Possible mechanism of delignification using firstly A)  $NaOH$ ,  $Na_2SO_3$  and B)  $H_2O_2$ .

### 3.1.2 Delignification by $NaClO$

The wood samples were put in 5%  $NaClO$  solution for 72 h, and the delignification process proceeded at room temperature. Then, the wood samples were washed using 50% ethanol solution several times to remove the residual  $NaClO$  solution. The experiment procedure was based on previous bibliography<sup>63</sup>.  $NaClO$  breaks the chromophores of lignin by its oxidation effect. In the figure 3.3 is observed the possible result of the reaction of  $NaClO$  with lignin. As a possible mechanism of the delignification, benzene rings will be disrupted, then the content of carboxyl will increase. First, the  $ClO^-$  ions will be hydrolyzed into  $HClO$  in water. There oxygen atom is negatively charged, and chlorine is positively charged. Then it can attack ortho positions of the  $-OR$  groups of lignin. Then, chlorination products of lignin can be formed

while  $H^+$  ions are eliminated from the intermediate, and the molecular weight of lignin will increase. Then the reaction will affect ether bonds. The phenolic-oxygen-methyl bonds will form phenolic hydroxyl and methanol after those bonds break. In this way, the molecular weight of lignin will break, and then it can provoke the cleavage of the chain of lignin, so phenolic-oxygen-R bonds also may break up and forming phenolic hydroxyl groups the fragments of lignin will be ROH, where R is the rest of lignin or H of the guaiacyl unit. If the reactions continue, the remains can react with more NaClO that can results in an o-benzenediol structure, decreasing more lignin molecular weight<sup>64</sup>.

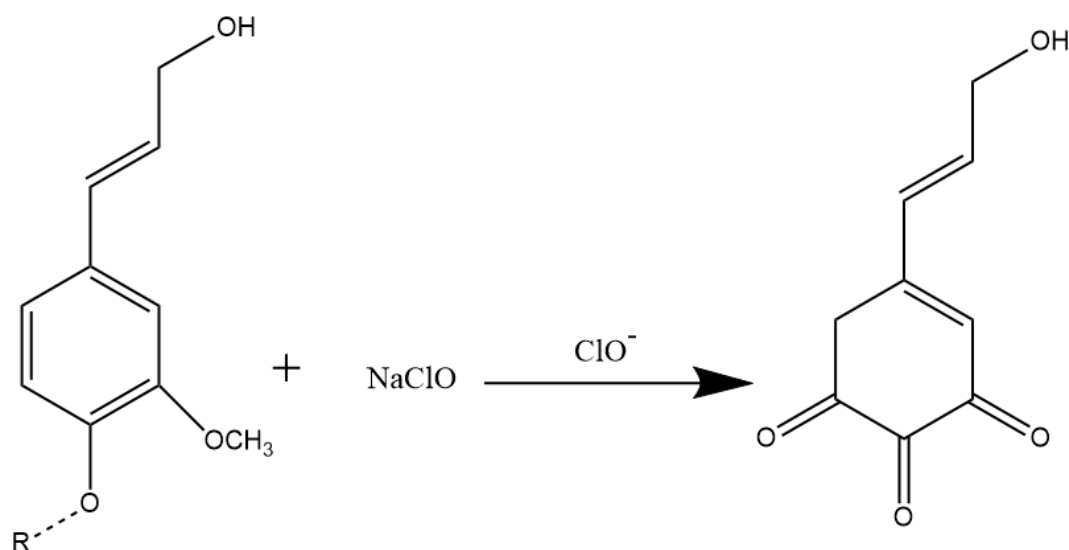


Figure 3.3: Possible mechanism of delignification using NaClO

### 3.1.3 Delignification by $NaClO_2$

The bleaching solution was performed by obtaining a 5%  $NaClO_2$  solution in distilled water, with the pH value adjusted to about 4.6 by adding acetic acid in the  $NaClO_2$  solution. The samples were immersed in boiling  $NaClO_2$  solution until the samples lost most of their dark coloring (about 2 hours of bleaching). Then, the samples were washed using 50% ethanol solution several times to remove any residual chemicals. The experiment procedure was based on previous bibliography<sup>63</sup>.

In this delignification process, some processes could happen as it is observed in figure 3.4. The aromatic structure of lignin will suffer an oxidative reaction that will open the ring to form acidic groups<sup>62</sup>. It will make the lignin more soluble in water. Three different paths could happen to lignin after  $\text{NaClO}_2$  treatment and are observed in the figure<sup>62</sup>. There we use the G unit of lignin as a sample. First, it can produce a quinone (it can be para and ortho). Second, it can create a muconic acid ester, and third a reactive intermediate. It can variate regarding the type of lignin. The third part can serve as an intermediate, and lignin can be degraded beyond the level of quinones and muconic acids<sup>10</sup>.

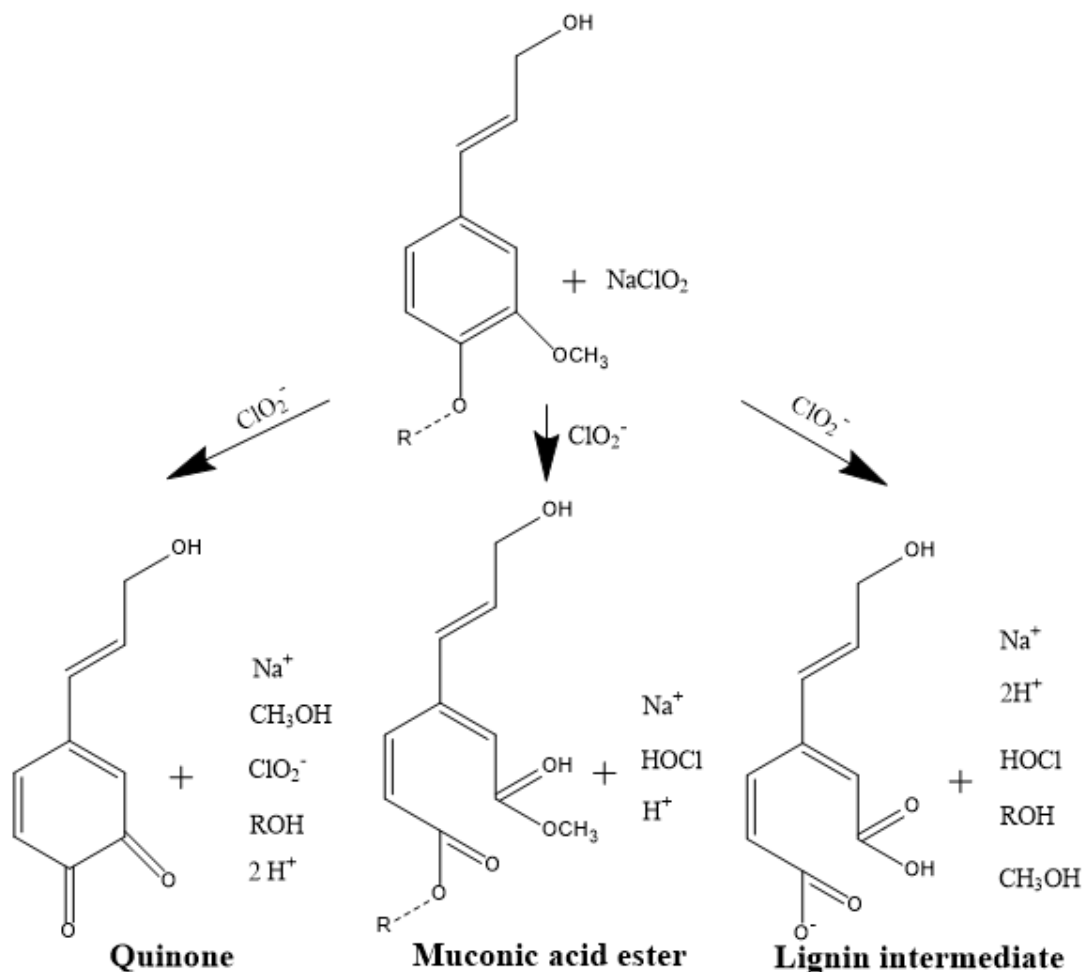


Figure 3.4: Possible mechanisms of delignification using  $\text{NaClO}_2$  adapted from<sup>10</sup>

### 3.2 Characterization using FTIR

We measured the transmittance of materials: untreated wood, wood after NaOH/Na<sub>2</sub>SO<sub>3</sub> treatment, and wood after H<sub>2</sub>O<sub>2</sub> treatment. FTIR spectra were measured by direct transmittance using a Cary 630 FTIR (Fourier transform infrared) Spectrometer with ATR (attenuated total reflectance ) accessory from the School of Biological Sciences and Engineering at Yachay Tech University. Spectral data were collected between 400-4,000 cm<sup>-1</sup> at a resolution of 4 cm<sup>-1</sup>. The materials were cut at 1 mm of width to be measured.

### 3.3 Characterization using XPS

We used XPS (X-ray photoemission spectroscopy) to identify the surface chemical composition of the materials by studying its binding energies obtained from the XPS spectra. We studied three wood types: untreated wood, wood after NaOH/Na<sub>2</sub>SO<sub>3</sub> treatment, and finally, after the full treatment adding H<sub>2</sub>O<sub>2</sub> (cooling wood material). The XPS measurements were performed in a VERSAPROBE PHI 5000 from Physical Electronics at Yachay Tech University. The equipment has a monochromatic source of aluminum K $\alpha$  for the X-ray source. The analyzer angle with respect to the sample's surface was about 90° for maximum penetration of the beam (about 7 nm approximately). The spot size used during the experiment was 100  $\mu$ m. The pass energy for the survey was 250 eV, for the individual core level region was 55 eV, and the energy resolution is about 0.5 eV. In the XPS equipment, an electrostatic field within the hemispherical analyzer only permits electrons of a given energy, the pass energy, to arrive at the detector. Pass energy is then the energy of the electron traveling from the analyzer entrance to the exit slit along the equipotential plane of the XPS<sup>65</sup>. Finally, we used an electron gun and an argon ion gun for charge neutralization. Charge neutralization is necessary to avoid sample charging during data acquisition that could distort the photoelectron lines, resulting in shifts of the binding energies<sup>66</sup>.

### 3.4 Cooling performance

#### Measurement of temperature and cooling power

Since radiative cooling measurements during the day are difficult because of fluctuating conditions, we designed equipment that minimized heat load on the cooling material to observe below ambient temperatures. The equipment with the sample is designed to be under direct sunlight, and to reduce the material's convection and conduction. The equipment is observed in figure 3.5 and a scheme is observed in figure 3.7 with the internal structure of the box in figure 3.6.

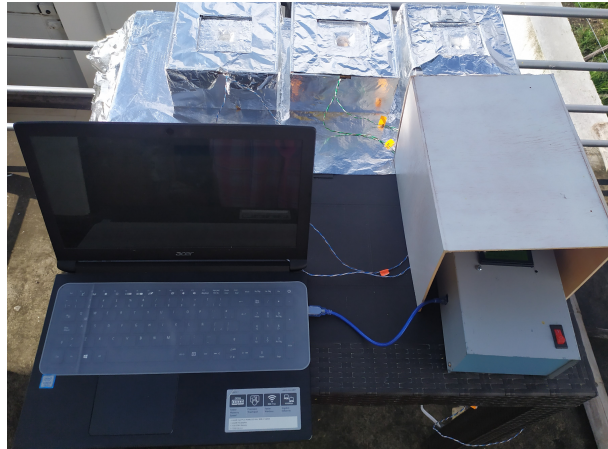


Figure 3.5: Equipment for the measurement of temperature differences and cooling power.

The measurement setup consists of a wooden box with all edges sealed. Inside it, polystyrene foam serves as an insulator to minimize conductive and convective losses. In order to monitor the temperature distribution in the box, temperature sensors are placed within the polystyrene foam in reference locations. The sample is placed in an exposed opening at the top of the wooden box, which is covered to reduce convective effects with a polyethylene film that serves as an infrared-transparent windshield. The hole structure allows having an air pocket between the sample and the polyethylene film. The structure of the boxes is observed in the diagram in figure 3.6. The cooling wood sample box has a heater and copper film attached to it, similar to the sample size, to deliver heat to it in a uniform manner. The role of the heater

is to monitor the amount of heat that must be delivered to the cooling wood to offset its lower temperature and thus measure its cooling power per unit area. This box is labeled *box 1*. Simultaneously, we designed another similar box to measure the temperature of the untreated wood or of another cooling material, but without the heater; this box is named *box 2*. Depending on what we want to measure, we place the cooling material or untreated wood in this box.

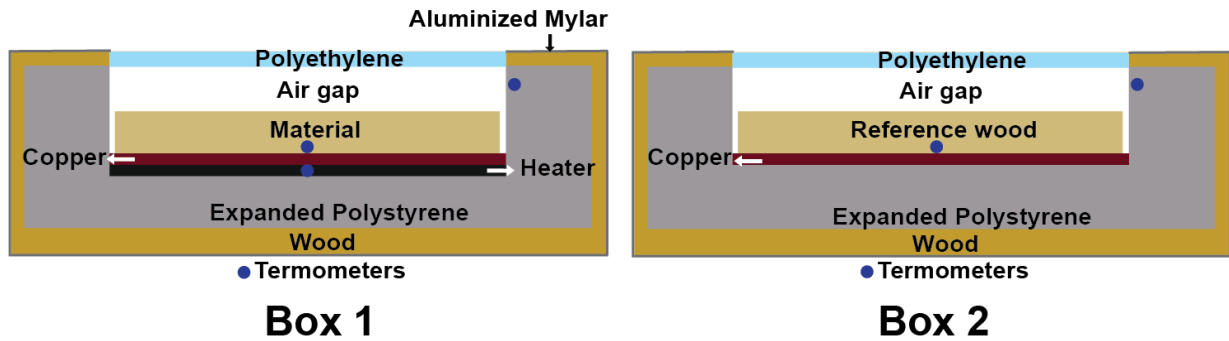


Figure 3.6: Graphical illustration of experimental setup for the measurement of temperatures and cooling power.

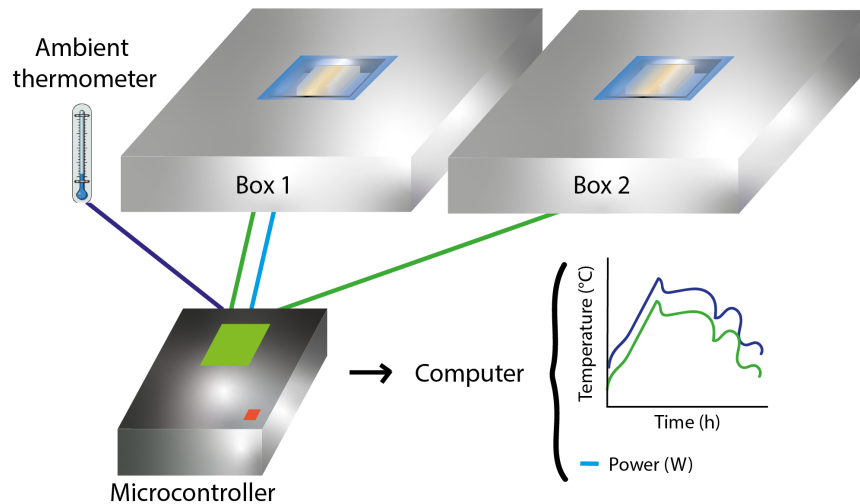


Figure 3.7: Graphical illustration of experimental setup for the measure of temperatures and cooling power.

In this work, we measured the non-treated wood, cooling wood, and ambient temperature comparing

with each other. We measured in the first-day Colorado cooling wood in box 1 with the heater on and Colorado cooling wood in box 2 without heater. We also measured the second-day Copal cooling wood in box 1 with the heater on and Copal cooling wood in box 2 without the heater. Finally, on the third day, we measure Eucalipto cooling wood in box 1 with the heater and Eucalipto cooling wood in box 2 without heater. Each day, the samples were measured in the morning, the box closed, and in the afternoon with the open box. Results of the closed box are added to the annex.

A reference thermometer measures the ambient temperature in free air in shadow conditions. Other temperature measurements were performed on the cooling wood in box 1, and another thermometer measures the heater's temperature. Extra thermometers were added as a control to measure the temperature inside each box and some other measure the ambient temperature. All thermometers were connected to the equipment box controlled by an Arduino microcontroller. The circuit was done thanks to Professor Werner Escamilla, Ph.D. The microcontroller transfers the data measured (temperatures, time, and power) to the computer. Additionally, Arduino has a temperature feedback control; when the temperature of the cooling wood material (in box 1 with the heater) is below ambient temperature, the heater turns on. It heats the sample until it is at ambient temperature, and it reads the power of the heater in Watts with an error of  $\pm 0.002$ . This is directly the *cooling power* of the cooling wood. The Arduino code can be found in the appendix. The average cooling power is obtained by dividing the average power (area under the curve) of the heater by the surface of the sample ( $0.0002 \pm 0.00003 \text{ m}^2$  Colorado area and  $0.0004 \pm 0.00004 \text{ m}^2$  Eucalipto and Copal area). To assure the thermometers' correct performance within the error expected, we monitored their readings under the same conditions by placing them in close contact. The thermometers have an expected error of  $\pm 0.2 \text{ }^\circ\text{C}$ . Figure 3.5 shows the full setup of the equipment used.

### Calculation of expected cooling performance

We measured the expected cooling power at day using the temperatures we obtained for the ambient and the material in the previously part, and the emissivity in the range of 8 to 13 micrometers obtained from the FTIR measurements. For the emissivity, we calculate the area under the curve of the transmission



spectrum of FTIR, and, considering no reflectance of the material in that range, we obtain the emissivity by subtracting by one. We are aware that this FTIR is more a qualitative measure, and we can not trust the intensity found on the spectrum. Nonetheless, as being the first time to develop a thesis project related to this area, and due to the situation, we use the available equipment at YachayTech University. Thus, we use FTIR spectrum results to identify emissivity. The equations used to measure the net cooling power expected were explained in Chapter 2, and the calculation was done in Mathematica software.

The net cooling power  $P_{net}$  was measured in the atmospheric window of 8 to 13 micrometers as follows<sup>16</sup>:

$$P_{net} = P_{rad} - P_{atm} - P_{solar} - P_{norad}, \quad (3.1)$$

where the radiative cooling power of the system  $P_{rad}$  is given by:

$$P_{rad}(T) = 2\pi \int_0^{\pi/2} \int_{8\mu m}^{13\mu m} I_{BB}(T, \lambda) \xi_{film}(\lambda, \theta) \sin(\theta) \cos(\theta) d\lambda d\theta, \quad (3.2)$$

where the emissivity of the sample  $\xi_{film}(\lambda, \theta)$  used is in Table 4.6. The Environmental thermal absorption  $P_{atm}$  is given by:

$$P_{atm}(T_{amb}) = 2\pi \int_0^{\pi/2} \int_{8\mu m}^{13\mu m} I_{BB}(T_{amb}, \lambda) \xi_{film}(\lambda, \theta) \xi_{atm}(\lambda, \theta, pw) \sin(\theta) \cos(\theta) d\lambda d\theta, \quad (3.3)$$

where we consider atmospheric emissivity  $\xi_{atm}(\lambda, \theta, pw)$ , based on the literature as follows<sup>22</sup>:

$$\xi_{atm}(\lambda, \theta) = 1 - [1 - \xi_{atm}(0, \lambda)]^{1/\cos \theta}, \quad (3.4)$$

where  $\xi_{atm}(0, \lambda)$  is the spectral emissivity when  $\theta = 0$  (it means in the vertical direction)<sup>22</sup>. The spectral emissivity is computed from

$$\xi_{atm}(\lambda, \theta) = 1 - 0.871^{1/\cos \theta}. \quad (3.5)$$

For the solar absorption,  $P_{solar}$ , we consider its value equal to zero by definition in the range of study

between 8 to 13 micrometers, while the solar spectral irradiance  $I_{solar}(\lambda)d\lambda$  is close to zero<sup>22</sup>.

$$P_{solar} = \cos\varphi \int_{8\mu m}^{13\mu m} \xi_{film}(\lambda, \varphi) I_{solar}(\lambda) d\lambda = 0. \quad (3.6)$$

For non-radiative power,  $P_{norad}$  we use

$$P_{norad} = P_{conv} + P_{cond} = h_c(T_{amb} - T), \quad (3.7)$$

where heat conduction to the surroundings can be neglected in the limit of low humidity in the atmosphere, as is the case of Ibarra/Ecuador. Then the convective loss  $P_{conv}$  in the upper radiation surface is:

$$P_{conv} = h_{air/conv}(T_{amb} - T), \quad (3.8)$$

where  $h_{air}$  can be expressed as follows

$$h_{air} = a + bV_{wind}, \quad (3.9)$$

and

$$h_{air} = 8.6(\pm 0.9) + 2.6(\pm 0.3)V_{wind}. \quad (3.10)$$

The last equation came from bibliography<sup>22,35,36</sup>. Therefore a typical value for natural convection considered for these calculations is

$$h_{conv} = 8 \frac{W}{m^2 K}. \quad (3.11)$$

Finally, the previous expression using the temperature measurements in a give time were solved in Mathematica, to obtain the cooling power at each time. The results were plotted for the same time of the temperature measurements.

## Chapter 4

# Results & Discussion

### 4.1 Materials obtained

After the treatment process was done as stated in methodology, we obtain the materials observed in figure 4.1. There, it is observed that the whitest material is Colorado cooling wood. Another point that needed to be considered is that the size of the woods diminished after the chemical treatment with NaOH/Na<sub>2</sub>SO<sub>3</sub> and H<sub>2</sub>O<sub>2</sub> (cooling wood) as different from materials obtained after being treated with NaClO and NaClO<sub>2</sub>. As the main objective is to get the materials with the optimum cooling power, we should consider the use the whitest since we expect them to reflect more light in the optical range<sup>1</sup>. Therefore in the following sections, we decided to focus on the materials treated with NaOH/Na<sub>2</sub>SO<sub>3</sub> and H<sub>2</sub>O<sub>2</sub> (labeled as cooling wood).

### 4.2 FTIR

In this section is presented the results for the FTIR for Manzano Colorado, Eucalipto and Copal treated with NaOH/Na<sub>2</sub>SO<sub>3</sub> and H<sub>2</sub>O<sub>2</sub>. The resolution of the FTIR used is 4 cm<sup>-1</sup>. For each material, the FTIR spectrum was drawn for untreated wood, wood after NaOH/Na<sub>2</sub>SO<sub>3</sub> treatment, and finally the wood after H<sub>2</sub>O<sub>2</sub> (the whole treatment gives the material we name Cooling Wood (CW)). In Chapter 2 section 2.7,



Figure 4.1: In this figure one observes the materials obtained from Colorado, Copal and Eucalipto woods, after chemical treatment with NaOH/Na<sub>2</sub>SO<sub>3</sub> and H<sub>2</sub>O<sub>2</sub> (cooling wood), NaClO and NaClO<sub>2</sub>.

was explained some basics of FTIR theory and some results that we may expect here. In Table 4.1 can be observed the peaks involved in the FTIR spectra for the studied materials and from where they come from.

The main constituents of wood are cellulose, hemicellulose, and lignin<sup>67</sup>. Therefore those elements will be present in the FTIR spectrum of the three kinds of wood and for non-treated, treated, and cooling wood samples. Those contribute to the O-H stretching absorption bands around  $3326 \pm 4 \text{ cm}^{-1}$ , and C-H absorption bands at  $2937 \pm 4 \text{ cm}^{-1}$ . Therefore, in the fingerprint region, between  $600$  to  $2000 \pm 4 \text{ cm}^{-1}$  we can distinguish differences happening after the wood was treated. The peaks are assigned as in Table 4.1. In figure 4.2, we review the general chemical structure of wood. In the case of lignin, we have three main units S unit, G unit, and H unit; for hardwood, as is our case for the three kinds of wood, we only have S units and G units. Also, for hemicellulose, there exist for softwood and hardwood. In the figure 4.2, we show the structure of hemicellulose hardwood.

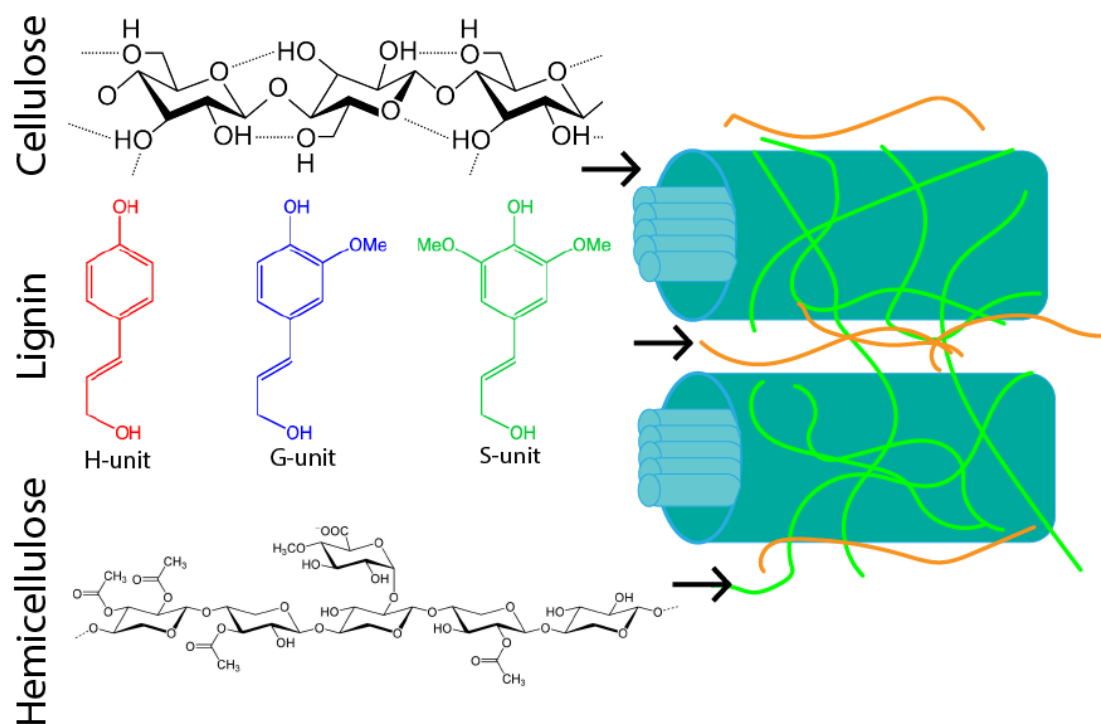


Figure 4.2: Wood structure is present here where cellulose, lignin and hemicellulose are observed. The main structure of wood is cellulose. The hemicellulose shown is for hardwood. In lignin Me means a methyl group ( $\text{CH}_3$ )<sup>11</sup>.

#### 4.2.1 Colorado

In figure 4.3, we observe the FTIR spectra of *Guarea Kunthiana* wood (Colorado). There, we have the spectra of Colorado wood after the entire treatment ( $\text{Na}_2\text{SO}_3/\text{NaOH}$  and  $\text{H}_2\text{O}_2$ ) named Colorado cooling wood (CCW), wood during the  $\text{Na}_2\text{SO}_3/\text{NaOH}$  treatment called treated Colorado wood (TCW), and finally, non-treated Colorado wood (NTCW).

In the spectra, we observe a peak at  $1736 \pm 4 \text{ cm}^{-1}$  related to the  $\text{C}=\text{O}$  stretch of hemicellulose<sup>68</sup> only for the NTCW and Colorado cooling wood. Here we have a shift in CCW for  $1719 \pm 4 \text{ cm}^{-1}$ . The  $\text{C}=\text{O}$  bond shows strong absorption between  $1750 \pm 4 \text{ cm}^{-1}$  and  $1700 \pm 4 \text{ cm}^{-1}$ . This wavenumber depends on the functional group. For carboxylic acid, it is present at  $1725\text{-}1700 \pm 4 \text{ cm}^{-1}$ ; for the ester, ketone, it is in the  $1725\text{-}1705 \text{ cm}^{-1}$  range, and for the aldehyde is in  $1740\text{-}1720 \pm 4 \text{ cm}^{-1}$ . It also depends on

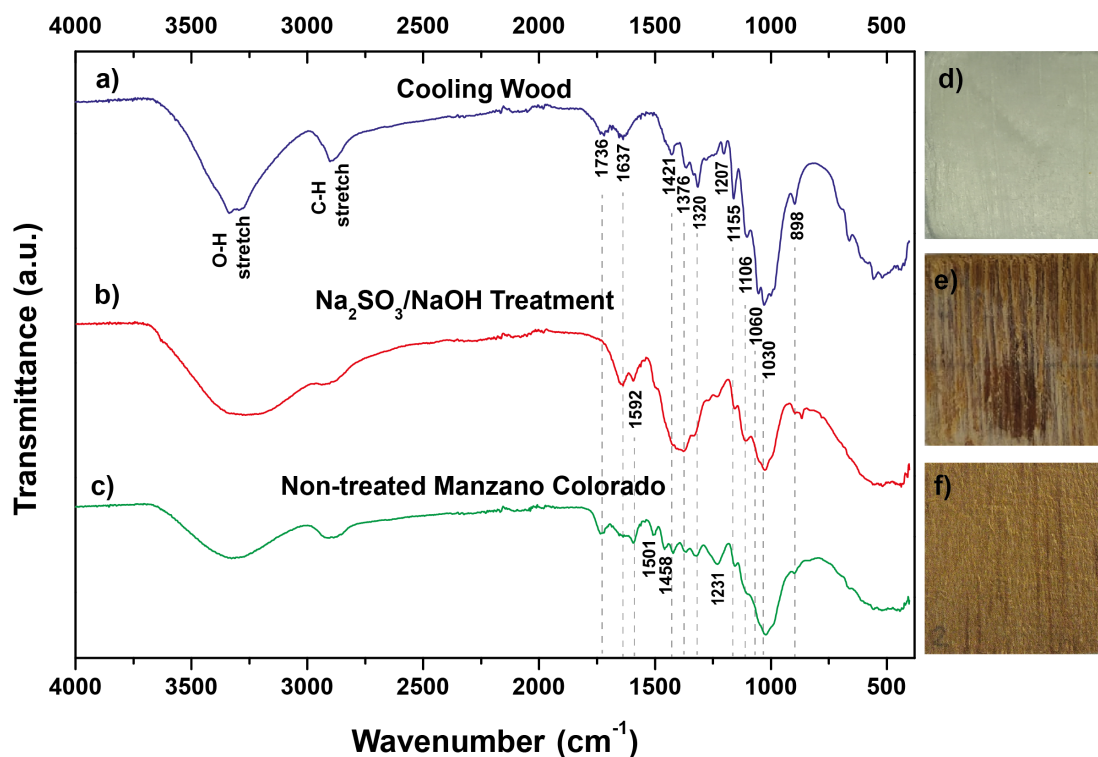


Figure 4.3: FTIR spectra of Colorado wood before the delignification, during the delignification and after of the delignification treatment to obtain Colorado cooling wood material.

its structural location. At lower wavenumbers, it is related to the conjugated C=O. In general, the band around  $1730 \pm 4 \text{ cm}^{-1}$  is almost exclusively due to the carbonyl groups of acetoxy groups in xylan, which means hemicellulose contribution<sup>67</sup>. In that way, the  $1736 \pm 4 \text{ cm}^{-1}$  peak of NTCW is due to carbonyl groups of acetoxy groups in xylan, and the  $1719 \pm 4 \text{ cm}^{-1}$  peak in CCW is related to ester and ketone. The shift of CCW might be due to the breaking of acetyl or acetoxy groups in xylan, which is related to the delignification treatment and with temperature used<sup>67</sup>. After the chemical treatment, not only is lignin eliminated at the beginning of the treatment, hemicelluloses are the first to degrade; therefore, we have a decrease of the  $1736 \text{ cm}^{-1} \pm 4 \text{ cm}^{-1}$  peak passing to TCW spectra; this is attributed to the cleavage of acetyl or acetoxy groups in xylan<sup>20</sup>.

Following that, we have the peak at  $1637 \pm 4 \text{ cm}^{-1}$ , representing the water associated with lignin and cellulose<sup>68</sup>, which is more observed in treated and cooling wood; the non-treated Colorado wood is dry; therefore, this peak is not observed. Also, this peak tells us that the cooling wood sample is not entirely dried.

Following, we have a  $1592 \pm 4 \text{ cm}^{-1}$  peak related to C=C stretching vibration from lignin<sup>68</sup> which is observed more in TCW and non-treated Colorado (NTCW). This peak is not present at cooling wood, which means that we have less to no lignin present. It probes that we delignified the wood since this peak is for aromatic skeletal lignin.

Similarly, the peak at  $1501 \pm 4 \text{ cm}^{-1}$  refers to the same interaction as the  $1592 \pm 4 \text{ cm}^{-1}$  peak for aromatic skeletal lignin<sup>68</sup> and is only present in non-treated wood. It was not identified its presence in TCW; nonetheless, if it is present, other peaks overlap it. Aromatic rings exhibit the band corresponding to benzene ring stretching vibrations. This band is very important because it varies for hardwood lignin and softwood<sup>20</sup>. The band at  $1505 \pm 4 \text{ cm}^{-1}$  is mainly visible for hardwood lignin (Guaiacyl - G and Syringyl - S), and at  $1510 \pm 4 \text{ cm}^{-1}$  for softwood lignin (Guaiacyl-G)<sup>67</sup>. Therefore we know Colorado wood has hardwood lignin which coincides with the information of Chapter 2. The shift in this band can be due to the decrease of the methoxyl groups in lignin which would lead to lignin more similar to softwood (G-lignin) or the loss of S units. As seen in figure 4.2, lignin S-unit has two methoxyl groups, and lignin G-unit has one methoxyl group. S-unit monomer is less condensed by C-C bonds than G-unit monomers, and therefore it can be easily liberated by a thermal degradation<sup>67,69</sup>. Lignin condensation is the re polymerization of lignin decomposition products through C-C linkages. Thus, the resulting lignin structure is highly recalcitrant (it is a stable structure, difficult to degraded) to further degradation<sup>70</sup>. So having a structure less condensate as is S-unit monomer, we were able to liberate lignin. In this case, we eliminated lignin, and it is attributed to the breaking of aliphatic side-chains in lignin and/or condensation reactions<sup>68</sup>. The peak at  $1458 \pm 4 \text{ cm}^{-1}$  is for C-H asymmetric deformation in  $-\text{OCH}_3$  (of xylan),  $\text{CH}_2$  in pyran ring symmetric scissoring<sup>71</sup>. It is only present in non-treated wood, indicating that lignin has been reduced/eliminated in the chemical treatment.

The peak of  $1421 \pm 4 \text{ cm}^{-1}$  is related to the C-H asymmetric deformation of  $-\text{OCH}_3$ . The band

corresponds to the vibration of the aromatic ring of lignin and the C-H bending in cellulose<sup>71</sup>. This peak is present in the non-treated and cooling wood. In cooling wood, it is shifted to  $1427 \pm 4 \text{ cm}^{-1}$ . In TCW, it seems to not exist, and if it is present, it is overlapped. The shift in CCW may be related to lignin content in the sample, which is reduced; now, all the contribution is for cellulose deformation. This band is important since it is used to identify crystallinity changes<sup>72</sup>. In this band, as in the  $897 \pm 4 \text{ cm}^{-1}$  band, the FTIR spectrum differs for cellulose I and cellulose II and amorphous cellulose. If cellulose fiber had crystalline cellulose I, the band is towards  $1421 \pm 4 \text{ cm}^{-1}$ , and the amount of cellulose II and amorphous cellulose decreases. Thus an increase in the ratio 1430/898 intensity relates to an increase in cellulose crystallinity<sup>71,72</sup>. The ratio of peaks of  $1430 \pm 4 \text{ cm}^{-1}$  and  $898 \pm 4 \text{ cm}^{-1}$  is calculated to monitor an increase in crystallinity.

In Table 4.1 we identify the ratio of intensities I (1421/898), there we can notice that the ratio increases for cooling woods (it means after the chemical treatment). A higher increase was identified for Colorado cooling wood. We can consider that the delignification process increases cellulose's crystallinity, but additional studies should be made to confirm the statement.

The peak for  $1365 \pm 4 \text{ cm}^{-1}$  is for C-H deformation vibration in cellulose and hemicellulose<sup>20</sup>. It is presented in 3 graphs non-treated, treated, and cooling wood. Nonetheless, it is predominant in treatment. Also, for TCW, the peak is shifted to  $1376 \pm 4 \text{ cm}^{-1}$ . According to Esteves *et al.*, for the band at  $1333 \pm 4 \text{ cm}^{-1}$  all structural components of wood contributes because this peak is related to C-H bending of polysaccharides, which joins the band at  $1327 \pm 4 \text{ cm}^{-1}$  of S and G lignin condensed units<sup>67</sup>. Therefore the  $1320 \pm 4 \text{ cm}^{-1}$  peak is related to the C-O vibration of the syringyl ring units<sup>68</sup>. This is predominant in cooling wood than in non treated. For CCW, the peak is shifted to  $1315 \pm 4 \text{ cm}^{-1}$ . This can be due to condensation reactions in the lignin units. This peak increased and is shifted to small wavenumbers. Since we are supposed to have lower or non-lignin content in cooling wood, it can be related to lignin remaining condense and therefore making it more difficult to eliminate those remainings of lignin<sup>68</sup>. So delignification at 100 percent is not possible.

For the case of  $1231 \pm 4 \text{ cm}^{-1}$  C-O stretching in lignin and hemicellulose (C-O carbonyl band in lignin and xylan units)<sup>21</sup>, the peak is reduced/eliminated for treated and cooling wood, which means we



are diminishing the presence of lignin of the sample and also we are reducing hemicellulose thanks to the treatment.

The  $1203 \pm 4 \text{ cm}^{-1}$  peak is related to OH in-plane bending in cellulose I and cellulose II<sup>71</sup>. This peak is only identified in cooling wood. After the treatment, cellulose has more liberty to move and is more exposed to the material's surface, therefore, contributing more to this peak. At the same way as proposed in the mechanism of methodology. The delignification process forms OH bonds in the remains of lignin.

We also have  $1155 \pm 4 \text{ cm}^{-1}$  peak of C-O-C vibration in polysaccharides (asymmetric stretching in cellulose I and cellulose II)<sup>68</sup>. This peak is present in the three spectra; it is predominant in cooling wood, where it is shifted to  $1160 \pm 4 \text{ cm}^{-1}$ .  $1160 \pm 4 \text{ cm}^{-1}$  peak can also be assigned to the C-H in-plane deformation of the G ring, but as is more present in cooling wood, it is related more to cellulose<sup>68</sup>.

The band at  $1140 \pm 4 \text{ cm}^{-1}$  results from the sum of the contribution of C-H deformation in aromatic rings and C-O stretching in primary alcohols. This peak has a shoulder at  $1140 \pm 4 \text{ cm}^{-1}$  in woods with G lignin<sup>67</sup>.  $1128 \pm 4 \text{ cm}^{-1}$  peak came from the woods with G and S lignin. Therefore we have a G lignin predominant. Also, in this band, no consistent variation was found. This G lignin contribution may be related as that as we remove some methoxyl groups in lignin we have before the presence of S and G units in our non-treated wood, and after the whole treatment, we have the presence of G units (G units have just one methoxyl group attached)<sup>54</sup>.

$1106 \pm 4 \text{ cm}^{-1}$  peak is related to the O-H association of cellulose units. This peak is present in the three spectra; it is predominant in cooling wood and shifted to  $1102 \pm 4 \text{ cm}^{-1}$ , in non-treated Colorado is not even well see in the graph and data. The increase in Colorado cooling wood may be due to new alcohol and ester groups forming after the treatment.  $1110 \pm 4 \text{ cm}^{-1}$ , are also assigned to the aromatic C-H in-plane deformation (typical for S units), secondary alcohols, C<sup>1</sup>/4O stretch, and ring asymmetric stretching in cellulose I and cellulose II<sup>54</sup>.  $1052 \pm 4 \text{ cm}^{-1}$  peak is related to C-O valence vibration mainly from O-CH<sub>3</sub> (assigned to C-C and C-O stretching (in polysaccharides))<sup>54</sup>. It is only present in cooling wood as a shoulder.

The  $1022 \pm 4 \text{ cm}^{-1}$  peak is related to the C-O-C stretching of a primary alcohol in cellulose and hemicelluloses<sup>73</sup>. This is present in 3 of the FTIR spectra. We have a shift to  $1024 \text{ cm}^{-1} \pm 4$  in TCW

and in CCW a change to  $1030 \pm 4 \text{ cm}^{-1}$ . As stated in reference, a peak closed to  $1030 \text{ cm}^{-1} \pm 4$  can be assigned to Calkyl–O ether vibrations,  $-\text{OCH}_3$ , and b–O–4 in guaiacol and C–C and C–O stretching in cellulose I and cellulose II, which is the main peak related to the atmospheric window. So it is important to notice that it is mainly due to cellulose contribution<sup>73</sup>.

Finally, the peak of  $897 \pm 4 \text{ cm}^{-1}$  of C1–H deformation of the glucose ring in cellulose and hemicellulose is related to the crystallinity ratio<sup>68,73</sup>. The peak is better defined in cooling wood. It is also present in the NCW, but in TCW, it is almost non-existent or shifted to  $894 \pm 4 \text{ cm}^{-1}$  with a smaller contribution. This peak corresponding to the sugar ring tension seemed to increase with ring-closing. Also, The absorption peak at  $897 \pm 4 \text{ cm}^{-1}$  indicated the asymmetric deformation of cellulose and hemicellulose units<sup>68</sup>.

#### 4.2.2 Eucalipto

For Eucalipto, we have peaks similar as before as seen in figure 4.4, we measure FTIR spectra of Eucalipto for non-treated wood (ENW), Eucalipto treated wood (ETW), and Eucalipto cooling wood (ECW). In the fingerprint region, the peak of  $1736 \pm 4 \text{ cm}^{-1}$  is only present in Eucalipto. For  $1637 \pm 4 \text{ cm}^{-1}$ , it is only present in ETW and ECW, which is related to the water in the sample. Similar to before, the treated sample is the one that contains more water. The peak of  $1592 \pm 4 \text{ cm}^{-1}$  is present in ENW, ETW, and a little in ECW.  $1501 \pm 4 \text{ cm}^{-1}$  peak is only present in ENW. Similar as  $1458 \pm 4 \text{ cm}^{-1}$  peak. As mentioned before, this peak comes from lignin<sup>71</sup> that has been removed in the chemical treatment.  $1421 \pm 4 \text{ cm}^{-1}$  peak is present in ENW, and in ECW, at  $1425 \pm 4 \text{ cm}^{-1}$ .  $1365 \pm 4 \text{ cm}^{-1}$  peak is present in Colorado. For this case is shifted to  $1376 \pm 4 \text{ cm}^{-1}$  in ETW, and ECW is present in  $1365 \pm 4 \text{ cm}^{-1}$ , which is moved with respect to the ETW.  $1320 \text{ cm}^{-1}$  peak of Colorado here is shifted to  $1322 \text{ cm}^{-1}$ . It is present in NCW at  $1322 \pm 4 \text{ cm}^{-1}$  and moved for ECW to  $1319 \pm 4 \text{ cm}^{-1}$ . For  $1231 \pm 4 \text{ cm}^{-1}$ , it is present in ENW, in ETW is almost depreciable and shifted to  $1233 \pm 4 \text{ cm}^{-1}$  and in ECW is shifted to  $1227 \pm 4 \text{ cm}^{-1}$ .  $1592 \pm 4 \text{ cm}^{-1}$ ,  $1501 \pm 4 \text{ cm}^{-1}$ ,  $1458 \pm 4 \text{ cm}^{-1}$ , and  $1231 \pm 4 \text{ cm}^{-1}$  peaks are related more to lignin<sup>68</sup>, and their decrease or their nonpresence after the chemical treatment gives us an insight of the removal of lignin from the samples. Here  $1592 \pm 4 \text{ cm}^{-1}$  is still present in ECW,  $1501 \pm 4 \text{ cm}^{-1}$  and  $1458 \pm 4 \text{ cm}^{-1}$  peaks are not present in

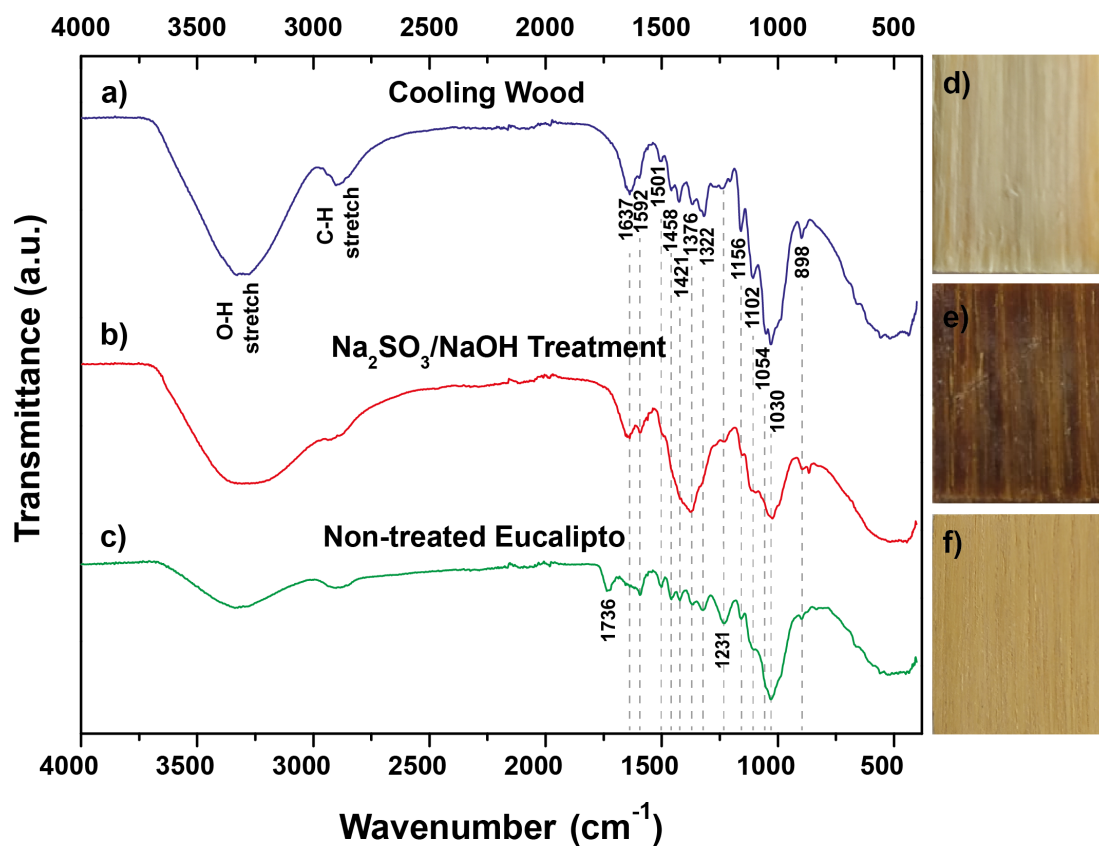


Figure 4.4: FTIR spectra of Eucalypto wood before the delignification, during the delignification and after of the delignification treatment to obtain Eucalypto cooling wood material

ECW, and  $1231 \pm 4 \text{ cm}^{-1}$  is slightly present. Therefore we remove some lignin from our sample, and we still have remains of lignin. In this case, different from Colorado, we do not have the peak at  $1203 \pm 4 \text{ cm}^{-1}$ , which is related to OH in-plane bending in cellulose I and cellulose II<sup>71</sup>, and was only identified in Colorado cooling wood. After the treatment, cellulose has more liberty to move and is more exposed to the material's surface. In this case, as seen in the figure 4.4, the color of our cooling wood is not as white as for Colorado. We still have some remains of lignin in Eucalypto cooling wood. For the  $1155 \pm 4 \text{ cm}^{-1}$  peak present in Colorado, here we have that peak at  $1156 \pm 4 \text{ cm}^{-1}$  for ENW, for ETW at  $1153 \pm 4 \text{ cm}^{-1}$

and for ECW at  $1158 \pm 4 \text{ cm}^{-1}$ . For  $1106 \pm 4 \text{ cm}^{-1}$  peak in Colorado, here we have the peak at  $1102 \pm 4 \text{ cm}^{-1}$  for ENW, for ETW  $1095 \pm 4 \text{ cm}^{-1}$ , and for ECW at  $1106 \pm 4 \text{ cm}^{-1}$ . The peak of  $1052 \text{ cm}^{-1}$  present in Colorado cooling wood here is present in Eucalipto cooling wood but shifted to  $1054 \pm 4 \text{ cm}^{-1}$ . For  $1022 \pm 4 \text{ cm}^{-1}$  present in Colorado wood, here is at  $1030 \pm 4 \text{ cm}^{-1}$  for ENW, at  $1022 \pm 4 \text{ cm}^{-1}$  for ETW and  $1030 \pm 4 \text{ cm}^{-1}$  for ECW. Finally,  $898 \pm 4 \text{ cm}^{-1}$  peak is present in ENW and ECW and shifted in ETW to  $894 \pm 4 \text{ cm}^{-1}$  and is almost inexistent. In table 4.1, it is shown how the crystallinity of cellulose increases with respect to non-treated wood.

### 4.2.3 Copal

For Copal, we have the contribution of the peaks similar as before and mentioned in table 4.2, we measure Copal non-treated wood (CpNW), Copal treated wood (CpTW), and Copal cooling wood (CpCW) as seen in figure 4.5. In the fingerprint region: the peak of  $1736 \pm 4 \text{ cm}^{-1}$  is only present in Copal. For  $1637 \pm 4 \text{ cm}^{-1}$ , it is only present in CpTW (with a shift to  $1639 \pm 4 \text{ cm}^{-1}$ ) and CpCW, which is related to the water in the sample<sup>68</sup>.  $1592 \pm 4 \text{ cm}^{-1}$  peak is present in CpNW, CpTW.  $1501 \pm 4 \text{ cm}^{-1}$  peak of Colorado is only present in CpNW (shifted to  $1503 \pm 4 \text{ cm}^{-1}$ ) and CpCW, here also we have hardwood lignin in accordance with bibliography<sup>20,41</sup>.  $1458 \pm 4 \text{ cm}^{-1}$  peak is only present in CpNW and CpCW.  $1421 \pm 4 \text{ cm}^{-1}$  is present in CpNW and CpCW, but there is shifted to  $1425 \pm 4 \text{ cm}^{-1}$ .  $1365 \pm 4 \text{ cm}^{-1}$  peak is present in CpNW, CpTW shifted to  $1378 \pm 4 \text{ cm}^{-1}$  and CpCW in  $1369 \pm 4 \text{ cm}^{-1}$ .  $1320 \pm 4 \text{ cm}^{-1}$  peak is present in CpNW and CpCW at  $1317 \pm 4 \text{ cm}^{-1}$ . For  $1231 \pm 4 \text{ cm}^{-1}$  peak present in Colorado wood, it is present in CpNW but shifted to  $1227 \pm 4 \text{ cm}^{-1}$ .

$1592 \pm 4 \text{ cm}^{-1}$ ,  $1501 \pm 4 \text{ cm}^{-1}$ ,  $1458 \pm 4 \text{ cm}^{-1}$ , and  $1231 \pm 4 \text{ cm}^{-1}$  peaks are related more to lignin<sup>68</sup>, and their decrease or their nonpresence after the chemical treatment gives us an insight into the removal of lignin from the samples. Here  $1592 \pm 4 \text{ cm}^{-1}$  is non present in CpCW,  $1501$  and  $1458 \pm 4 \text{ cm}^{-1}$  are present in CpCW, and  $1231 \pm 4 \text{ cm}^{-1}$  is non present. Therefore we remove some lignin from our sample, and we still have remains of lignin.

Colorado has a peak at  $1203 \pm 4 \text{ cm}^{-1}$  for CCW, and here it is at  $1205$  for CpCW. Eucalipto does not

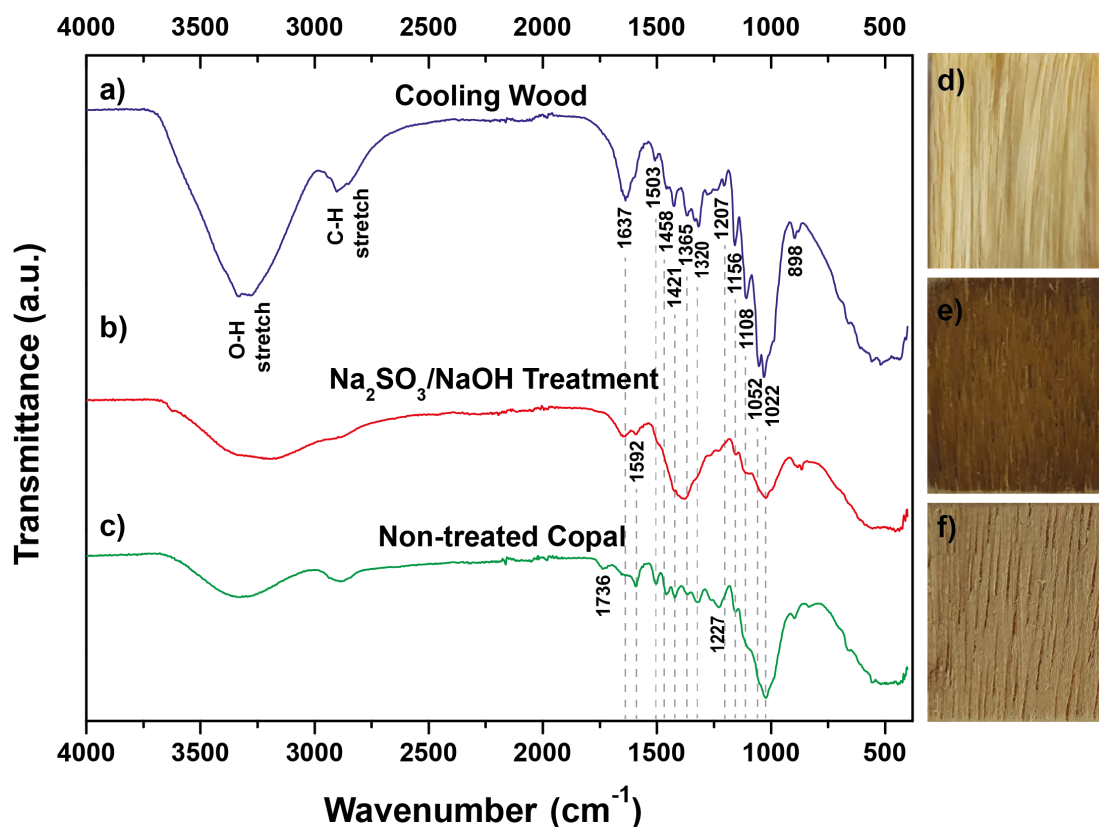


Figure 4.5: FTIR spectra Copal wood before the delignification, during the delignification and after of the delignification treatment to obtain Copal cooling wood material

have the presence of this peak. We consider that as more lignin is removed, this peak is present since it is related to OH in-plane bending in cellulose I and cellulose II<sup>71</sup> and also to possible creation of OH bonds in remains of lignin. After the removal of lignin, cellulose is more exposed to the surface of the material. For  $1155 \pm 4 \text{ cm}^{-1}$  of Colorado, here we have that peak at  $1156 \pm 4 \text{ cm}^{-1}$  for CpNW, for CpTW at  $1155 \pm 4 \text{ cm}^{-1}$ , and CpCW at  $1158 \pm 4 \text{ cm}^{-1}$ . For  $1106 \pm 4 \text{ cm}^{-1}$  in Colorado here we have the peak at  $1108 \pm 4 \text{ cm}^{-1}$  for CpNW, for CpTW  $1095 \pm 4 \text{ cm}^{-1}$ , for CpCW at  $1108 \pm 4 \text{ cm}^{-1}$ . The peak of  $1052 \pm 4 \text{ cm}^{-1}$  present in Colorado cooling wood and Eucalipto cooling wood shifted to  $1054 \pm 4 \text{ cm}^{-1}$ , here is present for CpCW at  $1052 \pm 4 \text{ cm}^{-1}$ .  $1022 \pm 4 \text{ cm}^{-1}$  peak, we have in CpNW, CpTW, and at  $1030 \pm 4 \text{ cm}^{-1}$  for

CpCW, Finally,  $898 \pm 4 \text{ cm}^{-1}$  peak is present in CpNW and CpCW and shifted in CpTW to  $866 \pm 4 \text{ cm}^{-1}$ . This peak help us to identify an increase in crystallinity shown in table 4.1. Where is observed how the crystallinity of cellulose increases after the chemical treatment.

Since we have more formed cellulose fibers, the increase of the I (1421/898) ratio is observed for the three kinds of wood that give us an insight into the crystallinity of cellulose<sup>72</sup>. Nonetheless, we need to confirm that increase in cellulose crystallinity by making other essays. In general, we identify the removal of lignin in the three samples, being more efficient for Colorado cooling wood where almost all the peaks related to lignin were eliminated, therefore considering its absence. In Eucalipto and Copal, we still have some peaks related to lignin but with lower contribution as different from non-treated wood.

<b>Material</b> <b>I(1421/898)</b>	<b>Non treated Wood</b>	<b>Cooling Wood</b>
Manzano Colorado	$1.08 \pm 0.01$	$1.23 \pm 0.02$
Eucalipto	$1.08 \pm 0.01$	$1.201 \pm 0.001$
Copal	$1.07 \pm 0.01$	$1.11 \pm 0.01$

Table 4.1: Ratio of intensities I(1421/898) measured for the spectra in order to identify the increase of crystallinity.

Wavenumber ( $\pm 4 \text{ cm}^{-1}$ )	Functional Groups	Compounds	R
3000-3600 (s)	O-H stretching, acid, methanol	Cellulose-hemicellulose	R <sup>20,53,54,68</sup>
2860-2970 (m)	C-H stretch, alkyl, aliphatic and aromatic	Cellulose-hemicellulose-lignin	R <sup>20,53,54,68</sup>
1736 (w)	C=O stretch, ketone and carbonyl	Hemicellulose	R <sup>20,21,54,68</sup>
1637 (w)	Water associated with lignin and cellulose	Water	R <sup>54,68</sup>
1592 (m)	C=C stretching vibration	Lignin	R <sup>20,21,68</sup>
1501 (w)	C=C stretching vibration	Lignin	R <sup>20,21,68</sup>
1458 (w)	C-H asymmetric deformation in -OCH <sub>3</sub> , CH <sub>2</sub> in pyran ring symmetric scissoring	Lignin	R <sup>68,71</sup>
1421 (w)	C-H asymmetric deformation in -OCH <sub>3</sub>	Lignin	R <sup>68,71</sup>
1365 (w)	C-H deformation vibration	Cellulose-hemicellulose	R <sup>20,68</sup>
1320 (m)	C1-O vibrations in S derivatives, CH in-plane bending in cellulose I and II and CH <sub>2</sub> wagging in cellulose I, II	Cellulose-lignin	R <sup>68,71</sup>
*1231 (m)	C-O stretching	Lignin-hemicellulose	R <sup>20,21,68</sup>
*1203 (w)	OH in-plane bending in cellulose I and cellulose II	Cellulose	R <sup>68,71</sup>
*1155 (m)	C-O-C stretching vibration pyranose ring skeletal	Cellulose-hemicellulose	R <sup>54,68</sup>
*1106 (m)	O-H association C-OH	Cellulose-hemicellulose	R <sup>54,68</sup>
*1052 (w)	C-O stretching and C-O deformation ethanol C-OH	Cellulose-hemicellulose	R <sup>54,68</sup>
*1022 (s)	COC stretching of primary alcohol	Cellulose-hemicellulosen	R <sup>68,73</sup>
*898 (m)	C1-H deformation of glucose ring	Cellulose-hemicellulose	R <sup>68,73</sup>
*700-400 (s)	C-C stretching		R <sup>54</sup>

Table 4.2: FTIR peaks of wood and its main components: cellulose, hemicellulose and lignin measured in the samples, \* refers to the peaks in the atmospheric window regions of 8 to 13  $\mu\text{m}$ , the peaks intensity are denoted by (s) strong, (m) medium and (w) weak.

### 4.3 XPS

We use a XPS to measure some chemical properties of the materials. The resolution of the XPS used is 0.5 eV. In figure 4.6 we have figures obtained from the SEM that has the XPS. There is observed the fiber structure of wood and finally of the cooling wood, that in Colorado seem to be more fibrous.

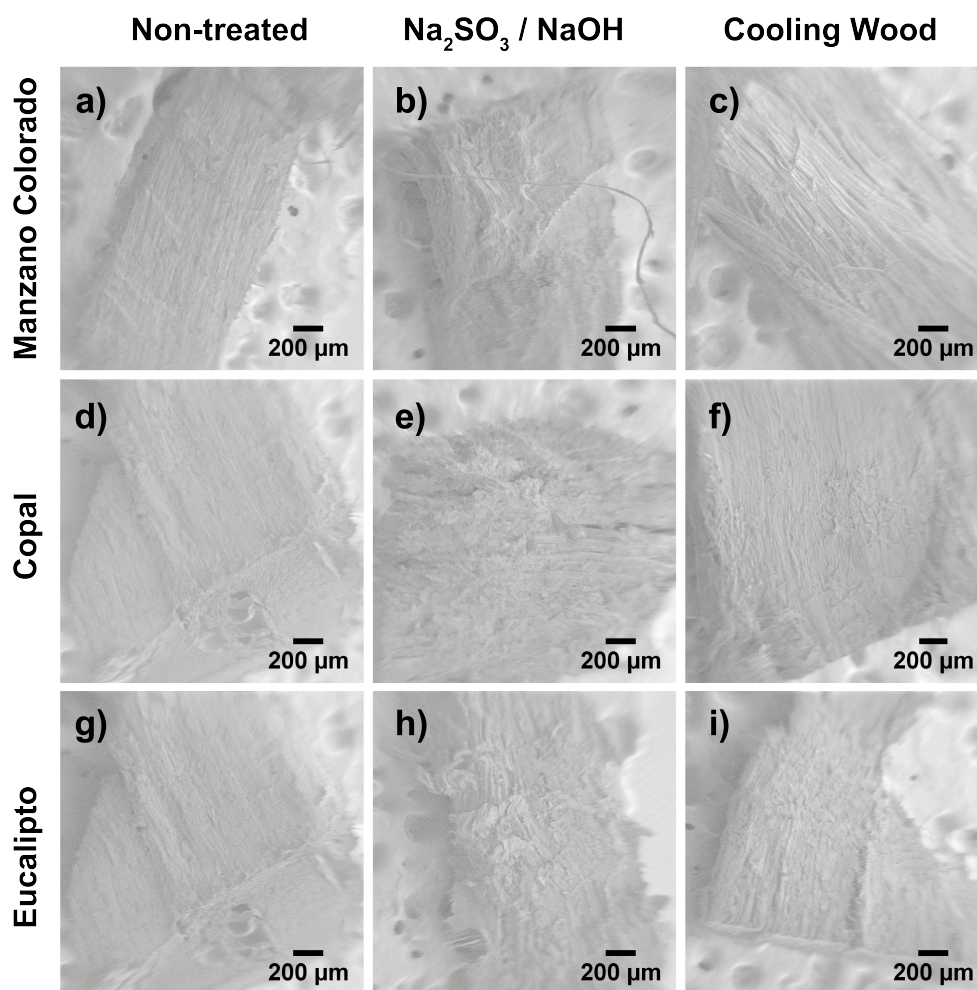


Figure 4.6: SEM XPS

The data obtained from the XPS are shown in the following sections. In order to understand the XPS spectra, it's essential to remember wood composition. Wood is mainly composed of cellulose 40-50



wt%, lignin 25-30 wt%, and hemicellulose 20-25 wt%.<sup>58</sup>. Wood also has small amounts (0-10wt % ) of extractives<sup>74</sup>, consisting of compounds like resin, fatty acids, triglycerides, sterols, and steryl esters. Those compounds can be removed by organic solvents like dichloromethane, ethanol, or acetone<sup>58</sup>. In Chapter 2 section 2.7, was explained some basics of XPS theory and some results that we may expect here. Considering that, we will identify and discuss the results of XPS spectra.

### 4.3.1 Colorado

As seen in figure 4.7 are presented the fitting for carbon C1s spectrum and oxygen O1s spectrum for Colorado wood (NTW), Colorado treated wood (TW), and Colorado cooling wood (CW). In table 4.3 we summarize the peaks present in the whole XPS spectra and where they come from. In carbon C1s spectra, for Colorado was identified 4 peaks centered at  $284.9 \pm 0.5$ ,  $286.3 \pm 0.5$ ,  $287.3 \pm 0.5$ , and  $288.8 \pm 0.5$  eV. The first is related to C-C/C-H (C2), the second for C-O (C3), the third C=O/C-O-C (C4), and the last for O-C=O (C5). For treated wood, there were identified peaks centered at  $283.8 \pm 0.5$ ,  $284.8 \pm 0.5$ ,  $286.0 \pm 0.5$ ,  $287.4 \pm 0.5$ ,  $289.7 \pm 0.5$ , and  $291.2 \pm 0.5$  eV. Different from non-treated and cooling wood, here, the first peak comes from silicon carbide SiC (C1). The others came from C-C/C-H, C-O, C=O, and O-C=O with a shake-up line (C6) at  $291.2 \pm 0.5$  eV. For cooling, wood was identified four peaks centered at  $284.7 \pm 0.5$ ,  $285.8 \pm 0.5$ ,  $286.9 \pm 0.5$ , and  $288.4 \pm 0.5$  eV, related to C-C/C-H, C-O, C=O, and O-C=O, respectively, similar for non-treated wood. Those contributions are in good relation with the bibliography and the chemical constituents of cellulose, lignin, and hemicellulose<sup>59</sup>.

In oxygen O1s spectra for Colorado non-treated, we can identify 4 peaks at  $528.7 \pm 0.5$ ,  $530.8 \pm 0.5$ ,  $532.2 \pm 0.5$ , and  $533.3 \pm 0.5$  eV. The first is an unnamed peak (O2) that can be related to some contamination since it has a vast FWHM, the second is related to C=O (O3), the third to C-O (O4), and the fourth to O-C=O (O5). O3, O4, and O5 present here are well related to the peaks identified in C1s spectra. For treated wood, we obtained the peaks centered at  $524.3 \pm 0.5$  eV from satellite (O1),  $530.9 \pm 0.5$  eV from C=O,  $532.2 \pm 0.5$  eV from C-O,  $533.1 \pm 0.5$  eV from O-C=O, and  $537.0 \pm 0.5$  eV related to Na auger electron (O6). In cooling wood, we identified 4 peaks centered at  $529.4 \pm 0.5$ ,  $531.0 \pm 0.5$ ,

532.2  $\pm$  0.5, and 533.3  $\pm$  0.5 eV. The first peak is related to some contamination and is also present in non-treated wood; the second is associated with C=O, the third to C-O, and the fourth to O-C=O, here Na auger is removed.

In figure 4.8 are presented the XPS spectra with the fittings of nitrogen N1s and silicon Si2p. For N1s spectra, we identified a peak in non-treated wood at 399.8  $\pm$  0.5 eV, in treated wood at 399.4  $\pm$  0.5 eV related to peptide bond CO-NH originating from protein in pulps it could be related to amine/amide functional groups<sup>75</sup>. Those came from naturally occurring proteins in wood. Nonetheless, contamination could also be considered<sup>58</sup>. We could not identify a well-defined peak for Colorado wood N1s, so we removed nitrogen from the sample after the whole treatment, confirming a well-done chemical treatment.

For silicon Si2p in non-treated wood, we identify a peak centered at 102.3  $\pm$  0.5 eV for treated wood at 102.3  $\pm$  0.5 eV and for cooling wood at 102.6  $\pm$  0.5 eV. This peak in the three samples is mainly to silicon oxide's SiO contribution, attributed to some dust particles impregnated in the sample.

In C1s spectra, C-C/C-H (C2) contribution decreased during and after the treatment, C-O (C3) increases during the treatment and decreases after the treatment. C=O/C-O-C (C4) contribution reduces in treatment, and in cooling wood increases, and O-C=O (C5) contribution increases during and after the treatment but at a lower rate. C2 partial reduction is related to the loss of lignin contribution. Colorado cooling wood is the sample with lower lignin remains. On the other hand, cellulose also contributes to C-C and C-H peaks, making this peak bigger than others. Additionally, the ratio of C2/C3 was obtained before the treatment 3.3  $\pm$  0.1 and after the treatment 5.6  $\pm$  0.1. Thus, we consider that C2 increases its contribution compared to C3. C-H contribution is related to cellulose I and II. FTIR peak at 1320  $\pm$  4 cm<sup>-1</sup> related to CH in-plane bending of cellulose I and II, and CH<sub>2</sub> wagging in cellulose I, II increase noticeable contribution. Also, 1365  $\pm$  4 cm<sup>-1</sup> related to C-H deformation vibration of cellulose 1 also increases after the delignification process. Even a peak of C-H stretch identified around 2800  $\pm$  4 cm<sup>-1</sup> in the FTIR spectra is more defined after the delignification process. Thus it shows the remain of C2 (C-C/C-H) peak as the main contribution of C1s spectra, even when lignin was removed, and this peak reduce a bit. The increase in C1s in C=O/C-O-C (C4) can be related to the FTIR peak increase for cooling wood at 1022  $\pm$  4 cm<sup>-1</sup> of C-O-C stretching of primary alcohol cellulose and hemicellulose. Consequently, we have an increase in cellulose. The

contribution of C-O-C is essential for the cooling power of the material; an increase in this FTIR peak means a higher emission in the atmospheric window which means an increase in the cooling power.

In O-C=O (C5), we cannot consider an increase or decrease for analyzing its contribution in C1s spectra since it is low. We can identify real increases or decreases by analyzing O1s spectra related to this peak.

Thus, in oxygen spectra, C=O/C-O-C (O3) contribution increases for treated wood, and for cooling wood, C-O (O4) increases during the treatment and reduces after the treatment, and O-C=O (O5) during the treatment increases and after the treatment decreases. The reduction of O-C=O functional groups after the treatment is related to hemicellulose structure disintegration. As observed in figure 4.2 in hemicellulose structure, O-C=O is connected to CH<sub>3</sub> groups. The removal of O-C=O functional groups reduces CH<sub>3</sub> groups as proved by the reduction of FTIR peak at  $1458 \pm 4 \text{ cm}^{-1}$  related to C-H asymmetric deformation in -OCH<sub>3</sub> in Colorado wood FTIR spectra (figure 4.3). The reduction of O-C=O and CH<sub>3</sub> functional groups lead us hemicellulose more similar to cellulose structure. The decrease of O-C=O can be that this transforms to C=O, therefore increasing this peak's contribution. In FTIR spectra for Colorado, cooling wood peak at  $1736 \pm 4 \text{ cm}^{-1}$  related to C=O stretch ketone and carbonyl remains after the treatment. However, it was partially reduced.  $1736 \pm 4 \text{ cm}^{-1}$  peak is related to hemicellulose. Thus, some hemicellulose was transformed by eliminating O-C=O groups, and others were dissolved and eliminated through the chemical treatment. Simultaneously, the increase of C=O/C-O-C (O3) in C1s and O1s spectra can be mainly for C-O-C since in FTIR spectra of cooling wood, the peak at  $1022 \pm 4 \text{ cm}^{-1}$ , related to C-O-C stretching of primary alcohol cellulose and hemicellulose, increases. The bigger the FTIR peak at  $1022 \pm 4 \text{ cm}^{-1}$  help in the cooling power.

C-O contribution is present in all components, hemicellulose, lignin, and cellulose. Its decrease can be related to reducing hemicellulose and lignin in the wood after the treatment since we have a lower contribution of C-O from hemicellulose and lignin. As observed in the FTIR spectrum, the peak at  $1231 \pm 4 \text{ cm}^{-1}$  of C-O stretching of lignin from wood reduce in cooling wood. As in the C1s spectrum, in O1s, C-O seems to be reduced to, but still appears strong. This is related mainly to the C-OH contribution in cellulose.

Something remarkable is that O4 and O5 vary together. Its ratio O4/O5 before the treatment is  $0.6 \pm 0.1$ , during the treatment  $1.2 \pm 0.1$ , and after the treatment  $1.2 \pm 0.1$ . Initially, in natural wood, O4 is higher than O5. During the treatment, O4 and O5 are almost similar, being bigger the contribution of O5 than O4. Finally, after the treatment (cooling wood), the contribution of O5 is higher than O4, as shown by the higher O4/O5 ratio. As we reduce O-C=O contribution, we increase C-O contribution even that C-O contribution, in general, is diminished after the delignification process where lignin and hemicellulose are removed. The reduction of O-C=O leads to some increase in C-O (with respect to each other) could be attributed to that as in hemicellulose O-C=O breaks liberating  $\text{CH}_3$  hydrogen could be attached to the oxygen in hemicellulose, resulting in a contribution of C-OH and a structure more similar to cellulose. This is confirmed by reducing FTIR peak at  $1231 \pm 4 \text{ cm}^{-1}$  of C-O stretching of lignin and hemicellulose. It demonstrates the reduction observed in C-O of C1s and O1s spectra of XPS. At the same time, FTIR peak at  $1052 \pm 4 \text{ cm}^{-1}$  of C-O stretching of C-OH of cellulose increase in FTIR. This probe the ratio relation of O4/O5, the reduction of O-C=O and C-O increase.

Additionally, Sodium auger electron (O6) contribution is present in treated wood even if we do not have the peak of Na1s spectra. This is a lower contribution from the chemical treatment with  $\text{Na}_2\text{SO}_3$  and NaOH that remains in the sample. But they were efficiently removed after the last washes and the treatment with  $\text{H}_2\text{O}_2$  that lead us to cooling wood where this peak is no longer present.

#### 4.3.2 Eucalipto

As seen in figure 4.9 is presented the fitting for C1s and O1s spectra for Eucalipto wood, Eucalipto treated wood, and Eucalipto cooling wood. In table 4.4 we summarize the binding energy (BE) of the peaks and its assignment for Eucalipto non-treated wood (BWNTW), Eucalipto treated wood (BETW), and Eucalipto cooling wood (BECW) for the whole elements identified in the XPS. For spectra of C1s, in Eucalipto NTW, we have a shift of the equipment, and we have the spectra cut. However, two peaks were identified at  $284.7 \pm 0.5$  and  $286.3 \pm 0.5 \text{ eV}$  corresponding to carbon bonded to carbon C-C and C-H and carbon

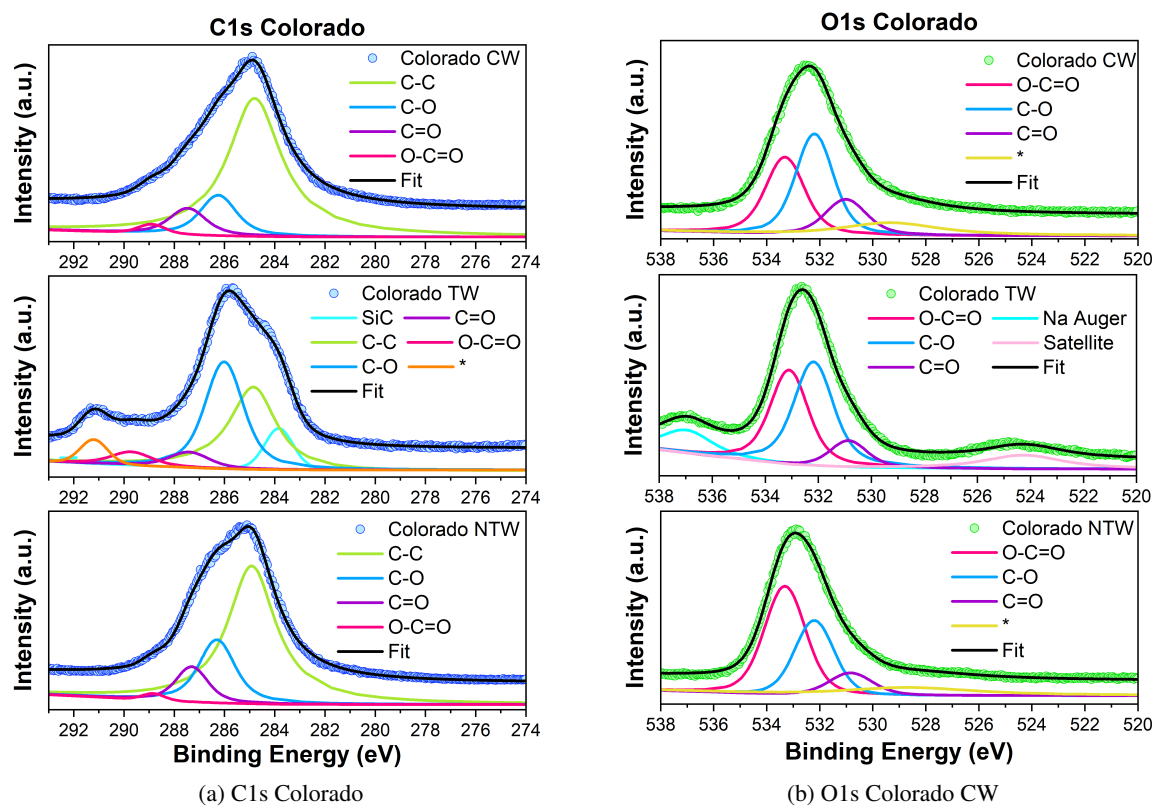


Figure 4.7: C1s and O1s XPS spectra of Colorado for non-treated wood (NTW), treated wood (TW) and cooling wood (CW).

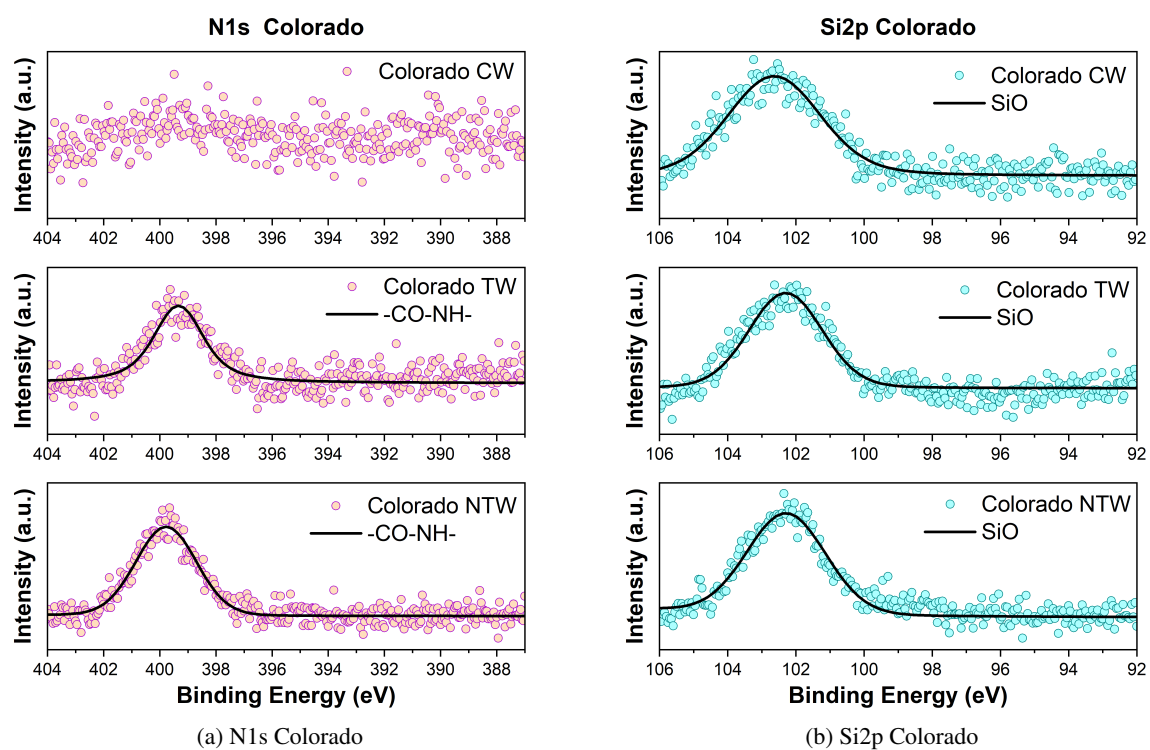


Figure 4.8: N1s and Si2p XPS spectra of Colorado for non-treated wood (NTW), treated wood (TW) and cooling wood (CW).

Colorado					
C1s	BE NTW ( $\pm 0.5$ eV)	BE TW ( $\pm 0.5$ eV)	BE CW ( $\pm 0.5$ eV)	RBE (eV)	Assignment
C1	-	283.8	-	283.8 <sup>76</sup>	SiC
C2	284.9	284.8	284.8	284.8 <sup>77</sup>	C-C/C-H
C3	286.3	286.0	286.2	286.3 <sup>78</sup>	C-O
C4	287.3	287.4	287.5	287.3 <sup>79</sup> 287.8 <sup>78</sup>	C=O/O-C-O
C5	288.8	289.7	288.9	288.7 <sup>80</sup> 289.8 <sup>81</sup>	O-C=O
C6	-	291.2	-	291.3 <sup>80</sup>	Shake up
O1s	BE NTW	BE TW	BE CW	RBE	Assignment
O1	-	524.2	-	-	Satellite
O2	528.7		529.3	-	*
O3	530.8	530.9	531.0	531.0 <sup>77</sup>	C=O
O4	532.2	532.2	532.2	532.2 <sup>75,82</sup>	C-O
O5	533.3	533.1	533.3	533.3 <sup>75,78</sup>	O-C=O
O6	-	537.0	-	536.0	Na Auger
N1s	BE NTW	BE TW	BE CW	RBE	Assignment
N1s	399.8	399.3	-	399.9 <sup>75</sup>	-CO-NH-
Si2p	BE NTW	BE TW	BE CW	RBE	Assignment
Si2p	102.3	102.3	102.6	102.3 <sup>83</sup>	SiO

Table 4.3: Peaks assignments for XPS spectra C1s, O1s, N1s and Si2p for Colorado for non-treated wood (NTW), treated wood (TW) and cooling wood (CW).

bonded to oxygen C-O, for treated wood were identified 5 peaks at  $284.9 \pm 0.5$ ,  $286.2 \pm 0.5$ ,  $287.4 \pm 0.5$ ,  $289.7 \pm 0.5$ , and  $291.4 \pm 0.5$  eV. The first is C-C/C-H, the second C-O, the third C=O, the fourth O-C=O, and the last to the satellite. In Colorado, wood was identified four peaks centered at  $284.8 \pm 0.5$ ,  $286.3 \pm 0.5$ ,  $287.8 \pm 0.5$ , and  $289.1 \pm 0.5$  eV. The first is C-C/C-H, the second for C-O, the third C=O, and the last for O-C=O.

For spectra of O1s, for Eucalipto non-treated, we can just identify one peak at  $532.9 \pm 0.5$  eV related to the O-C=O. This peak tells us that even we have cut that part for the C1s spectra, we can consider if the

whole C1s spectra were showed we could observe this part's contribution. For treated wood, was identified five peaks centered at  $524.9 \pm 0.5$ ,  $531.1 \pm 0.5$ ,  $532.2 \pm 0.5$ ,  $533.3 \pm 0.5$ , and  $537.5 \pm 0.5$  eV. The second peak comes from C=O, the third from C-O, the fourth to O-C=O, and the last to Na auger electron. In the cooling wood, case were identified 3 peaks centered at  $531.0 \pm 0.5$ ,  $532.2 \pm 0.5$ , and  $533.3 \pm 0.5$  eV. The first is related to C=O, the second to C-O, and the third to O-C=O, which are related to the peaks identified in C1s spectra.

Figure 4.10 shows the spectra of N1s and Si2p. For N1s spectra, we could not identify a well-defined peak in non treated wood, for treated wood we have a peak centered at  $399.8 \pm 0.5$  eV, and for cooling wood, we have a main peak centered at  $399.8 \pm 0.5$  eV, which is related to -CO-NH-.<sup>75</sup>

For Si2p in non-treated wood, we identify a peak centered at 102.06 eV for treated wood at 103.08 and for cooling wood at  $102.3 \pm 0.5$  eV. This is mainly to the contribution of SiC.

In C1s spectra, C-C/C-H (C2) contribution decreased during and after the treatment, C-O (C3) decreases during the treatment and increases after the treatment. C=O/C-O-C (C4) contribution could not be observed due to XPS spectra' shift, so the graph is incomplete. But from treatment to cooling wood, this contribution increases, and O-C=O (C5) contribution is also not present in non-treated; with respect to treatment, in cooling wood, this contribution increases. C2 partial reduction is related to the loss of lignin contribution. Even Eucalipto cooling wood is not completely white; it delignificates partially. On the other hand, cellulose also contributes to C-C and C-H peaks, making this peak bigger than others. Additionally, the ratio of C2/C3 was obtained before the treatment  $6.1 \pm 0.1$ , during the treatment  $1.7 \pm 0.1$ , and after the treatment  $3.8 \pm 0.1$ . Thus, we consider that C2 decreases its contribution as C3 increases as contrary as Colorado cooling wood. In Colorado, C3 contribution increases after the treatment at lower rates; this could be related to that the C1s spectrum is not complete, so that leads us to a higher FWHM as observed in the figure, and that could be the misreading of this peak. Nonetheless, C-O contribution changes can be observed better in O1s spectra. Even after the treatment, C2 (C-C/C-H) decreases a little due to the decrease of C-C of lignin, it still a stronger contribution in C1s spectra. That because, similar to Colorado, C-H contribution is related to cellulose I and II. FTIR peak at  $1322 \pm 4$  cm<sup>-1</sup> related to CH in-plane bending of cellulose I and II, and CH<sub>2</sub> wagging in cellulose I, II increase noticeably for Eucalipto cooling



wood. Also,  $1376 \pm 4 \text{ cm}^{-1}$  related to C-H deformation vibration of cellulose 1 also increases after the delignification process. Even a C-H stretch peak identified around  $2800 \pm 4 \text{ cm}^{-1}$  in the FTIR spectra is more defined after the delignification process.

The increase in C1s after the treatment with respect to during the treatment in C=O/C-O-C (C4) can be related to the FTIR peak increase for cooling wood at  $1030 \pm 4 \text{ cm}^{-1}$  of C-O-C stretching of primary alcohol cellulose and hemicellulose. Consequently, we have an increase in cellulose. The contribution of C-O-C is essential for the cooling power of the material; an increase in this FTIR peak means a higher emission in the atmospheric window which means an increase in the cooling power.

In O-C=O (C5), we cannot consider an increase or decrease for analyzing its contribution in C1s spectra since it is low. We can identify real increases or decreases by analyzing O1s spectra related to this peak. In principle, this contribution increases with respect to treated wood.

Thus, in oxygen spectra due to XPS shift, we were unable to identify an entire O1s spectrum for non-treated wood; thereby, the relations of changes in contribution will be related to treatment wood. C=O/C-O-C (O3) contribution increases for cooling wood, C-O (O4) reduces after the treatment, and O-C=O (O5) after the treatment decreases. The reduction of O-C=O functional groups is similar for Colorado after the treatment; this is related to hemicellulose structure disintegration. The reduction seems not to be highly representative as for Colorado. In Colorado, the removal of O-C=O functional groups reduces CH<sub>3</sub> groups as proved by the reduction of FTIR peak at  $1458 \pm 4 \text{ cm}^{-1}$  related to C-H asymmetric deformation in -OCH<sub>3</sub> in Colorado wood FTIR spectra (figure 4.3). However, for Eucalipto (figure 4.4), the peak at  $1458 \pm 4 \text{ cm}^{-1}$  in FTIR spectra still contributing. The reduction of O-C=O and CH<sub>3</sub> functional groups leads us hemicellulose more similar to cellulose structure, increasing cellulose's contribution as observed in Colorado where we remove almost all lignin and some cellulose. The low reduction of O-C=O and therefore the remaining of CH<sub>3</sub> groups confirm the presence of some entire hemicellulose or more lignin present in the sample that makes it hard to delignify the wood. We may have more hemicellulose in Eucalipto wood, which is more intertwined with lignin, and cellulose, which takes longer to separate cellulose and make free lignin. Nonetheless, this theory can be probed by analyzing the O1s entire spectra of non-treated Eucalipto. The small decrease of O-C=O can be that this transforms to

C=O, therefore increasing this peak's contribution. In FTIR spectra for Colorado, cooling wood peak at  $1736 \pm 4 \text{ cm}^{-1}$  related to C=O stretch ketone and carbonyl remains after the treatment here for Eucalipto; this peak disappears.  $1736 \pm 4 \text{ cm}^{-1}$  peak is related to hemicellulose. Thus, some hemicellulose was eliminated, and the contribution of CH<sub>3</sub> is of lignin and O-C=O groups too. Here as the difference from Colorado, hemicellulose is not transformed; it is more dissolved or eliminated. This gives us an insight that the problem of Eucalipto of delignified lower than Colorado can be due to the lignin is strong, and hemicellulose was more superficial than lignin, so after removing the hemicellulose, lignin star to being eliminated. Simultaneously, the increase of C=O/C-O-C (O3) in C1s and O1s spectra can be mainly for C-O-C since in FTIR spectra of cooling wood, the peak at  $1030 \pm 4 \text{ cm}^{-1}$ , related to C-O-C stretching of primary alcohol cellulose and hemicellulose, increases. The bigger the FTIR peak at  $1030 \pm 4 \text{ cm}^{-1}$  help in the cooling power. So from non-treated Eucalipto wood to cooling wood, the emissivity in this range will increase.

C-O (O4) contribution is present in all components, hemicellulose, lignin, and cellulose. Its decrease can be related to reducing hemicellulose and lignin in the wood after the treatment since we have a lower C-O contribution from hemicellulose and lignin because hemicellulose was more eliminated. As observed in the FTIR spectrum, the peak at  $1231 \pm 4 \text{ cm}^{-1}$  of C-O stretching of lignin from wood reduce in Eucalipto cooling wood. Nonetheless, as in the C1s spectrum, C-O seems to increase, but we are not sure since the spectra are not complete, but if there were an increase in C-O, this would be related mainly to the C-OH contribution in cellulose. In Colorado, there was identified that O4 and O5 vary together. Initially, in natural wood, O4 is higher than O5. During the treatment, O4 and O5 are almost similar, being bigger the contribution of O5 than O4. Finally, after the treatment (cooling wood), the contribution of O5 is higher than O4, as shown by the higher O4/O5 ratio. In this case of Eucalipto, we do not have that; we just have, as mentioned earlier, the reduction of O4 and O5 on their own as different of Colorado where the both are reduced but O5 increases with respect to the other. This can be related that now we do not have much the elimination of O-C=O peaks that gets free CH<sub>3</sub> and therefore could be some new peaks formed like C-O, C-OH because here in Eucalipto, the hemicellulose was more liberated or dissolved it was not transformed.

Additionally, Sodium auger electron (O6) contribution is present in treated wood even if we do not

have the peak of Na1s spectra. This is a lower contribution from the chemical treatment with  $\text{Na}_2\text{SO}_3$  and NaOH remains in the sample. But they were efficiently removed after the last washes and the treatment with  $\text{H}_2\text{O}_2$  that lead us to cooling wood where this peak is no longer present.

Here in Eucalipto, as different from Colorado, nitrogen was not present in the sample, but during and after treatment, it is present. It can be that the proteins happening in wood are more inside the wood, and the piece of non-treated wood measured was superficial, so we may not take a sample with that contribution. As the chemical process is carried out, wood loses some fibers of the surface, and inside it, we can find the proteins. The proteins were more exposed, and after the last treatment, their contribution is reduced. In this wood, we do not have the contribution of nitrogen.

### 4.3.3 Copal

As seen in figure 4.11 are presented the fitting for C1s and O1s spectrum for Copal non-treated wood (NTW), Copal treated wood (TW), and Copal cooling wood. In table 4.5 we summarize the peaks present in the whole XPS spectra and its assignment for Copal non-treated wood, treated, and Copal cooling wood. For Copal, there four peaks were identified centered at  $284.9 \pm 0.5$  and  $286.2 \pm 0.5$ ,  $287.4 \pm 0.5$ , and  $288.5 \pm 0.5$  eV. The first is C-C/C-H (O2), the second for C-O (O3), the third C=O (O4), and the last for O-C=O (O5). For treated wood, we have peaks at  $284.8 \pm 0.5$ ,  $286.4 \pm 0.5$ ,  $287.8 \pm 0.5$ ,  $289.9 \pm 0.5$ , and  $291.5 \pm 0.5$  eV. The first comes from C-C/C-H, the second for C-O, the third C=O, the fourth O-C=O with its shake-up line. For cooling wood, the spectrum is incomplete due to a shift of the XPS. However, two peaks were identified at  $284.7 \pm 0.5$ ,  $286.1 \pm 0.5$  eV, which are related to C-C/C-H and C-O, respectively.

For the spectra of O1s, for Copal non-treated, we can identify peaks at  $530.6 \pm 0.5$ ,  $532.4 \pm 0.5$ , and  $533.7 \pm 0.5$  eV. The first is related to C=O, the second to C-O, and the third to O-C=O, which are related to the peaks identified in C1s spectra. For treated wood, we recognized peaks at  $530.9 \pm 0.5$ ,  $532.1 \pm 0.5$ , and  $533.3 \pm 0.5$  eV; similar to non-treated wood, we have additional peaks at  $524.2 \pm 0.5$  and  $536.7 \pm 0.5$  eV related to satellite and sodium auger electron, respectively. In the cooling wood case, there was

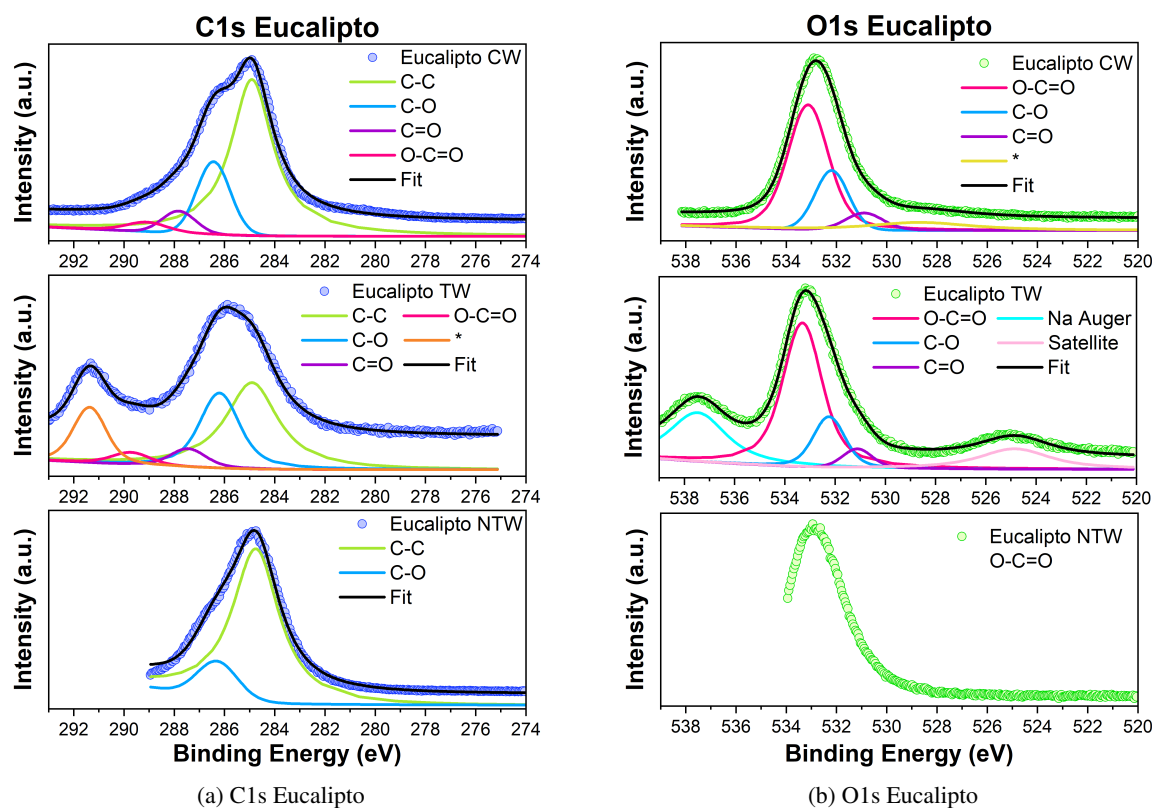


Figure 4.9: C1s and O1d XPS spectra of Eucalypto for non-treated wood (NTW), treated wood (TW) and cooling wood (CW).

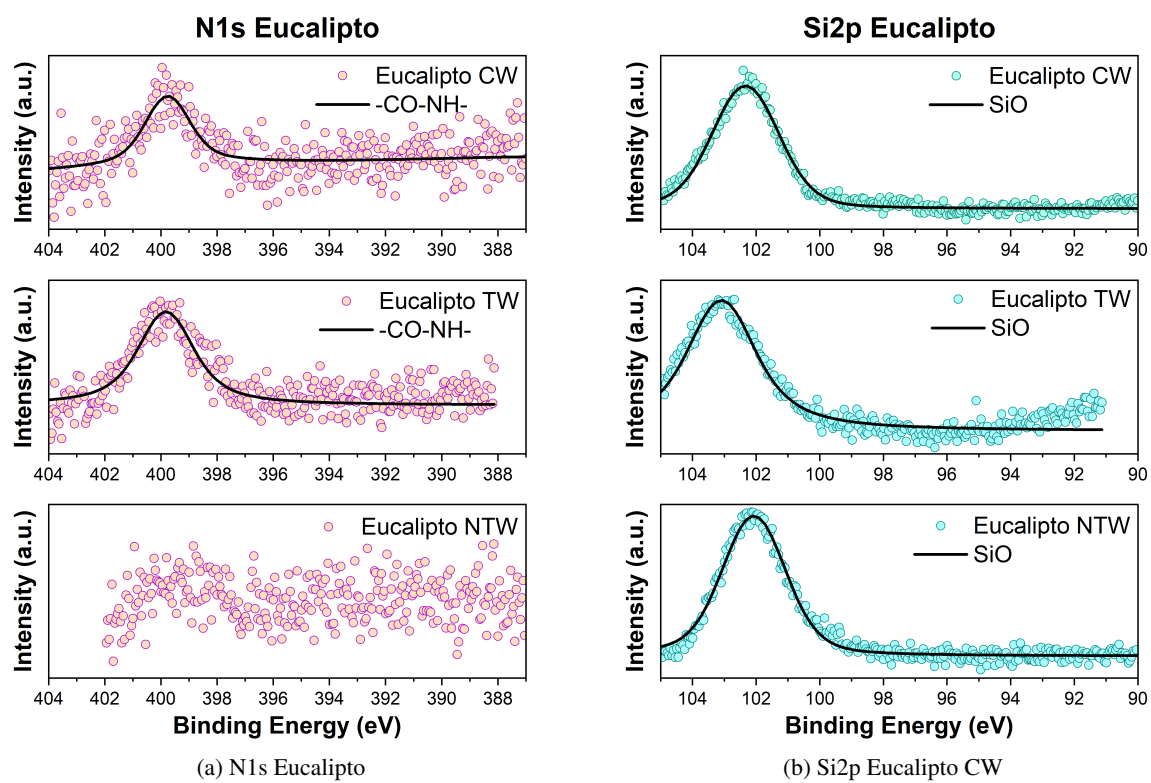


Figure 4.10: N1s and Si2p XPS spectra of Eucalypto for non-treated wood (NTW), treated wood (TW) and cooling wood (CW).

<b>Eucalipto</b>					
<b>C1s</b>	<b>BE NTW</b> ( $\pm 0.5$ eV)	<b>BE TW</b> ( $\pm 0.5$ eV)	<b>BE CW</b> ( $\pm 0.5$ eV)	<b>RBE</b> (eV)	<b>Assignment</b>
C1	284.7	284.9	284.9	284.8 <sup>77</sup>	C-C/C-H
C2	286.3	286.2	286.4	286.3 <sup>78</sup>	C-O
C3	-	287.4	287.8	287.8 <sup>78</sup>	C=O/C-O-C
C4	-	289.7	289.1	289.1 289.8 <sup>81</sup>	O-C=O
C5	-	291.4	-	291.3 <sup>80</sup>	Shake up
<b>O1s</b>	<b>BE NTW</b>	<b>BE TW</b>	<b>BE CW</b>	<b>RBE</b>	<b>Assignment</b>
O1	-	524.9	-	-	Satellite
O2	-	-	528.7	-	*
O3	-	531.1	530.9	531.0 <sup>77</sup>	C=O
O4	-	532.2	532.2	532.2 <sup>75,82</sup>	C-O
O5	532.9	533.3	533.1	533.3 <sup>75,78</sup>	O-C=O
O6		537.5	-		Na Auger
<b>N1s</b>	<b>BE NTW</b>	<b>BE TW</b>	<b>BE CW</b>	<b>RBE</b>	<b>Assignment</b>
N1s	-	399.8	399.8	399.9 <sup>75</sup>	-CO-NH-
<b>Si2p</b>	<b>BE NTW</b>	<b>BE TW</b>	<b>BE CW</b>	<b>RBE</b>	<b>Assignment</b>
Si2p	102.1	103.1	102.3	102.3 <sup>83</sup>	SiO

Table 4.4: Peaks assignments for XPS spectra C1s, O1s, N1s and Si2p for Eucalipto for non-treated wood (NTW), treated wood (TW) and cooling wood (CW).

a significant shift, so it is impossible to identify a peak, but it looks as if it will have similar behavior as non-treated wood. For N1s spectra, we could not identify well-defined peaks in non-treated wood, treated wood neither to cooling wood. As in the first part, we talk that wood is conformed of cellulose, hemicellulose, lignin, and some extractives. Copal have lower amounts of extractives used to contribute to nitrogen. Thus we have not nitrogen contribution as in Colorado and Eucalipto. For Si2p in non-treated wood, we identify a peak centered at  $102.6 \pm 0.5$  eV for treated wood at  $102.9 \pm 0.5$  eV and for cooling wood at  $102.1 \pm 0.5$  eV. This is mainly to the contribution of SiO. This contribution is primarily due to dust particles deposited in the sample at the time of measurements.

In C1s spectra, C-C/C-H (C2) contribution decreased during and after the treatment, C-O (C3) decreases

during the treatment and after the treatment. C=O/C-O-C (C4) contribution decreases during the treatment, and after it could not be observed due to XPS spectra's shift, the graph is incomplete. O-C=O (C5) contribution increases during the treatment and after the treatment could not be observed due to XPS spectrum shift. C2 partial reduction is related to the loss of lignin contribution. Even Copal cooling wood is not completely white; it delignifies partially. On the other hand, cellulose also contributes to C-C/C-H peaks, making this peak bigger than others. Additionally, the ratio of C2/C3 was obtained before the treatment  $1.3 \pm 0.1$ , during the treatment  $1.5 \pm 0.1$ , and after the treatment  $4.3 \pm 0.1$ . Thus, we consider that C2 increases its contribution as C3 decreases, similar to Colorado cooling wood and different from Eucalipto wood. C1s spectrum of Copal cooling wood is not complete, so talking to contribution and C2/C3 ratio may be a little confused due to the area measured of C3 is not complete. Nonetheless, during the treatment, we also observe an increase in the ratio C2/C3 and a decrease in C2 contribution that give us an insight. During and after the treatment, C2 (C-C/C-H) decreases slightly due to the decrease of C-C of lignin. Nonetheless, C2 still is the stronger contribution in C1s spectra. That because, similar to Colorado, C-H contribution is related to cellulose I and II. FTIR peak at  $1320 \pm 4 \text{ cm}^{-1}$  related to CH in-plane bending of cellulose I and II, and CH<sub>2</sub> wagging in cellulose I, II increase noticeably for Copal cooling wood. Also,  $1365 \pm 4 \text{ cm}^{-1}$  related to C-H deformation vibration of cellulose one also increases after the delignification process. Even a peak of C-H stretch identified around  $2800 \pm 4 \text{ cm}^{-1}$  in the FTIR spectra (figure 4.5) is more defined after the delignification process.

The decrease in C=O/C-O-C (C4) during the treatment with respect to non-treated wood is similar to Eucalipto, also in Eucalipto, after the treatment, it increases. We can not identify that increase after the treatment in Copal since we do not have that part of the spectrum after the treatment. The decrease during the treatment is related to having some hemicellulose removed. We are not transforming that hemicellulose as in Colorado. C=O contribution of hemicellulose in FTIR peak at  $1736 \pm 4 \text{ cm}^{-1}$  is no longer present during treatment.

In O-C=O (C5), we cannot consider an increase or decrease of contribution in C1s spectra since C5 contribution is low. We can identify real changes by analyzing O1s spectra related to this peak, but we do not have the entire spectrum for cooling wood. In the C1s spectrum, this contribution increases during the

treatment.

Thus, in oxygen spectra due to XPS shift, we could not identify an entire O1s spectrum for cooling wood; thereby, the relations of contribution changes will be related to non-treated wood to treated wood. C=O/C-O-C (O3) contribution decrease for treated wood, C-O (O4) reduces during the treatment and O-C=O (O5) during the treatment increases. The increment of O-C=O functional groups is similar for Colorado during the treatment. In Colorado, after the treatment, that contribution decreases; this is related to hemicellulose structure disintegration that happens during the treatment where hemicellulose is more exposed to the surface, giving more interaction. Simultaneously, the decrease of C=O/C-O-C (O3) during the treatment can be mainly for C=O reduction as hemicellulose is reduced, as happens a similar decrease in the C1s spectra during the treatment. In Colorado, during the treatment, C=O contribution increases as different from here since we were not transforming the hemicellulose as in Colorado. C-O (O4) contribution is present in all components, hemicellulose, lignin, and cellulose. Its decrease during the treatment can be related to partially reducing hemicellulose and lignin in the wood. We have a lower C-O contribution from hemicellulose and lignin because hemicellulose is eliminated apart during the process. As observed in the FTIR spectrum of treated wood, the peak at  $1231 \pm 4 \text{ cm}^{-1}$  of C-O stretching of lignin from wood reduce /eliminated. Also, in the C1s spectrum, C-O during the treatment decreases.

In Colorado, we identified that O4 and O5 vary together before, during, and after the treatment. Initially, in natural wood, O4 is higher than O5. During the treatment, O4 and O5 are almost similar, being bigger the contribution of O5 than O4. Finally, after the treatment (cooling wood), the contribution of O5 is higher than O4, as shown by the higher O4/O5 ratio. In this case of for Copal, we have, as mentioned earlier, a bigger reduction of O4 and increment of O5 during the treatment different from Colorado wood. This can be related that during the treatment in Copal, there is a significant reduction of lignin and hemicellulose, which means the reduction of O4. On the other hand, we do not have the elimination of O-C=O peaks that liberates  $\text{CH}_3$ , and that permits the material to build some new peaks like C-O, C-OH. Here in Copal, some hemicellulose is still present during treatment, and others were more liberated or dissolved; hemicellulose was not transformed.

Similar to Colorado and Eucalipto we have, Sodium auger electron (O6) contribution is present in



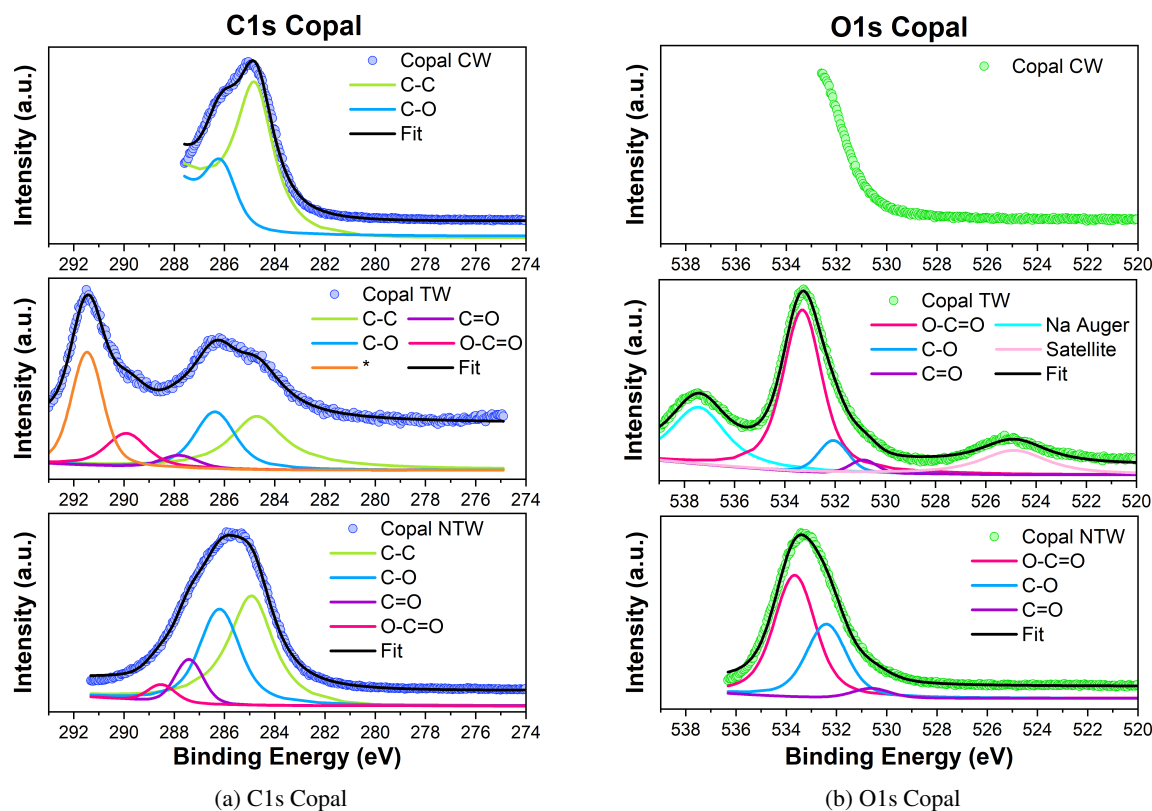


Figure 4.11: C1s and O1s XPS spectra of Copal for non-treated wood (NTW), treated wood (TW) and cooling wood (CW).

treated wood. This is a lower contribution from the chemical treatment with  $\text{Na}_2\text{SO}_3$  and NaOH remains in the sample. But they were efficiently removed after the last washes that lead us to cooling wood where this peak is no longer present.

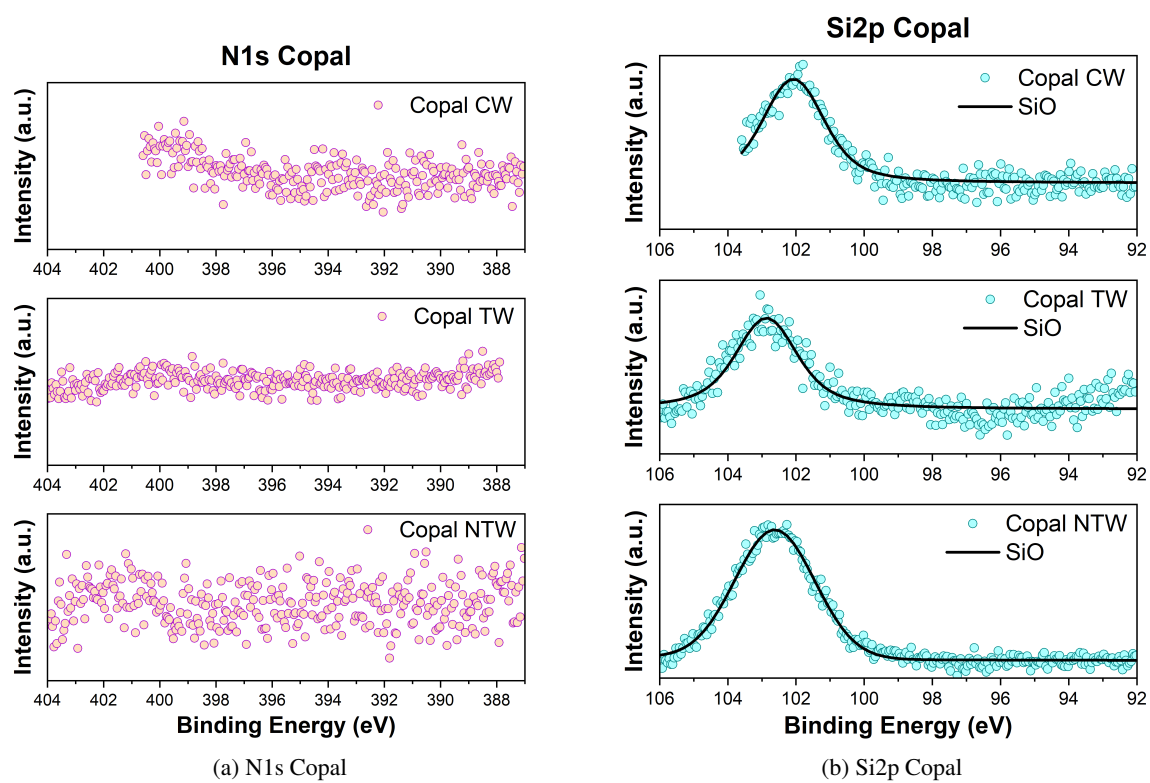


Figure 4.12: N1s and Si2p XPS spectra of Copal for non-treated wood (NTW), treated wood (TW) and cooling wood (CW).

<b>Copal</b>					
<b>C1s</b>	<b>BE NTW</b> ( $\pm 0.5$ eV)	<b>BE TW</b> ( $\pm 0.5$ eV)	<b>BE CW</b> ( $\pm 0.5$ eV)	<b>RBE</b> (eV)	<b>Assignment</b>
C2	284.9	284.8	284.7	284.8 <sup>77</sup>	C-C/C-H
C3	286.2	286.4	286.1	286.3 <sup>78</sup>	C-O
C4	287.4	287.8	-	288.3 <sup>77</sup>	C=O/C-O-C
C5	288.5	289.9	-	289.8 <sup>81</sup>	O-C=O
C6	-	291.5	-	291.5	Shake up <sup>84</sup>
<b>O1s</b>	<b>BE NTW</b>	<b>BE TW</b>	<b>BE CW</b>	<b>RBE</b>	<b>Assignment</b>
O1	-	524.2	-	-	Satellite
O3	530.6	530.9	-	531.1 <sup>77</sup>	C=O
O4	532.4	532.1	-	532.2 <sup>75,82</sup>	C-O
O5	533.7	533.3	-	533.3 <sup>75,78</sup>	O-C=O
O6	-	536.7	-	536.0	Na Auger
<b>Si2p</b>	<b>BE NTW</b>	<b>BE TW</b>	<b>BE CW</b>	<b>RBE</b>	<b>Assignment</b>
Si2p	102.6	102.9	102.1	102.3 <sup>83</sup>	SiO

Table 4.5: Peaks assignments for XPS spectra C1s, O1s, N1s and Si2p for Copal for non-treated wood (NTW), treated wood (TW) and cooling wood (CW).

## 4.4 Cooling Performance

In order to identify the cooling performance of the materials, we study their emissivity in the range of the atmospheric window. In figure 4.13, we observe the FTIR spectra for Colorado (blue), Copal (purple), and Eucalipto (pink) cooling woods in terms of the emissivity with the atmospheric transmission spectra (observed as light blue), in the 8 to 13 micrometers range (atmospheric window). We measured the transmittance with the FTIR spectra and we put it in terms of emissivity by considering 1 minus transmittance, just for visible purposes. In Table 4.6 we have the emissivity values in the atmospheric

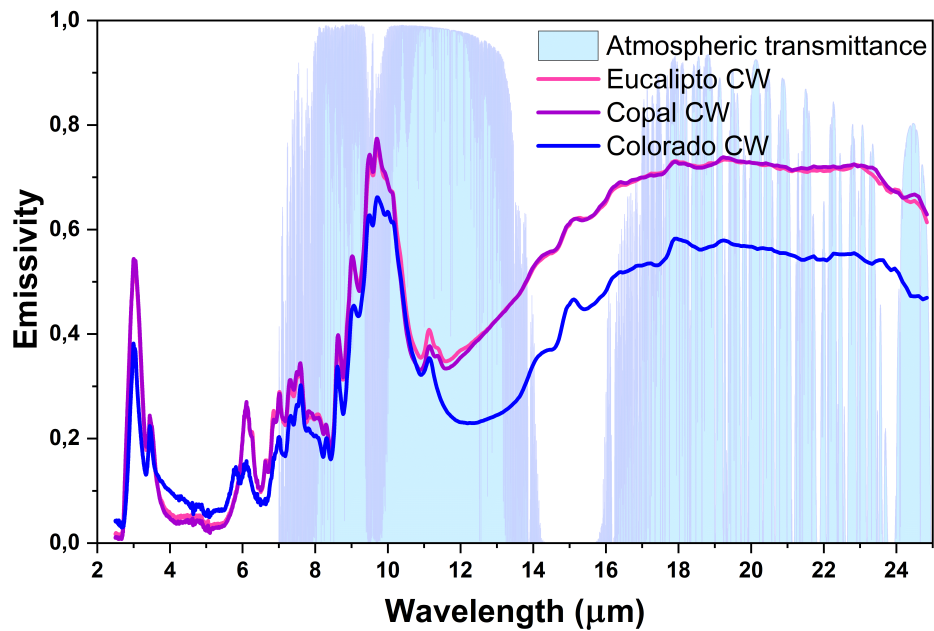


Figure 4.13: Emissivity of cooling woods: Colorado (blue), Copal (purple) and Eucalipto (pink) with respect to the atmospheric transmission where the atmospheric window is observed. Transmission and emissivity is dimensionless<sup>3</sup>

window region. Using only emissivity in this range, we should judge which material could be the best cooling wood considering only its behavior at night when radiation in the optical range is not an issue. In

Table 4.6, the material with the best emissivity is Eucalipto, which should be the material with the best cooling power at night. Nonetheless due to the errors of the values we can not confirm the material with the best emissivity. We can affirm that the three materials have a value really close to each other. Therefore, the three materials should a similar cooling power at night.

By day, Eucalipto and Copal are not as reflective in the optical range (not as white) as Colorado; therefore, Eucalipto and Copal should be heated more at day that will make us difficult to identify cooling power during the day. Also, we find that the emissivity increases with the delignification process. Cooling wood materials have higher emissivity than non-treated wood. Nonetheless, the FTIR equipment used to obtain the infrared spectra of transmittance may be subject to misreadings; this equipment give us more a qualitative measurement. Since the ATR (attenuated total reflectance) accessory used for FTIR measures good reflectance but in our case, was considering export the data in terms of transmittance. In this equipment, the light bounces up to the sample, and it reflects and goes back and then arrived at the detector. Thus the path length for measurement is very small. In relation to that, the equipment process that data and gives the FTIR spectrum in terms of transmittance. Transmittance measurements are not feasible since, for that, the path length must be larger. Thus higher intensities from one material to the other are not reliable. Nonetheless, this measurement gives us the qualitative characterization of the material and some insights that the cooling wood's main peaks are in the atmospheric window range. Additionally, as stated in the methodology, the piece of the material used for this measurement was approximately 1 mm of thickness. Nonetheless, the size measured could influence the intensity measurement of (attenuated total reflectance) since as it can be thin enough to be partially transparent, the transmittance can be higher. Therefore, that could contribute to having lower emissivity than the real one. In order to analyze those relations of increases in emissivity correctly, it is essential to measure the IR spectrum with other equipment and directly the emissivity of the material in the region from 8 to 13 micrometers of the entire material or with a more considerable thickness.

Until now to diminished that error, the values of emissivity were obtained by making an average of three FTIR spectra of different pieces of the same material.

Material/Emissivity	Non treated Wood	Cooling Wood
Manzano Colorado	$0.26 \pm 0.02$	$0.36 \pm 0.09$
Eucalipto	$0.24 \pm 0.04$	$0.43 \pm 0.09$
Copal	$0.27 \pm 0.07$	$0.43 \pm 0.01$

Table 4.6: Emissivity in the range of the atmospheric window (8 to 13 micrometers). It is important to notice that emissivity is dimensionless.<sup>3</sup>

Next, we measured the materials' temperature in relation to the ambient reference temperature: Colorado, Copal, and Eucalipto cooling wood and the ambient temperature as stated in the methodology. The temperature was measured during the day and night. First, during the day, we measured with the box closed and then with the box open; by open box, we mean without polyethylene cover film. In the appendix we explain the results for the closed box. We identify a difference in temperature lower or non-existent for a closed box in contrast with the open box. It may be possible that the polyethylene film is not totally invisible in the infrared region since, at night, it is also difficult to identify a difference in temperature in the closed box. In the future, the infrared spectra of polyethylene film used must be checked.

In the day, it may be that the insulator box is exposed to direct sunlight due to the hole of the box covered by polyethylene film, the box heats inside, and the box preserves that heat, making it more challenging to identify the temperature difference produced by passive cooling. Once the heat is in the box, it is difficult to cold; therefore, the materials are in a heater environment than outside. Also, we need to consider that the material we study is too small, making us more difficult to identify a temperature difference from the material to the ambient temperature at day. Since the materials are small, the sun can quickly heat them, even if they are white, and try to reflect all solar radiation or emit in the atmospheric window spectrum. While, we measured the temperature difference for the three materials, we measured the cooling power in another sealed box to eliminate heat loss due to convection and conduction. Then, we calculated the average power needed to heat the sample until ambient temperature, and we divide by the area of the materials and obtain the average cooling power per area<sup>1</sup>. Similarly, we also study the cooling performance of the

materials at night. For this case, we measure with the open box 1 hour for each material, and in the same way, we estimate the average cooling power. The measures with the open box will be discussed here. The boxes were exposed to direct sunlight in Ibarra/Ecuador during the day and in the same place for the night measurements. Finally, since cooling power at day is challenging to identify, we calculated the cooling power expected at day using the temperatures measured (at day) for the ambient and the material and the emissivity obtained previously. The equations used were explained in Chapter 2. The net cooling power  $P_{net}$  was measured in the atmospheric region 8 to 13 micrometers as<sup>1</sup>:

$$P_{net} = P_{rad} - P_{atm} - P_{solar} - P_{norad} \quad (4.1)$$

It is important to highlight that the way of calculating the cooling power during the day is similar to the night time measurements since we are studying in the region of the atmospheric window, considering a structure that reflects strongly the solar radiation and therefore considering  $P_{solar}=0$ . The difference will be in the temperature measured since at night we identified lower temperatures of the cooling wood with respect to ambient temperature.

#### 4.4.1 Colorado

In figure 4.14, we observe the results for temperature measurements of Colorado cooling wood during the day (a) and night (b). There the green line is the material temperature, the purple line the ambient temperature, and the pink line the untreated wood. During the day, the average difference in temperature is  $0.6 \pm 0.2$  °C but can reach  $2.0 \pm 0.2$ °C. Some increases in difference in temperature in some times are related to the absence of clouds; with clouds there is an increase in downwelling sky radiation than for a clear sky. Thus bigger surface radiation losses on clear days results in greater and faster temperature drops<sup>85</sup>. We measured the temperature for approximately 2 hours in the afternoon (13:00 h -15:00 h). In the morning, the weather was hotter without clouds, and in the afternoon, the weather was colder and cloudy. The measured cooling power of Colorado was an average of  $0.012 \pm 0.002$  W and over the area ( $0.0002 \pm 0.00003$  m<sup>2</sup>) is  $60 \pm 20$  Wm<sup>-2</sup>. This results are consistent with the values obtained in

bibliography. According to Li *et al.*, for basswood cooling wood, they obtained an average cooling power at day of  $37 \text{ Wm}^{-2}$  and a sub-ambient temperature of  $4^\circ\text{C}$ <sup>23</sup>. Materials reviewed in the theoretical framework like photonic material performed by Raman *et al.* at sunlight has a temperature of  $4.9^\circ\text{C}$  below ambient temperature and a cooling power of  $40.1 \text{ Wm}^{-2}$ <sup>5</sup>; a glass-polymer hybrid metamaterial performed by Zhai *et al.* has a cooling power of  $93 \text{ Wm}^{-2}$ <sup>27</sup>; and a polymer coating made by Mandal *et al.* has a sub ambient temperature of  $6^\circ\text{C}$  and a cooling power of  $96 \text{ Wm}^{-2}$ <sup>8</sup>. Colorado cooling wood has a lower temperature difference with respect to ambient temperature but a higher cooling power than basswood cooling wood performed by Li *et al.* Since we have a material with a lower difference in temperature, we should have lower cooling power, but it is not the case. Concerning cooling power higher for Colorado, it could be due to measurement error since the value of basswood from theory is still in the range of the error measured. Additionally, we can say that we have lower cooling power than the basswood of Li *et al.* because we have a lower temperature difference. In the paper of Li *et al.*, the emissivity of basswood cooling wood is closed to 1. Therefore, its cooling power and difference in temperature with respect to ambient should be higher during the day and during the night. Nonetheless, the difference in temperature reported in Colorado of  $0.6 \pm 0.2^\circ\text{C}$  should be higher, but at the same time lower than  $4 \pm 0.2^\circ\text{C}$ . This can be due to the error in thermometers and also the insulating box used for the measurements. For the difference in temperature measurements, in our case, we used open boxes due to the lack of a complete transparent windshield of polyethylene. Therefore, hot air could heat our samples, so we could not identify a difference in temperature since nonradiative contribution increases for those conditions.

In order to prove if the material has passive radiative cooling, we measure its performance at night figure 4.14 b. For Colorado, the difference in temperature at night is on average  $2.7 \pm 0.2^\circ\text{C}$ . The cooling power average is  $0.015 \pm 0.02 \text{ W}$  and over the area of the material ( $0.0002 \pm 0.00003 \text{ m}^2$ ) is  $80 \pm 20 \text{ Wm}^{-2}$ . This cooling power and difference in temperature obtained is well related to the one obtained by Li *et al.* basswood cooling wood<sup>23</sup>. During the night they obtained an average cooling power of  $101 \text{ Wm}^{-2}$  with a sub-ambient temperature of  $9^\circ\text{C}$ . Also in other studies Zhai *et al.* performed a glass-polymer hybrid metamaterial with a cooling power of  $110 \text{ Wm}^{-2}$ <sup>27</sup>. Those materials of bibliography increases its cooling power and temperature differences for night measurements as in our case. As compared with



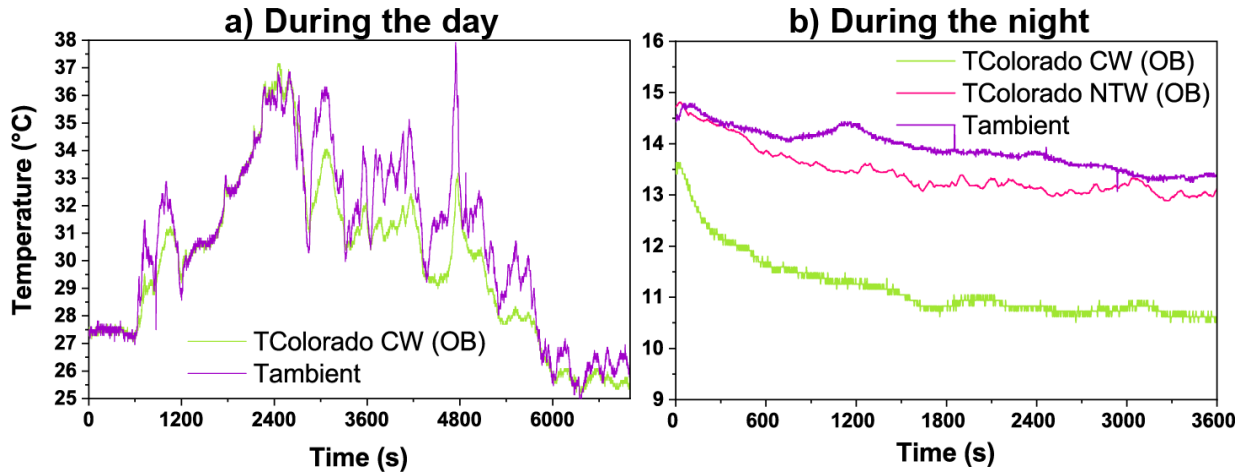


Figure 4.14: Manzano Colorado cooling wood temperature during the day (a), and during the night (b), where (green) is the temperature of Colorado cooling wood, (purple) ambient temperature, and (pink) untreated Colorado wood over time in an open box.

nanowood of Li *et al.*, they achieved a high emissivity in the atmospheric window on their material. Thus, its cooling power is higher than the one obtained by us. Therefore we obtained values in well relation with bibliography.

It is also observed in figure 4.14 b that the nontreated wood has a temperature higher than the cooling wood. Thus, the delignification process increases the cooling power at night of the material by increasing the emissivity in the atmospheric window range.

Theoretically, we study the cooling power based on the temperature results during the day of figure 4.14 and the emissivity in Table 4.6. The equations used were explained in theory section. In figure 4.15 we study the cooling power expected for the previous temperatures in the atmospheric window spectrum. For Colorado, we obtained an average net cooling power of  $40 \pm 10 \text{ Wm}^{-2}$ .

Thus, the cooling power measured during the day is on average  $60 \pm 20 \text{ Wm}^{-2}$  and the expected  $40 \pm 10 \text{ Wm}^{-2}$  where this is calculated just in the region of 8-13 micrometers which will be the same if we consider an entire reflective material in the whole spectrum except in the atmospheric window. In the same way the cooling power at night is  $80 \pm 20 \text{ Wm}^{-2}$ . which is higher than during the day and as the cooling

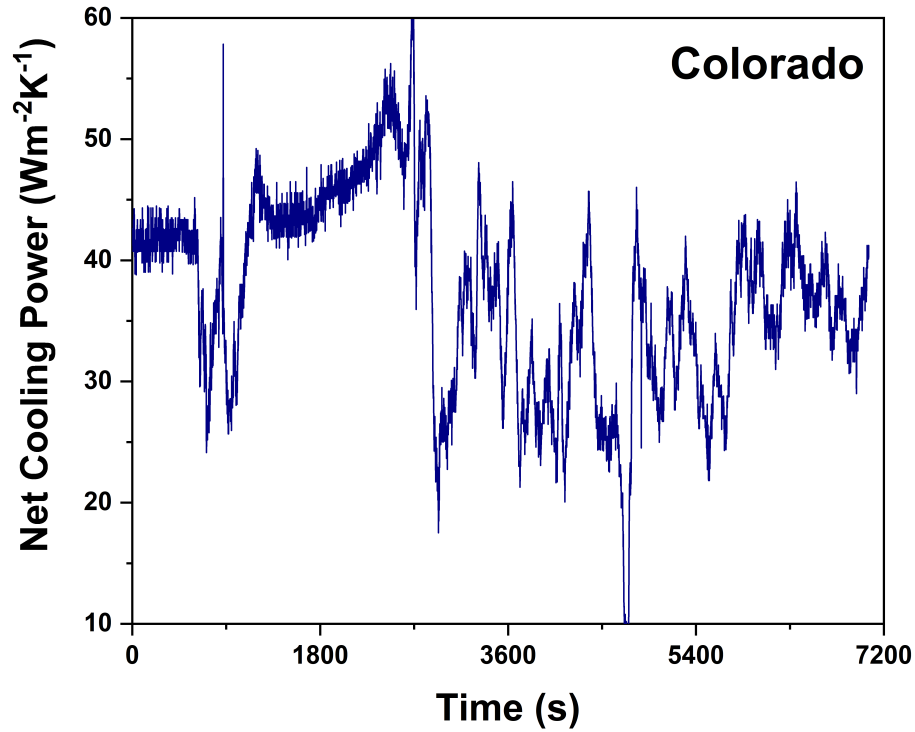


Figure 4.15: Colorado net cooling power with respect to time expected during the day.

power expected. We are confirming indeed that the emissivity is higher than that measured by FTIR. Additionally, we confirm the theory that the cooling power is better at night. For the expected values, we may have lower values than the measured ones since the emissivity we consider is very low and could be lower than the real one.

#### 4.4.2 Eucalipto

In the case of Eucalipto, in figure 4.16 we have the temperature difference during the day (a), and at night (b) in an open box. During the day, the temperature difference is almost non-existent for both cases for closed box (see appendix) and open box. The average difference in temperature for the open box is  $0.02 \pm$

0.2 °C. The measured cooling power of Eucalipto was  $0.008 \text{ W} \pm 0.002 \text{ W}$ , and the net cooling power over the area of the sample ( $0.0004 \pm 0.00004 \text{ m}^2$ ), is  $20 \text{ Wm}^{-2} \pm 7 \text{ Wm}^{-2}$ .

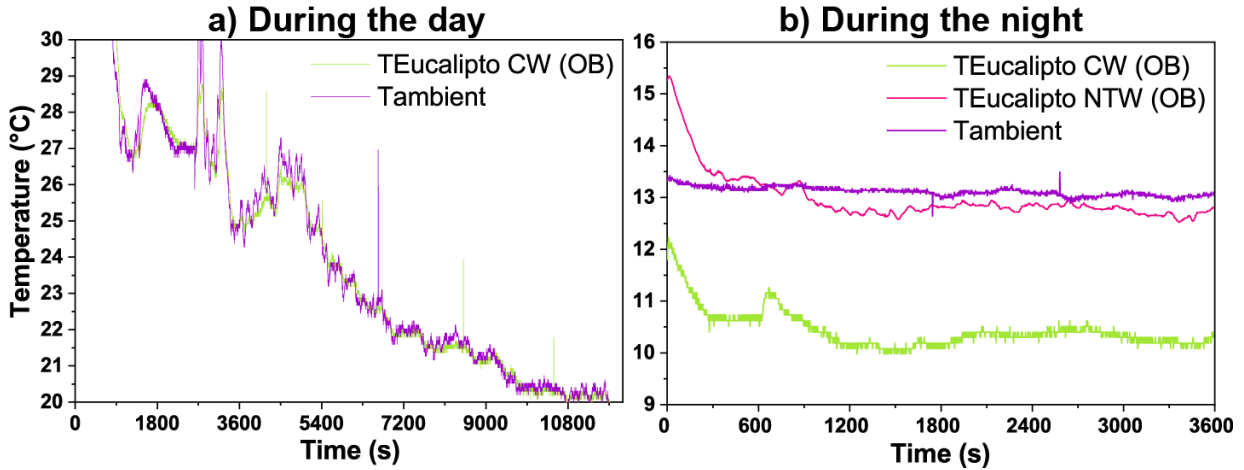


Figure 4.16: Eucalipto cooling wood temperature during the day (a) and during the night (b), where (green) is the temperature of Eucalipto cooling wood, (purple) ambient temperature, and (pink) untreated Eucalipto wood over time in an open box.

On the other hand, at night the average difference in temperature between ambient and the material is  $2.7 \text{ °C} \pm 0.2 \text{ °C}$ . The cooling power measured is  $0.013 \pm 0.002 \text{ W}$  and over the area of the material  $33 \pm 8 \text{ Wm}^{-2}$ . Similar as before is observed in figure 4.16 b that the non-treated wood has higher temperature than the cooling wood of Eucalipto. For Eucalipto the expected cooling power at day is observed in figure 4.17 with an average net cooling power of  $40 \pm 10 \text{ Wm}^{-2}$ .

Thus, the cooling power measured is on average  $20 \text{ Wm}^{-2} \pm 7 \text{ Wm}^{-2}$  and the expected  $40 \pm 10 \text{ Wm}^{-2}$ . Also, the net cooling power over area at night is  $33 \pm 8 \text{ Wm}^{-2}$  which is higher than the day as expected. In contrast to Colorado, in Eucalipto, the expected net cooling power value at day is higher than the measured value. This is because the temperature difference is lower than Colorado cooling wood. This material is darker than Colorado, so it can not reflect entirely solar radiation, diminishing its passive cooling capacity when it is exposed to sunlight. Consequently, net cooling power's real values are lower than Colorado cooling wood and lower than the expected values for Eucalipto cooling wood. Simultaneously, since the

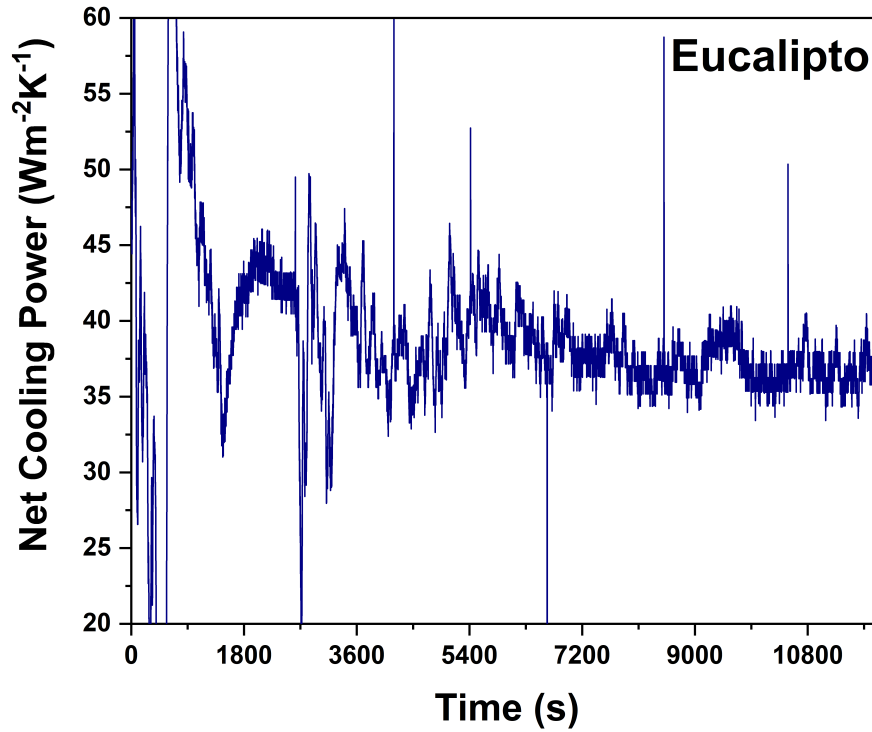


Figure 4.17: Eucalipto net cooling power expected over time

material is heated more quickly, it is difficult to detect a lower temperature in actual tests.

#### 4.4.3 Copal

In the case of Copal the temperature measurements of open box are observed in figure 4.18 during the day (a), and at night (b). At day, the temperature difference is almost in-existent for both cases for closed box and open box. The average difference in temperature for the open box is  $0.1 \pm 0.2$  °C , and the measured cooling power of Copal at day was  $0.009 \pm 0.002$  W and over the area measured ( $0.0004 \text{ m}^2 \pm 0.00004$ ), the net cooling power is  $22 \text{ Wm}^{-2} \pm 7$ .

In the other hand at night, the average of difference in temperature between ambient and the cooling

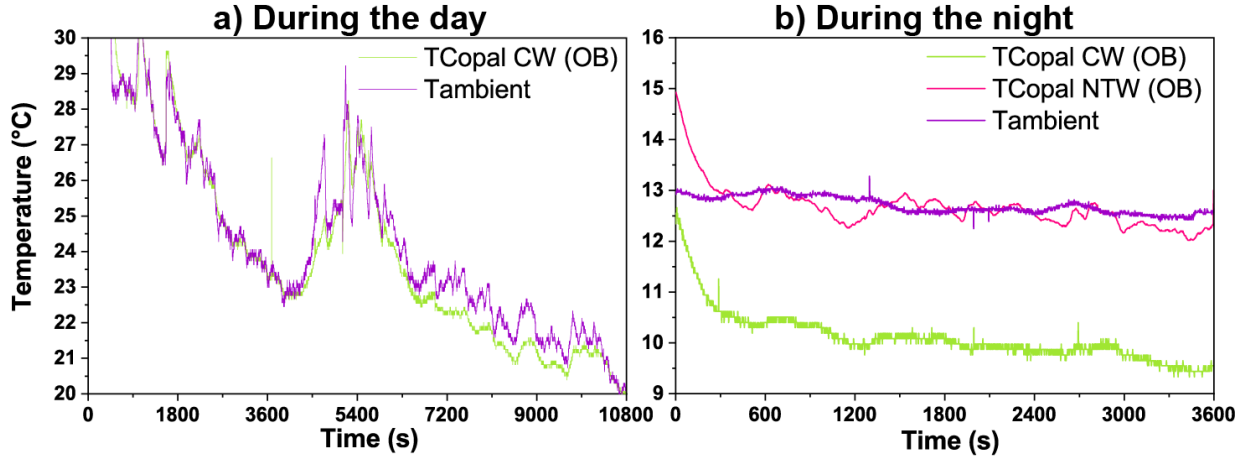


Figure 4.18: Copal cooling wood temperature during the day (a) and during the night (b), where (green) is the temperature of Copal cooling wood, (purple) ambient temperature, and (pink) untreated Copal wood over time in an open box.

wood is  $2,6 \text{ }^{\circ}\text{C} \pm 0,2 \text{ }^{\circ}\text{C}$ . Then the cooling power measured is  $0,028 \pm 0,002 \text{ W}$  and over the area  $70 \pm 10 \text{ Wm}^{-2}$ . Similar as before is observed in figure 4.18 b, that the nontreated wood has higher temperature than the cooling wood of Copal.

For Copal we obtained net cooling power expected at day in figure 4.19 with an average net cooling power of  $37 \pm 2 \text{ Wm}^{-2}$ . Thus, the cooling power measured at day is on average  $22 \pm 7 \text{ Wm}^{-2}$  and the expected  $37 \pm 2 \text{ Wm}^{-2}$ . The cooling power measured at night is  $70 \pm 12 \text{ Wm}^{-2}$ . We have that cooling power at night is higher than at day as expected. The value of the expected net cooling power of Copal can be lower than in real life. It could be confirmed with other measures of emissivity in the atmospheric window region.

In general, results observed in table 4.7 show that the cooling power at day and night is the highest in Colorado cooling wood, following this Copal cooling wood, and the last Eucalipto cooling wood. Also that the average difference in temperature is higher at day for Colorado and for Eucalipto and Copal we do not have average temperature difference. Therefore, based on the difference in temperature and the

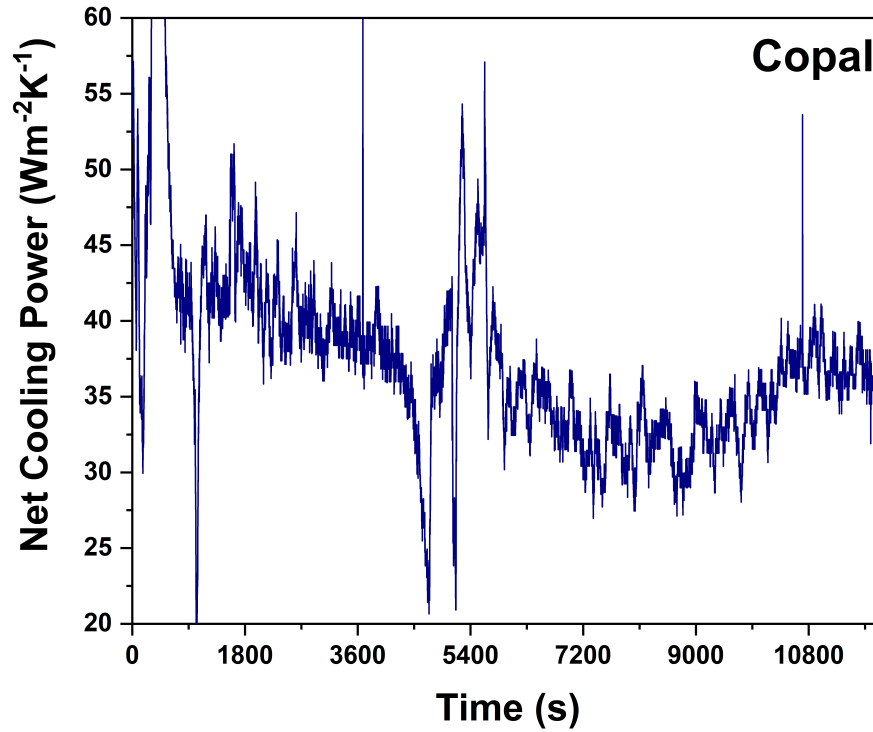


Figure 4.19: Copal net cooling power expected.

Material	Temperature difference (°C)		Cooling power (Wm <sup>-2</sup> )		Expected (Wm <sup>-2</sup> )
CW	Day	Night	Day	Night	Day
Colorado	0.6 ± 0.2	2.7 ± 0.2	60 ± 20	80 ± 20	40 ± 10
Eucalipto	0.0 ± 0.2	2.7 ± 0.2	20 ± 7	33 ± 8	40 ± 10
Copal	0.1 ± 0.2	2.6 ± 0.2	22 ± 7	70 ± 10	37 ± 2

Table 4.7: Cooling performance results for Colorado, Eucalipto and Copal cooling wood (CW).

thermometers' error, we can barely consider that we have a sub-ambient temperature for Eucalipto and Copal during the day, so just for Colorado cooling wood, we prove it has a cooling power performance. For Eucalipto and Copal cooling wood, we can not say that the material has a passive cooling performance

at day by analyzing its temperature differences. Therefore we measured its performance at night since, in principle, Colorado, Eucalipto and Copal have a similar emissivity in the atmospheric window. So they must work at night. Copal and Eucalipto cooling wood are not as white as Colorado cooling wood, due to some lignin remain in woods (confirmed by FTIR and XPS characterization), which affects the passive cooling at day and night. Since at day Copal and Eucalipto cooling, wood can not reflect all the solar radiation received. Therefore the material is heated quickly, making it very difficult to perform passive cooling during the day. To identify passive cooling, we should do some experiments like delignify more the materials until the light yellow color disappears completely. However, this gives us an insight that for now, Colorado wood must be more studied. Since we need to make a material for cooling purposes, we need to use the most efficient wood: the one that needs lower times for delignification which means lower chemicals used and less money. On the other hand, at night, we probed that the materials have cooling power since the difference in the cooling wood materials' temperatures and the ambient temperature is existent and higher as observed in the table 4.7. The average difference in temperature of Colorado, Eucalipto, and Copal cooling wood at night is almost similar among them and are considerable higher than average difference in temperature at day. Those results show us that the cooling wood materials obtained emit radiation to outer space and, therefore, can be cooled by themselves. The difference in temperature higher at night is expected since we do not have solar radiation as a factor that heats our material at night. The temperature difference is similar from one material to other since they have similar emissivity at the atmospheric region, as observed in previous results. Just at day was identified differences between the materials Colorado CW, Eucalipto CW, and Copal CW. Since the delignification process most perfectly obtained helps us have the material that reflects more solar radiation, it allows the material not to be heated.

Following that, for the measured cooling power over the area of the material during the temperature experiment at day, we have that Colorado has the highest value. Considering this, we can confirm that the one with higher cooling power is Colorado. It goes along with the fact that Colorado cooling wood has a higher sub-ambient temperature. From the three kinds of wood that we study, Colorado cooling wood is the only one we can confirm with passive cooling behavior at day.

As mentioned earlier, the emissivity values may be subjected to the thickness of the material measured;

therefore, we can not be based on this data. During night and day measurements, it was proved that the material with higher cooling power is Colorado cooling wood, followed by Copal and finally Eucalipto. Therefore, we confirm that the delignification process not only increases the reflection of solar radiation it also improves the emissivity in the atmospheric window range. Therefore after the delignification we have a material with higher cooling power at day and night. Similarly, in the experiments, we observed that the cooling wood materials at night have a lower temperature compared to the non-treated wood where they come from. Therefore, we can confirm that the delignification process increases the emissivity in the atmospheric window range as observed in emissivity values, where an increase is considerable.

Concerning the expected net cooling power at day, we have for Colorado, Eucalipto the same value  $40 \pm 10 \text{ Wm}^{-2}$  and Copal a close value  $37 \pm 2 \text{ Wm}^{-2}$ . As mentioned for the temperature difference results and the net cooling power measured, we may consider that Copal and Eucalipto have not passive cooling behavior during the day. However, if we check the emissivity in the atmospheric regions previously obtained, we reported emissivity in that range, so the material has passive cooling. Also, the expected cooling power values and the night measurements Copal and Eucalipto cooling wood shows that they have passive cooling behavior, but that is not observable during the day. The last result highlights the importance of reflecting solar radiation to have passive cooling during the day.

We confirm the theory that to have a passive cooling material during the day, the material should be highly emissive in the atmospheric region, and at the same time, this should reflect solar radiation in the optical range. The latter capacity is related to the color of the sample. The whiter the material, the more reflective it is in the optical range and the presence of lignin works against such reflectivity. Therefore an efficient delignification is needed<sup>23</sup>.



## Chapter 5

# Summary and Conclusions

### 5.1 Summary

In this thesis project, we studied the principles behind passive radiative cooling. We elaborated passive cooling materials and designed a procedure to measure their passive cooling properties. In Chapter 2, we analyzed the parameters that make a material with passive cooling behavior. Radiative cooling is a natural cooling method since heat is dissipated to space via thermal radiation through the natural atmospheric window<sup>1</sup>. While it is more effective at night, it is more needed during the daytime but more challenging to achieve because of solar radiation. Other factors to consider for passive cooling materials is the cooling power is lost due to the wind and/or by conduction and convection<sup>5</sup>.

In, Chapter 3 we explained the methods used to obtain the passive cooling material based on wood. We explained how FTIR and XPS are useful techniques to characterize these materials and quantify the cooling power of these materials. The passive cooling materials used in this project were obtained from the delignification of three Ecuadorian kinds of wood: *Eucalyptus globulus* (Eucalipto), *Guarea kunthiana* (Manzano Colorado), *Dacryodes peruviana* (Copal). For the delignification process, we tested three different treatments: NaOH/Na<sub>2</sub>SO<sub>3</sub> and H<sub>2</sub>O<sub>2</sub>, with NaClO, and with acetic acid and NaClO<sub>2</sub>. The NaOH/Na<sub>2</sub>SO<sub>3</sub> and H<sub>2</sub>O<sub>2</sub> treatment delignified the woods better than the other treatments.

The materials obtained by the aforementioned treatment labeled cooling woods were characterized by FTIR and XPS (before, during, and after the treatment). Also, we developed a thermally insulated box and a circuit to monitor the temperature of the cooling wood material and untreated wood with respect to the ambient temperature and the cooling power of each sample. For that, the samples were placed in the box with an opening exposed to sunlight. Finally, the cooling performance expected for each sample was computed based on the emissivity estimated in the range from 8 to 13 micrometers and the ambient temperature and cooling wood temperature measured with the insulated boxes.

In Chapter 4 we discussed the results of the materials obtained, their characterization, and their cooling performance.

## 5.2 Conclusion

After the chemical treatments described, we obtained that the most reflective material in the optical range is the *Colorado* cooling wood. In general, materials treated with NaOH/Na<sub>2</sub>SO<sub>3</sub> and H<sub>2</sub>O<sub>2</sub> resulted in a whiter sample and, thus, a better delignification process. Thus, to accomplish our objectives of obtaining materials with the optimal cooling power, we considered the whitest material, Colorado cooling wood, since we expect them to reflect more light in the optical range.

Using the analytical techniques FTIR and XPS, we identified the removal of lignin in the three samples, Colorado, Eucalipto, and Copal cooling wood. The whitest material, Colorado cooling wood, had almost all the peaks coming from the chemical structure of lignin removed. Using the FTIR spectra of Colorado, Eucalipto, and Copal cooling woods, we obtained the emissivity in the range from 8 to 13 micrometers (in the atmospheric window). The three materials cooling wood have similar emissivity values, so the three of them have passive cooling behavior. The darker color due to the remaining lignin hampered the cooling capacity of Eucalipto and Copal below Colorado cooling wood by day.

We acquired the temperature difference for the cooling performance measurements ( ambient minus cooling wood temperature) between the cooling woods and the ambient temperature. The highest difference in temperature during the day is Colorado cooling wood with  $0.6\text{ }^{\circ}\text{C} \pm 0.2\text{ }^{\circ}\text{C}$ . The error bars evidenced

that Eucalipto and Copal cooling wood, on average, did not cool in any measure during the day. Therefore, some methods must be devised to further delignify the materials until most of the radiation absorbing lignin disappears.

On the other hand, at night, the passive cooling materials have a considerably higher cooling performance than during the daytime. The average difference in temperature at night of Colorado cooling wood is  $2.7\text{ }^{\circ}\text{C} \pm 0.2\text{ }^{\circ}\text{C}$ , for Eucalipto  $2.7\text{ }^{\circ}\text{C} \pm 0.2\text{ }^{\circ}\text{C}$  and for Copal  $2.6\text{ }^{\circ}\text{C} \pm 0.2\text{ }^{\circ}\text{C}$ . Compared with the results obtained by day, the difference in temperature increases at night for all the samples. This confirms that the cooling wood materials emit radiation to outer space through the atmospheric window, thus cooling themselves. Since we do not have solar radiation as a factor that heats our material at night, we readily identified lower temperatures for the passive cooling materials. At night, the temperature difference is similar from one material to another since they have similar emissivity at the atmospheric region, as observed in previous results. Interestingly we also found that delignifying increases the cooling performance at night, a feature that would be interesting to understand.

For the measured cooling power, by day, we have for Colorado an average cooling power over the area  $60\text{ }Wm^{-2} \pm 20\text{ }Wm^{-2}$  which was the only one that cooled within measurement error. From the three kinds of wood that we study, we may consider that Colorado cooling wood is the only one with passive cooling behavior during the day.

In the case of the measured cooling power at night, for Colorado, the cooling power averaged  $80 \pm 20\text{ }Wm^{-2}$ ; for Eucalipto  $33 \pm 8\text{ }Wm^{-2}$ ; and for Copal  $70 \pm 10\text{ }Wm^{-2}$  higher than at daytime. In this case, the cooling power per unit area at night is higher for Colorado cooling wood than the others materials and higher than Colorado CW by day measurements.

We also conclude that the delignification process improves the emissivity in the atmospheric window range, resulting in higher cooling power. Similarly, in the experiments, we observed that the cooling wood at night has lower temperatures compared to the non-treated wood where it comes from. Therefore, we can confirm that the delignification process increases the emissivity in the atmospheric window range, increasing the cooling power at night.

Concerning the expected net cooling power at day, we have for Colorado an average of  $40 \pm 10\text{ }Wm^{-2}$ ;

for Eucalipto, an average of  $40 \pm Wm^{-2}$  and for Copal, an average net cooling power of  $37 \pm 2 Wm^{-2}$ . Those values are in accordance with the emissivities obtained that are similar for the three samples.

For a material to have passive radiative cooling at night, it should have high emissivity in the atmospheric transparency window close to that of a perfect *Blackbody*. But for a material to have passive radiative cooling during the day, it should have high emissivity in the infrared window and simultaneously reflect or scatter visible sunlight efficiently. The reflection of the solar radiation is related to the whiter color of our samples. In our case, that is related to removing lignin. The more lignin is removed, the whiter the wood, and more reflection of solar radiation.

Finally, we conclude that passive cooling material at day is harder to achieve but can be an alternative to air conditioners used for structures. Cooling wood can be manufactured at a large scale cheaply. This thesis project is a step forward to achieve the most efficient material in terms of their cooling power by the day. In particular, Colorado takes the shortest time to delignify and shows good cooling power at night and cooling power by the day. In that way, we also conclude that the delignification process improves the passive cooling at day by reflecting solar radiation. It also increases the emissivity in the range of the atmospheric window.

### 5.3 Outlook

As a future, to understand the structure of the cooling wood material deeply, we can characterize the material before and after the characterization process with Raman, an X-ray diffractometer, and a Scanning electron microscope. Additionally, using a rheometer, we could measure the mechanical properties of the samples before and after the treatment. Finally, to confirm the value of emissivity in the atmospheric window, it is essential to measure the emissivity of the material with a new IR spectrometer.

## **Appendix A**

### **Cooling performance closed box**

Here are the results of the temperature measurements during the day for closed boxes it means with the wind shield of polyethylene which may be not highly transparent in the infrared spectrum. Thus results in lower difference in temperature. Here we have the results for Colorado Figure A.1, for Eucalipto Figure A.2 and for Copal Figure A.3

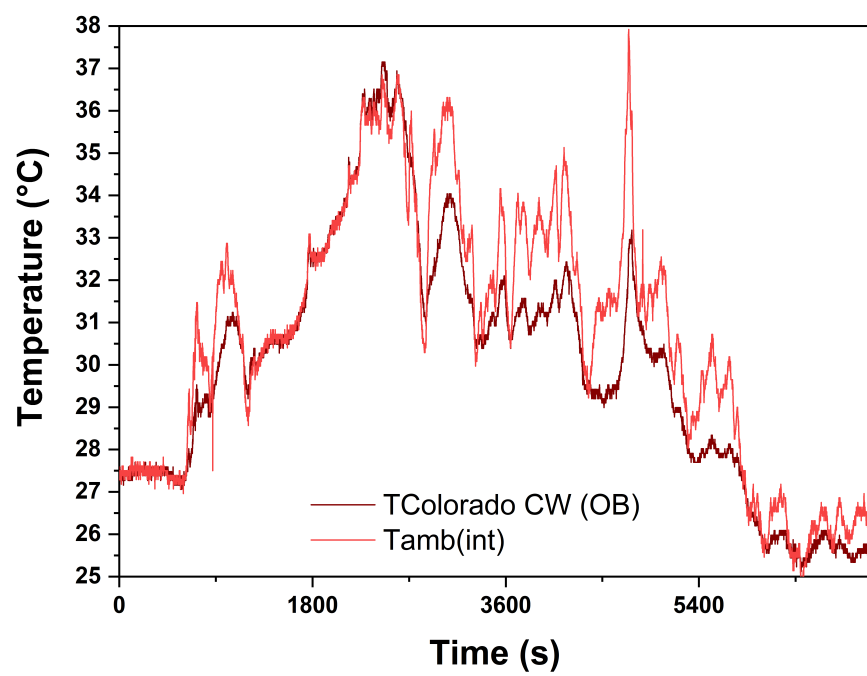


Figure A.1: Manzano Colorado registered temperature differences closed.

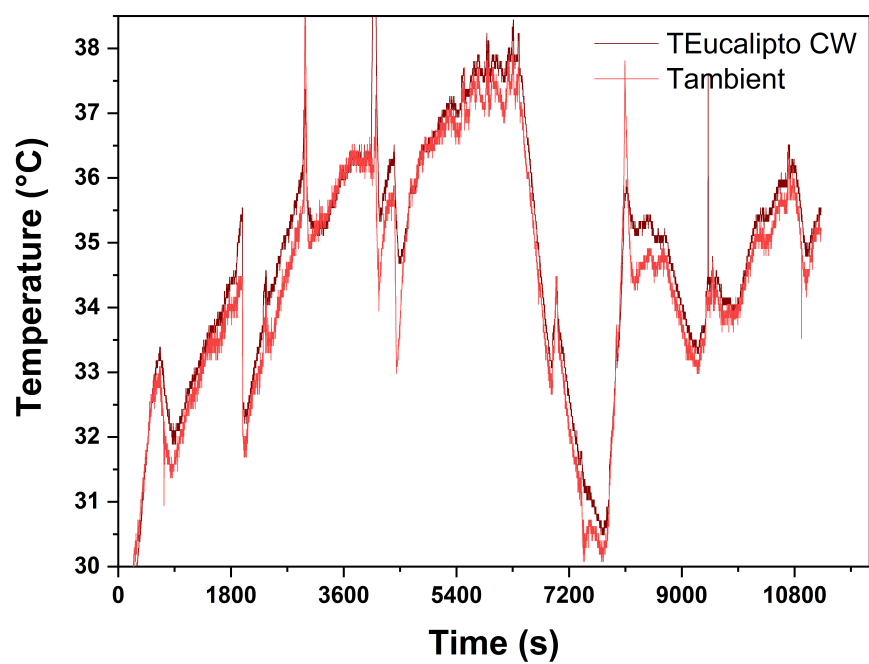


Figure A.2: Eucalipto registered temperature differences closed.

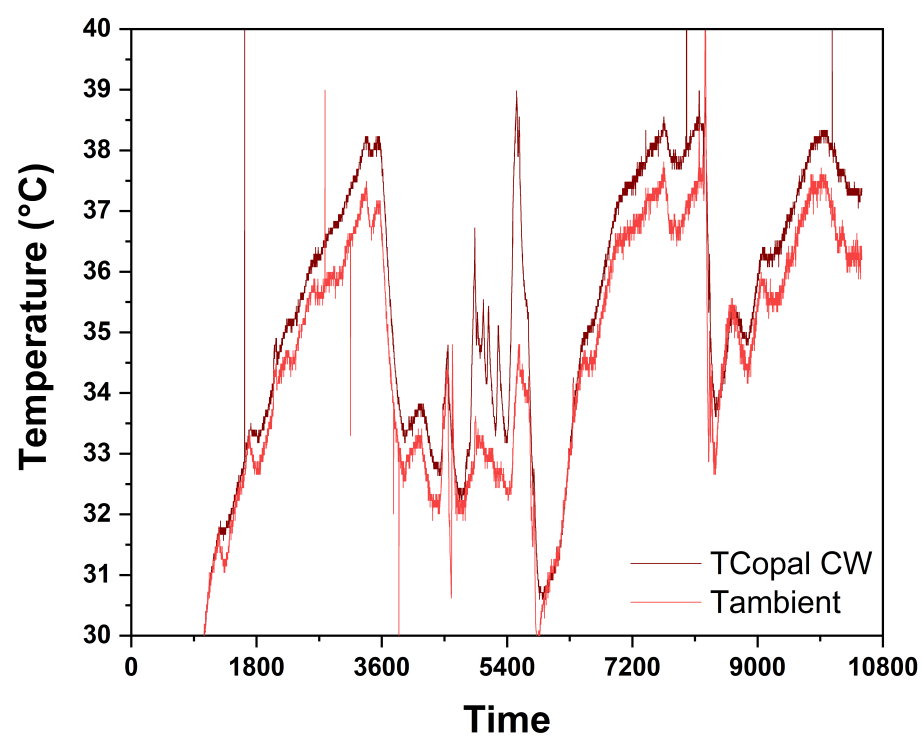


Figure A.3: Copal registered temperature differences closed box.



## **Appendix B**

### **XPS data of fitting**

In the next tables we have the fitting information of area and FWHM (full width in an half maximum) for the XPS spectra of Colorado Table B.1, of Eucalipto Table B.2 and of Copal Table B.3.

COL	Area NTW	FWHM NTW	Area TW	FWHM TW	Area CW	FWHM CW
C1	-	-	1400 ± 100	1.35 ± 0.04	-	-
C2	10800 ± 400	2.32 ± 0.5	5400 ± 400	2.19 ± 0.5	9400 ± 400	2.56 ± 0.5
C3	3310 ± 50	1.71 ± 0.5	5500 ± 600	1.82 ± 0.08	1700 ± 100	1.72 ± 0.07
C4	1580 ± 20	1.51 ± 0.5	900 ± 400	1.9 ± 0.4	1100 ± 100	1.7 ± 0.1
C5	160 ± 10	1.03 ± 0.5	700 ± 300	1.9 ± 0.5	260 ± 50	1.3 ± 0.1
C6	-	-	740 ± 90	1.28 ± 0.05	-	-
Error	$R^2 = 0.998$		$R^2 = 0.998$		$R^2 = 0.998$	
COL	Area NTW	FWHM NTW	Area TW	FWHM TW	Area CW	FWHM CW
O1	-	-	3300 ± 300	3.6 ± 0.2	-	-
O2	2100 ± 200	6.2 ± 0.4	-	-	1800 ± 200	4.4 ± 0.5
O3	1740 ± 30	2.0 ± 0.5	2900 ± 200	1.67 ± 0.04	1960 ± 70	1.9 ± 0.5
O4	4920 ± 30	1.8 ± 0.5	12100 ± 500	1.78 ± 0.04	4810 ± 30	1.7 ± 0.5
O5	7640 ± 30	1.8 ± 0.5	10300 ± 300	1.71 ± 0.02	3850 ± 30	1.8 ± 0.5
O6	-	-	3200 ± 200	2.30 ± 0.08	-	-
Error	$R^2 = 0.998$		$R^2 = 0.998$		$R^2 = 0.998$	
COL	Area NTW	FWHM NTW	Area TW	FWHM TW	Area CW	FWHM CW
N1	270 ± 20	2.55 ± 0.06	190 ± 10	2.10 ± 0.10	-	-
Error	$R^2 = 0.904$		$R^2 = 0.715$			
COL	Area NTW	FWHM NTW	Area TW	FWHM TW	Area CW	FWHM CW
Si1	115 ± 7	2.72 ± 0.07	176 ± 9	2.54 ± 0.08	110 ± 4	3.22 ± 0.08
Error	$R^2 = 0.890$		$R^2 = 0.789$		$R^2 = 0.879$	

Table B.1: Area and FWHM (full width in a half maximum) of peaks present in XPS spectra C1s, O1s, N1s and Si2p for Colorado (COL) non-treated wood (NTW), treated wood (TW) and cooling wood (CW)

EUC	Area NTW	FWHM NTW	Area TW	FWHM TW	Area CW	FWHM CW
C1	-	-	-	-	-	-
C2	19400 ± 400	2.3 ± 0.5	4500 ± 400	2.5 ± 0.5	15000 ± 400	2.0 ± 0.5
C3	3200 ± 200	1.89 ± 0.05	2700 ± 50	1.9 ± 0.5	3930 ± 50	1.6 ± 0.5
C4	-	-	590 ± 20	1.7 ± 0.5	1190 ± 30	1.6 ± 0.5
C5	-	-	440 ± 20	1.9 ± 0.5	700 ± 40	1.9 ± 0.5
C6	-	-	1540 ± 40	1.56 ± 0.02	-	-
Error	$R^2 = 0.997$		$R^2 = 0.996$		$R^2 = 0.998$	
EUC	Area NTW	FWHM NTW	Area TW	FWHM TW	Area CW	FWHM CW
O1	-	-	3800 ± 300	3.4 ± 0.2	-	-
O2	-	-	-	-	2100 ± 200	5.0 ± 0.3
O3	-	-	1300 ± 200	1.41 ± 0.06	1430 ± 80	1.76 ± 0.06
O4	-	-	3900 ± 300	1.50 ± 0.07	400 ± 200	1.57 ± 0.03
O5	-	-	14500 ± 200	1.86 ± 0.01	11700 ± 100	1.93 ± 0.01
O6	-	-	6800 ± 200	2.68 ± 0.05	-	-
Error	$R^2 = 0.997$		$R^2 = 0.997$		$R^2 = 0.999$	
EUC	Area NTW	FWHM NTW	Area TW	FWHM TW	Area CW	FWHM CW
N1	-	-	190 ± 10	2.4 ± 0.1	80 ± 5	1.9 ± 0.5
Error	$R^2 = 0.720$		$R^2 = 0.720$		$R^2 = 0.418$	
EUC	Area NTW	FWHM NTW	Area TW	FWHM TW	Area CW	FWHM CW
Si1	280 ± 7	2.37 ± 0.03	370 ± 10	2.63 ± 0.06	299 ± 8	2.49 ± 0.03
Error	$R^2 = 0.975$		$R^2 = 0.925$		$R^2 = 0.971$	

Table B.2: Area and FWHM (full width in a half maximum) of peaks present in XPS spectra C1s, O1s, N1s and Si2p for Eucalipto (EUC) non-treated wood (NTW), treated wood (TW) and cooling wood (CW)

<b>COP</b>	<b>Area NTW</b>	<b>FWHM NTW</b>	<b>Area TW</b>	<b>FWHM TW</b>	<b>Area CW</b>	<b>FWHM CW</b>
C1	-	-	-	-	-	-
C2	9500 ± 400	2.2 ± 0.5	2300 ± 400	2.6 ± 0.5	9100 ± 400	1.8 ± 0.5
C3	7300 ± 400	1.92 ± 0.06	1540 ± 40	1.9 ± 0.5	2100 ± 100	1.29 ± 0.04
C4	2000 ± 100	1.31 ± 0.04	310 ± 20	1.8 ± 0.5	-	-
C5	730 ± 80	1.28 ± 0.06	870 ± 20	1.9 ± 0.5	-	-
C6	-	-	2100 ± 30	1.47 ± 0.01	-	-
Error	$R^2 = 0.998$		$R^2 = 0.993$		$R^2 = 0.995$	
<b>COP</b>	<b>Area NTW</b>	<b>FWHM NTW</b>	<b>Area TW</b>	<b>FWHM TW</b>	<b>Area CW</b>	<b>FWHM CW</b>
O1	-	-	5100 ± 400	3.2 ± 0.1	-	-
O2	-	-	-	-	-	-
O3	900 ± 100	1.8 ± 0.1	900 ± 100	1.24 ± 0.08	-	-
O4	700 ± 200	1.91 ± 0.04	2600 ± 300	1.39 ± 0.08	-	-
O5	11900 ± 100	2 ± 0.5	19200 ± 200	1.83 ± 0.01	-	-
O6	-	-	10500 ± 200	2.53 ± 0.04	-	-
Error	$R^2 = 0.998$		$R^2 = 0.996$			
<b>COP</b>	<b>Area NTW</b>	<b>FWHM NTW</b>	<b>Area TW</b>	<b>FWHM TW</b>	<b>Area CW</b>	<b>FWHM CW</b>
N1	-	-	-	-	-	-
<b>COP</b>	<b>Area NTW</b>	<b>FWHM NTW</b>	<b>Area TW</b>	<b>FWHM TW</b>	<b>Area CW</b>	<b>FWHM CW</b>
Si1	287 ± 4	2.76 ± 0.02	162 ± 9	2.2 ± 0.1	115 ± 4	2.15 ± 0.06
Error	$R^2 = 0.977$		$R^2 = 0.742$		$R^2 = 0.893$	

Table B.3: Area and FWHM (full width in a half maximum) of peaks present in XPS spectra C1s, O1s, N1s and Si2p for Copal (COP) non-treated wood (NTW), treated wood (TW) and cooling wood (CW)

## Appendix C

### Arduino temperature beedback circuit

Here is present the Arduino code used to measured cooling power at day and at night. We use TC as the thermometer of the heater that measures at the same time the material over it (cooling wood material). The ambient temperature we consider was an average of thermometers T1,T4 and T5. Those thermometers were placed at free air under shallow. When TC is lower than ambient temperature  $(T1+T4+T5)/3$  the heater turns on and measure its heating power, which is related to the cooling power. This code was provided by Ph.D. Werner Bramer professor of the School of Physical Sciences and Nanotechnology of YachayTech University.

<pre> #include &lt;Adafruit_ADS1015.h&gt; #include &lt;Wire.h&gt; #include &lt;hd44780.h&gt; #include &lt;hd44780ioClass/hd44780_I2Cexp.h&gt; hd44780_I2Cexp lcd;  int val_0, val_1, val_2, val_3, val_4, val_5, val_6, val_7, val_8, val_9, val_10, val_11, val_12; int tempPin_0 = 0; int tempPin_1 = 1; int tempPin_2 = 2; int tempPin_3 = 3; int tempPin_6 = 6; int tempPin_7 = 7; int RelayPin = 3; float repeticiones = 10.0; float TC, T1, T2, T3, T4, T5, T6, T7, T8, T9;  int16_t adc1_0, adc1_1, adc1_2, adc1_3; int16_t adc2_0, adc2_1;  //static float f_val; static char outstr_C[3]; static char outstr_1[3]; static char outstr_2[3]; static char outstr_3[3]; static char outstr_4[3]; static char outstr_5[3]; static char outstr_6[3]; static char outstr_7[3]; static char outstr_W[7]; </pre>	<pre> Adafruit_ADS1115 ads1; // Construct an ads1015 at the default address Adafruit_ADS1115 ads2 (0x49); // construct an ads1115 at address 0x49 //this is for measure current and voltage and for calculate Watts. const float multiplier = 5.05648F;  void setup() {   ads1.begin(); // Initialize first ads1115   ads2.begin(); // Initialize second ads1115   ads1.setGain(GAIN_TWOTHIRDS);   ads2.setGain(GAIN_TWOTHIRDS);   analogReference(INTERNAL);   lcd.begin(16,4); // initialize the lcd and   //specify that the LCD is 16x4,   //without this code the LCD do not work!   lcd.clear();   pinMode(RelayPin, OUTPUT);   Serial.begin(9600);    lcd.backlight();   lcd.setCursor(0,0);   lcd.print("TC=");   lcd.setCursor(8,0);   lcd.print("T1=");   lcd.setCursor(0,1);   lcd.print("T2=");   lcd.setCursor(8,1);   lcd.print("T3=");   lcd.setCursor(0,2);   lcd.print("T4="); </pre>
---	--

Figure C.1: Arduino code part 1 (page 1 and 2)

```

lcd.setCursor(8,2);
  lcd.print("T5=");
lcd.setCursor(0,3);
lcd.print("W=");
TC=24.0;
T1=24.0;
T2=24.0;
T3=24.0;
T4=24.0;
T5=24.0;
T6=24.0;
T7=24.0;
T8=24.0;
T9=24.0;
unsigned long time_2;
}

unsigned long time_1 = micros();
void loop()
{
  val_0 = 0.0;
  val_1 = 0.0;
  val_2 = 0.0;
  val_3 = 0.0;
  val_4 = 0.0;
  val_5 = 0.0;
  adc1_0 = 0.0;
  adc1_1 = 0.0;
  adc1_2 = 0.0;
  adc1_3 = 0.0;

```

3

```

  adc1_3 = 0.0;
  adc2_0 = 0.0;
  adc2_1 = 0.0;

  for (int i = 0; i < repeticiones; i++) { // Loop for measuring the values of
    //the voltage and making a mean value of each of them
  }

  analogReference(INTERNAL);
  val_0 = analogRead(tempPin_0) + val_0;
  analogReference(INTERNAL);
  val_1 = analogRead(tempPin_1) + val_1;
  analogReference(INTERNAL);
  val_2 = analogRead(tempPin_2) + val_2;
  analogReference(INTERNAL);
  val_3 = analogRead(tempPin_3) + val_3 ;
  analogReference(INTERNAL);
  val_4 = analogRead(tempPin_6) + val_4;
  analogReference(INTERNAL);
  val_5 = analogRead(tempPin_7) + val_5;

  adc1_0 = adsl.readADC_SingleEnded(0) ;
  adc1_1 = adsl.readADC_SingleEnded(1) ;
  adc1_2 = adsl.readADC_SingleEnded(2) ;
  adc1_3 = adsl.readADC_SingleEnded(3) ;

  delay(20);
}

  adc1_0 = adsl.readADC_SingleEnded(0);
  delayMicroseconds(100);
  adc1_1 = adsl.readADC_SingleEnded(1);
  delayMicroseconds(100);

```

4

Figure C.2: Arduino code part 2 (page 3 and 4)

```

    adc1_2 = ads1.readADC_SingleEnded(2);
    delayMicroseconds(100);
    adc1_3 = ads1.readADC_SingleEnded(3);
    delayMicroseconds(100);
    adc2_0 = ads2.readADC_SingleEnded(0);
    delayMicroseconds(100);
    adc2_1 = ads2.readADC_SingleEnded(1);
    delayMicroseconds(100);

    val_0 = val_0/repeticiones;
    val_1 = val_1/repeticiones;
    val_2 = val_2/repeticiones;
    val_3 = val_3/repeticiones;
    val_4 = val_4/repeticiones;
    val_5 = val_5/repeticiones;
    val_6 = adc1_0/repeticiones;
    val_7 = adc1_1/repeticiones;
    val_8 = adc1_2/repeticiones;
    val_9 = adc1_3/repeticiones;

    float mv_0 = ( val_0/1024.0)*1100;
    float mv_1 = ( val_1/1024.0)*1100;
    float mv_2 = ( val_2/1024.0)*1100;
    float mv_3 = ( val_3/1024.0)*1100;
    float mv_4 = ( val_4/1024.0)*1100;
    float mv_5 = ( val_5/1024.0)*1100;

    float mv_6 = ( adc1_0/32767.0)*5.0;
    float mv_7 = ( adc1_1/32767.0)*5.0;
    float mv_8 = ( adc1_2/32767.0)*5.0;
    float mv_9 = ( adc1_3/32767.0)*5.0;

    float cel_1 = mv_1/10.0;
    float cel_2 = mv_2/10.0-0.23;
    float cel_3 = mv_3/10.0;
    float cel_4 = mv_4/10.0+1.07;
    float cel_5 = mv_5/10.0+0.10;

    float cel_6 = mv_6*100.0+4.29+1.21;
    float cel_7 = mv_7*100.0+4.29+0.1;
    float cel_8 = mv_8*100.0+4.29;
    float cel_9 = mv_9*100.0+4.29+0.22;

    TC = cel_C;
    T1 = cel_1;
    T2 = cel_2;
    T3 = cel_3;
    T4 = cel_4;
    T5 = cel_5;
    T6 = cel_6;
    T7 = cel_7;
    T8 = cel_8;
    T9 = cel_9;

    lcd.setCursor(11,0);
    lcd.print(T1);

    if (TC < (T1+T4+T5)/3-0.1){
        // (T1+T4+T5)/3 it the temperature of ambient control,
        //TC:temperaure of the heater (temperature of the cooling wood)
        digitalWrite(RelayPin, HIGH);
        adc2_0 = ads2.readADC_SingleEnded(0);
        adc2_1 = ads2.readADC_SingleEnded(1);

```

Figure C.3: Arduino code part 3 (page 5 and 6)



```

    float W = (adc2_0/27138.0)*multiplier*(adc2_1/27138.0)*multiplier;
    delay(500);
    lcd.setCursor(2,3);
    dtostrf(W,1, 4, outstr_W);
    //function dtostrf() converts float to a string
    //that save in outstr_W with the format 2,1
    //three characters with one decimal.
    lcd.print(outstr_W);
    delay(50);
}
delay(100);
if (TC > (T1+T4+T5)/3-0.5){// 0.5 is the tolerance for the turn off
    digitalWrite(RelayPin, LOW);
    delay(100);
}
Serial.print("TC=");
Serial.print(CEL_C);
Serial.print(" ");
Serial.print("T1=");
Serial.print(CEL_1);
Serial.print(" ");
Serial.print("T2=");
Serial.print(CEL_2);
Serial.print(" ");
Serial.print("T3=");
Serial.print(CEL_3);
Serial.print(" ");
Serial.print("T4=");
Serial.print(CEL_4);
Serial.print(" ");
Serial.print("T5=");

```

7

Figure C.4: Arduino code part 4 (page 7)

<pre> Serial.print(cel_5); Serial.print(" "); Serial.print("T6="); Serial.print(cel_6); Serial.print(" "); Serial.print("T7="); Serial.print(cel_7); Serial.print(" "); Serial.print("T8="); Serial.print(cel_8); Serial.print(" "); Serial.print("T9="); Serial.print(cel_9); Serial.print(" ");  float W = (adc2_0/27138.0)*multiplier*(adc2_1/27138.0)*multiplier; Serial.print("W="); Serial.print(abs(W),5); Serial.print(" ");  unsigned long time_2= micros(); Serial.print("t="); Serial.println((time_2-time_1)*0.000001);  lcd.setCursor(3,0); dtostrf(cel_C,2,1, outstr_C); lcd.print(outstr_C);  lcd.setCursor(11,0); dtostrf(cel_1,2,1, outstr_1); lcd.print(outstr_1); </pre>	8	<pre> lcd.setCursor(3,1); dtostrf(cel_2,2,1, outstr_2); lcd.print(outstr_2);  lcd.setCursor(11,1); dtostrf(cel_3,2, 1, outstr_3); lcd.print(outstr_3);  lcd.setCursor(3,2); dtostrf(cel_4,2, 1, outstr_6); lcd.print(outstr_6);  lcd.setCursor(11,2); dtostrf(cel_5,2, 1, outstr_6); lcd.print(outstr_6);  lcd.setCursor(2,3); dtostrf(W,1, 4, outstr_W); lcd.print(outstr_W); delay(500); // Delay principal of the program. </pre>	9
---	---	--	---

Figure C.5: Arduino code part 5 (page 8 and 9)

# Bibliography

- [1] Pech-May, N. W.; Retsch, M. Tunable daytime passive radiative cooling based on a broadband angle selective low-pass filter. *Nanoscale Advances* **2020**, 2, 249–255.
- [2] Lord, S. D. *A new software tool for computing Earth's atmospheric transmission of near-and far-infrared radiation*; Ames Research Center, 1992; Vol. 103957.
- [3] Spiro, I.; Jones, R. C.; Wark, D. Atmospheric transmission: Concepts, symbols, units and nomenclature. *Infrared Physics* **1965**, 5, 11–36.
- [4] Rephaeli, E.; Raman, A.; Fan, S. Ultrabroadband photonic structures to achieve high-performance daytime radiative cooling. *Nano letters* **2013**, 13, 1457–1461.
- [5] Raman, A. P.; Anoma, M. A.; Zhu, L.; Rephaeli, E.; Fan, S. Passive radiative cooling below ambient air temperature under direct sunlight. *Nature* **2014**, 515, 540–544.
- [6] Hossain, M. M.; Jia, B.; Gu, M. A metamaterial emitter for highly efficient radiative cooling. *Advanced Optical Materials* **2015**, 3, 1047–1051.
- [7] Zhai, Y.; Ma, Y.; David, S. N.; Zhao, D.; Lou, R.; Tan, G.; Yang, R.; Yin, X. Scalable-manufactured randomized glass-polymer hybrid metamaterial for daytime radiative cooling. *Science* **2017**, 355, 1062–1066.
- [8] Mandal, J.; Fu, Y.; Overvig, A. C.; Jia, M.; Sun, K.; Shi, N. N.; Zhou, H.; Xiao, X.; Yu, N.; Yang, Y.

- Hierarchically porous polymer coatings for highly efficient passive daytime radiative cooling. *Science* **2018**, 362, 315–319.
- [9] Li, T.; Song, J.; Zhao, X.; Yang, Z.; Pastel, G.; Xu, S.; Jia, C.; Dai, J.; Chen, C.; Gong, A. Anisotropic, lightweight, strong, and super thermally insulating nanowood with naturally aligned nanocellulose.
- [10] Tarvo, V.; Lehtimaa, T.; Kuitunen, S.; Alopaeus, V.; Vuorinen, T.; Aittamaa, J. A model for chlorine dioxide delignification of chemical pulp. *Journal of Wood Chemistry and Technology* **2010**, 30, 230–268.
- [11] Horvat, A. A study of the uncertainty associated with tar measurement and an investigation of tar evolution and composition during the air-blown fluidised bed gasification of torrefied and non-torrefied grassy biomass. Ph.D. thesis, 2016.
- [12] Agencia de regulación y control de energía y recursos naturales no renovables, A. *Estadística anual y multianual del sector eléctrico ecuatoriano 2019*; Agencia de regulación y control de energía y recursos naturales no renovables and ARCONEL (agencia de regulación y control de electricidad), 2019.
- [13] CENACE, *Informe anual CENACE (operador nacional eléctrico) 2019*; CENACE, 2019.
- [14] Yang, Y.; Zhang, Y. Passive daytime radiative cooling: Principle, application, and economic analysis. *MRS Energy and Sustainability* **2020**, 7, E18.
- [15] Liu, C.-H.; Ay, C.; Tsai, C.-Y.; Lee, M.-T. The application of passive radiative cooling in greenhouses. *Sustainability* **2019**, 11, 6703.
- [16] Li, D.; Li, Y.; Su, Y.; Chi, C.; Huang, B. atmospheric-Window-Matching hierarchical Broadband infrared absorber realized by lithography-Free Fabrication. *Frontiers in Energy Research* **2018**, 6, 20.
- [17] Olaguer, E. P. *Atmospheric impacts of the oil and gas industry*; Academic Press, 2016.
- [18] Haldar, S. Mineral exploration. *Mineral Exploration* **2013**, 193–222.

- [19] Zhu, M.; Song, J.; Li, T.; Gong, A.; Wang, Y.; Dai, J.; Yao, Y.; Luo, W.; Henderson, D.; Hu, L. Highly anisotropic, highly transparent wood composites. *Advanced materials* **2016**, 28, 5181–5187.
- [20] Wu, Y.; Wu, J.; Yang, F.; Tang, C.; Huang, Q. Effect of H<sub>2</sub>O<sub>2</sub> bleaching treatment on the properties of finished transparent wood. *Polymers* **2019**, 11, 776.
- [21] Song, J.; Chen, C.; Yang, Z.; Kuang, Y.; Li, T.; Li, Y.; Huang, H.; Kierzewski, I.; Liu, B.; He, S. Highly compressible, anisotropic aerogel with aligned cellulose nanofibers.
- [22] Aili, A.; Zhao, D.; Lu, J.; Zhai, Y.; Yin, X.; Tan, G.; Yang, R. A kW-scale, 24-hour continuously operational, radiative sky cooling system: Experimental demonstration and predictive modeling. *Energy conversion and management* **2019**, 186, 586–596.
- [23] Li, T.; Zhai, Y.; He, S.; Gan, W.; Wei, Z.; Heidarinejad, M.; Dalgo, D.; Mi, R.; Zhao, X.; Song, J. A radiative cooling structural material.
- [24] Li, L.; Yu, L.; Wu, Z.; Hu, Y. Delignification of poplar wood with lactic acid-based deep eutectic solvents. *Wood Res* **2019**, 64, 499–514.
- [25] Iqbal, M. *An introduction to solar radiation*; Elsevier, 2012.
- [26] Howell, J. R.; Menguc, M. P.; Siegel, R. *Thermal radiation heat transfer*; CRC press, 2010.
- [27] Catling, D. C. *Encyclopedia of the solar system*; Elsevier, 2014; pp 343–357.
- [28] Kingston, R. H. *Optical sources, detectors, and systems: fundamentals and applications*; Academic Press, 1995.
- [29] Ribbing, C. G. *Optical Thin Films and Coatings*; Elsevier, 2013; pp 357–387.
- [30] McMahon, H. Thermal radiation from partially transparent reflecting bodies. *JOSA* **1950**, 40, 376–380.
- [31] Robitaille, P.-M. Kirchhoff's law of thermal emission: 150 years. *Progr. Phys* **2009**, 4, 3–13.

- [32] Trenberth, K. E. Earth's energy balance. **2014**,
- [33] Carlisle, C. M. The Oxford Companion to Cosmology, by Andrew Liddle and Jon Loveday. *Sky and Telescope* **2009**, 117, 52.
- [34] Zhao, D.; Aili, A.; Zhai, Y.; Lu, J.; Kidd, D.; Tan, G.; Yin, X.; Yang, R. Subambient cooling of water: Toward real-world applications of daytime radiative cooling. *Joule* **2019**, 3, 111–123.
- [35] Sharples, S.; Charlesworth, P. Full-scale measurements of wind-induced convective heat transfer from a roof-mounted flat plate solar collector. *Solar Energy* **1998**, 62, 69–77.
- [36] Test, F.; Lessmann, R.; Johary, A. Heat transfer during wind flow over rectangular bodies in the natural environment. **1981**,
- [37] Penín, L.; López, M.; Santos, V.; Alonso, J. L.; Parajó, J. C. Technologies for Eucalyptus wood processing in the scope of biorefineries: A comprehensive review. *Bioresource Technology* **2020**, 123528.
- [38] Heinze, T. *Cellulose chemistry and properties: fibers, nanocelluloses and advanced materials*; Springer, 2015; pp 1–52.
- [39] Hou, D.; Li, T.; Chen, X.; He, S.; Dai, J.; Mofid, S. A.; Hou, D.; Iddya, A.; Jassby, D.; Yang, R. Hydrophobic nanostructured wood membrane for thermally efficient distillation.
- [40] Chen, C.; Song, J.; Zhu, S.; Li, Y.; Kuang, Y.; Wan, J.; Kirsch, D.; Xu, L.; Wang, Y.; Gao, T. Scalable and sustainable approach toward highly compressible, anisotropic, lamellar carbon sponge.
- [41] Mendoza, Z. A.; Chalán, Á. F. L.; Ayala, C. S. Especies forestales más aprovechadas en la región sur del Ecuador. 2015.
- [42] Mejía, E.; Pacheco, P. *Aprovechamiento forestal y mercados de la madera en la Amazonía Ecuatoriana*; CIFOR, 2013; Vol. 97.

- [43] Jørgensen, P. M.; León-Yáñez, S. *Catalogue of the vascular plants of Ecuador*; Missouri Botanical Garden St. Louis, 1999; Vol. 75.
- [44] Ministerio del Ambiente del Ecuador (MAE), M.; Organización de las Naciones Unidas para la Alimentación y la Agricultura (FAO), O. *Propiedades anatómicas, físicas y mecánicas de 93 especies forestales*; MAE-FAO Ecuador, 2014.
- [45] León H, W. J. Anatomía de la Madera de 13 especies del orden Sapindales que crecen en el estado Mérida, Venezuela. *Acta Botánica Venezolánica* **2006**, 29, 269–296.
- [46] Kawasaki, M. L.; Holst, B. K.; Pérez, À. J. *Flora of Ecuador: Myrtaceae*/by Maria Lúcia Kawasaki, Bruce K. Holst and Álvaro J. Pérez; Department of biological and environmental sciences, University of Gothenburg, 2019.
- [47] Avilés Ramos, A. B. Posible amenaza del complejo *Gonipteris scutellatus* Gylenhall (1833) sobre las especies de *Eucalyptus* L'Hér (1789), debido a su introducción a Ecuador. M.Sc. thesis.
- [48] Renner, S.; Balslev, H.; Holm-Nielsen, L. Inventarion florístico de la Amazonia ecuatoriana], Flowering plants of Amazonian Ecuador-a checklist. *AAU reports* **1990**,
- [49] Alvarez Tacunga, D. M. Caracterización morfológica e identificación de zonas potenciales de conservación de copal (*dacryodes peruviana*) en los siete transectos del proyecto banco de germoplasma. B.S. thesis, Latacunga: Universidad Técnica de Cotopaxi; Facultad de Ciencias . . . , 2017.
- [50] Song, K. *Progress in Rubber Nanocomposites*; Elsevier, 2017; pp 115–152.
- [51] Titus, D.; Samuel, E. J. J.; Roopan, S. M. *Green Synthesis, Characterization and Applications of Nanoparticles*; Elsevier, 2019; pp 303–319.
- [52] Shameer, P. M.; Nishath, P. M. *Advanced Biofuels*; Elsevier, 2019; pp 181–213.
- [53] Shi, J.; Xing, D.; Lia, J. FTIR studies of the changes in wood chemistry from wood forming tissue under inclined treatment. *Energy Procedia* **2012**, 16, 758–762.

- [54] Yang, H.; Yan, R.; Chen, H.; Lee, D. H.; Zheng, C. Characteristics of hemicellulose, cellulose and lignin pyrolysis. *Fuel* **2007**, *86*, 1781–1788.
- [55] Lindau, I.; Pianetta, P.; Doniach, S.; Spicer, W. X-ray photoemission spectroscopy. *Nature* **1974**, *250*, 214–215.
- [56] Arnault, J.-C. X-ray Photoemission Spectroscopy applied to nanodiamonds: From surface chemistry to in situ reactivity. *Diamond and Related Materials* **2018**, *84*, 157–168.
- [57] Greczynski, G.; Hultman, L. X-ray photoelectron spectroscopy: Towards reliable binding energy referencing. *Progress in Materials Science* **2020**, *107*, 100591.
- [58] Johansson, L.-S.; Campbell, J.; Koljonen, K.; Stenius, P. Evaluation of surface lignin on cellulose fibers with XPS. *Applied surface science* **1999**, *144*, 92–95.
- [59] Wei, Y.; Huang, Y.; Yu, Y.; Gao, R.; Yu, W. The surface chemical constituent analysis of poplar fibrosis veneers during heat treatment. *Journal of Wood Science* **2018**, *64*, 485–500.
- [60] Kazzaz, A. E.; Feizi, Z. H.; Fatehi, P. Grafting strategies for hydroxy groups of lignin for producing materials. *Green Chemistry* **2019**, *21*, 5714–5752.
- [61] Li, J.; Wang, W.; Zhang, S.; Gao, Q.; Zhang, W.; Li, J. Preparation and characterization of lignin demethylated at atmospheric pressure and its application in fast curing biobased phenolic resins. *RSC advances* **2016**, *6*, 67435–67443.
- [62] Li, Y.; Fu, Q.; Rojas, R.; Yan, M.; Lawoko, M.; Berglund, L. Lignin-retaining transparent wood. *ChemSusChem* **2017**, *10*, 3445.
- [63] Jia, C.; Chen, C.; Mi, R.; Li, T.; Dai, J.; Yang, Z.; Pei, Y.; He, S.; Bian, H.; Jang, S.-H. Clear wood toward high-performance building materials.
- [64] Wang, R.; Zhou, B.; Wang, Z. Study on the Preparation and Application of Lignin-Derived Polycarboxylic Acids. *Journal of Chemistry* **2019**, 2019.



- [65] Greczynski, G.; Hultman, L. X-ray photoelectron spectroscopy: Towards reliable binding energy referencing. *Progress in Materials Science* **2020**, *107*, 100591.
- [66] Baer, D. R.; Artyushkova, K.; Cohen, H.; Easton, C. D.; Engelhard, M.; Gengenbach, T. R.; Greczynski, G.; Mack, P.; Morgan, D. J.; Roberts, A. XPS guide: Charge neutralization and binding energy referencing for insulating samples. *Journal of Vacuum Science & Technology A: Vacuum, Surfaces, and Films* **2020**, *38*, 031204.
- [67] Esteves, B.; Velez Marques, A.; Domingos, I.; Pereira, H. Chemical changes of heat treated pine and eucalypt wood monitored by FTIR. *Maderas. Ciencia y tecnología* **2013**, *15*, 245–258.
- [68] Moosavinejad, S. M.; Madhoushi, M.; Vakili, M.; Rasouli, D. Evaluation of degradation in chemical compounds of wood in historical buildings using FT-IR and FT-Raman vibrational spectroscopy. *Maderas. Ciencia y tecnología* **2019**, *21*, 381–392.
- [69] Faix, O.; Meier, D.; Fortmann, I. Gas chromatographic separation and mass spectrometric characterization of monomeric lignin derived products. *Holz als roh-und werkstoff* **1990**, *48*, 281–285.
- [70] Marella, T. K.; Tiwari, A. Marine diatom *Thalassiosira weissflogii* based biorefinery for co-production of eicosapentaenoic acid and fucoxanthin. *Bioresource technology* **2020**, *307*, 123245.
- [71] Kubovský, I.; Kačíková, D.; Kačík, F. Structural changes of oak wood main components caused by thermal modification. *Polymers* **2020**, *12*, 485.
- [72] Kljun, A.; Benians, T. A.; Goubet, F.; Meulewaeter, F.; Knox, J. P.; Blackburn, R. S. Comparative analysis of crystallinity changes in cellulose I polymers using ATR-FTIR, X-ray diffraction, and carbohydrate-binding module probes. *Biomacromolecules* **2011**, *12*, 4121–4126.
- [73] Popescu, C.-M.; Popescu, M.-C.; Singurel, G.; Vasile, C.; Argyropoulos, D. S.; Willfor, S. Spectral characterization of eucalyptus wood. *Applied spectroscopy* **2007**, *61*, 1168–1177.

- [74] Dobrzyńska-Mizera, M.; Knitter, M.; Woźniak-Braszak, A.; Baranowski, M.; Sterzyński, T.; Di Lorenzo, M. L. Poly (l-Lactic Acid)/Pine Wood Bio-Based Composites. *Materials* **2020**, *13*, 3776.
- [75] Chen, S.; Tanaka, H. Surface analysis of paper containing polymer additives by X-ray photoelectron spectroscopy I: Application to paper containing dry strength additives. *Journal of wood science* **1998**, *44*, 303–309.
- [76] Fujimoto, A.; Yamada, Y.; Koinuma, M.; Sato, S. Origins of sp<sup>3</sup>C peaks in C1s X-ray photoelectron spectra of carbon materials. *Analytical chemistry* **2016**, *88*, 6110–6114.
- [77] Ghavidel, A.; Scheglov, A.; Karius, V.; Mai, C.; Tarmian, A.; Vioel, W.; Vasilache, V.; Sandu, I. In-depth studies on the modifying effects of natural ageing on the chemical structure of European spruce (*Picea abies*) and silver fir (*Abies alba*) woods. *Journal of Wood Science* **2020**, *66*, 1–11.
- [78] Rouxhet, P. G.; Genet, M. J. XPS analysis of bio-organic systems. *Surface and Interface Analysis* **2011**, *43*, 1453–1470.
- [79] Ji, X.; Dong, Y.; Nguyen, T. T.; Chen, X.; Guo, M. Environment-friendly wood fibre composite with high bonding strength and water resistance. *Royal Society open science* **2018**, *5*, 172002.
- [80] Major, G. H.; Fairley, N.; Sherwood, P. M.; Linford, M. R.; Terry, J.; Fernandez, V.; Artyushkova, K. Practical guide for curve fitting in X-ray photoelectron spectroscopy. *Journal of Vacuum Science & Technology A: Vacuum, Surfaces, and Films* **2020**, *38*, 061203.
- [81] Belgacem, M.; Czeremuszkin, G.; Sapieha, S.; Gandini, A. Surface characterization of cellulose fibres by XPS and inverse gas chromatography. *Cellulose* **1995**, *2*, 145–157.
- [82] Nzokou, P.; Pascal Kamdem, D. X-ray photoelectron spectroscopy study of red oak-(*Quercus rubra*), black cherry-(*Prunus serotina*) and red pine-(*Pinus resinosa*) extracted wood surfaces. *Surface and Interface Analysis: An International Journal devoted to the development and application of techniques for the analysis of surfaces, interfaces and thin films* **2005**, *37*, 689–694.

- 
- [83] Nie, K.; Xu, L.; Qian, T.; Shen, X.; Sun, Q. Fabrication of a robust and flame-retardant aloooh-lignocellulose composite with a lotus-leaf-like superhydrophobic coating. *Journal of Wood Chemistry and Technology* **2020**, *40*, 44–57.
- [84] Bañuls-Ciscar, J.; Abel, M.-L.; Watts, J. F. Characterisation of cellulose and hardwood organosolv lignin reference materials by XPS. *Surface Science Spectra* **2016**, *23*, 1–8.
- [85] Goforth, M. A.; Gilchrist, G. W.; Sirianni, J. D. Cloud effects on thermal downwelling sky radiance. 2002.